Università degli Studi di Catania
Scuola Superiore di Catania

International PhD

In

Energy

XXIV cycle

Distributed Generation Systems Based on Hybrid Wind/Photovoltaic/Fuel Cell Structures

Aysar M.M. Yasin

Coordinator of PhD
Prof. Alfio Consoli

Tutor
Prof. Antonio Testa

Abstract

The distributed generation (DG) today attracts a large interest due to an even increasing demand of energy and the growth of awareness about the impact of conventional energy sources on the environment.

Photovoltaic (PV) and wind power are two of the most promising renewable energy technologies. Fuel cell (FC) systems also show enormous potential in future DG applications, due to a fast technology development, high efficiency, environment friendliness and modularity. Hybrid systems encompassing wind, photovoltaic and FC generators are today revised as a viable solution to overcome the inner unreliability of renewable energy sources.

The modelling and control of a hybrid wind/PV/FC DG system is addressed in this dissertation. Dynamic models for the main system components, namely: wind and PV energy generators, fuel cell, electrolyser, power electronic interfaces, battery, hydrogen storage tank, gas compressor, are developed and verified by experimental tests and simulation studies.

Five different architectures of stand-alone hybrid power systems are considered, exploiting connections through DC and AC buses. Each configuration is managed through a specific control methodology. Based on suitable dynamic models, the five proposed stand-alone hybrid energy system configurations have been simulated using the MATLAB/Simulink/SimPowSys^{TM} software environment.

A comparison among those configurations has been performed on the basis of purposely developed performance indexes. According to obtained results the high voltage DC bus (HVDC) configuration reaches the best score among the five configurations.

A Fuzzy logic based management of a stand-alone hybrid generator based on high voltage DC bus configuration has been developed to dynamically optimize the power flows among the different energy sources. The performances of the proposed strategy are evaluated by simulation in different operating conditions. The results confirm the effectiveness of the proposed strategy.

A further goal of the thesis has been the development of a probabilistic approach to size step-up transformers for grid-connected wind farms. This approach is mainly based on the evaluation of the Loss of Produced Power Probability index (LPPP); the costs of the wind farm equipments are also taken into consideration.

Acknowledgments

I am grateful to acknowledge and thank all persons and institutions who assisted me during the course of my PhD study.

This work has been done in collaboration with the Excellency School of Catania and National Research Council of Italy-Messina / Institute of Advanced Energy Technologies (CNR-ITAE/Messina). Acknowledgements are given to aforementioned institutions for their financial support.

The research activity was carried out under the supervision of Prof. Antonio Testa from the Department of Industrial Chemistry and Materials Engineering (DCIIM) at Messina University. My deepest gratitude goes to Prof. Testa for his valuable guidance, encouragement and professional support during the elaboration of my PhD thesis.

I'm deeply indebted to Prof. Alfio Consoli, the Coordinator of PhD program, from Department of Electrical Engineering, Electronics and Systems (DIEES) at Catania University for his support and professional guidance.

I would like to express my thanks to Eng. Gaetano Cacciola the director of CNR-ITAE/Messina for facilitating my research mission in the institution. I'm obliged to thank Dr. Vincenzo Antonucci the manager of energy technology system group (CNR-ITAE/Messina), Giuseppe Napoli and Marco Ferraro for their professional guidance, valuable hints and support. I want to thank also all of my colleagues in CNR-ITAE/Messina for their friendly companionship in particular Alessandro Stassi, Giorgio Dispenza, Francesco Sergi, Giovanni Brunaccini, Laura Andaloro and Alessandra Di Blasi.

I'm also grateful to Prof. Mario Cacciato and Giacomo Scelba from the University of Catania and Salvatore De Caro from the University of Messina for their guidance and friendship.

Special thanks to my PhD colleagues at the Excellency School of Catania; especially I'm obliged to thank Tommaso Scimone, Alberto Gaeta, Vittorio Crisafulli, Muhammad Alsayed, Novella Papa and Alessandro Contino for their assistance, helpful scientific discussion and friendship.

I should express the deepest and sincere appreciation to my parents, my wonderful wife Dalia and two sons Islam and Ali for their great sacrifices during my study in Italy.

Table of contents

Abstract ii
Acknowledgment iii
Table of Contents iv
Nomenclature vii

Chapter 1: Introduction 1

1.1 Background, Objectives and Motivation 1
1.2 Main Contribution 4
1.3 Thesis Outlines 5

Part I : Distributed Generation Systems Based on Hybrid Wind/Photovoltaic/Fuel Cell 7

Chapter 2: Fundamentals of the Renewable Energy Sources and Energy Storage Systems 8

2.1 Renewable Energy Sources 8
2.1.1 Photovoltaic Energy 8
2.1.1.1General Description of a PV Cell 9
2.1.1.2 Characteristics of a PV Module 10
2.1.1.3Maximum Power Point Tracker (MPPT) 11
2.1.2 Wind Energy System 15
2.1.2.1 Wind turbine types 15
2.1.2.2 Wind energy model 16
2.2.2.3 Wind energy control system 17
2.1.3 Fuel Cells 18
2.1.3.1 Fuel Cell work principle 19
2.1.3.2 Fuel Cell types and characteristics 19
2.1.3.3 Fuel cell Polarization Curve 20
2.2 Energy Storage System (ESS) 21
2.2.1 Lead Acid Battery Energy Storage System 21
2.2.2 Fuel cell - Electrolyser (FC/E-ESS) 23
2.2.3 Vanadium Redox Flow Battery (VRB- ESS) 26

Chapter 3: Stand-Alone Hybrid Distributed Generation System 28

3.1 Distributed Generation System 28
3.2 Hybrid Power Systems 29
3.3 Topologies of Hybrid Power Systems 30
3.3.1 DC Bus Coupled Topology 30
3.3.2 AC Bus Coupled Topology 30
3.4 Stand-alone Hybrid System versus Grid Connected System 31

3.5 Stand-Alone Hybrid System Plant Architectures 33
3.5.1 High Voltage DC Bus Configuration (HVDC) 33
3.5.2 Low Voltage DC Bus Configuration (LV-DC) 33
3.5.3 High voltage AC Bus configuration (HVAC) 34
3.5.4 High Voltage AC-rectified Bus Configuration (HVAC-Rect.) 34
3.5.5 Double Bus Low and High DC Voltage (LV/HV-DC) 35
3.6 Hybrid System Input Data 36
3.7 Hybrid system components parameters 37

Chapter 4: Modelling and Control of the Stand-Alone Hybrid System Components 40

4.1 Modelling and control of PVG 40
4.2 Modelling and control of WEG 43
4.3 Modelling and control of Fuel cell 46
4.4 Modelling and control of the electrolyser, H2 storage tank, Compressor and Dump load 48
4.5Modelling and control of BSS and DC bus 51

Chapter 5: Possible Configurations for a Stand-Alone Hybrid Generator 53

5.1 Introduction 53
5.2 Bus Voltage Configurations for a Stand-Alone Hybrid Generator 53
5.2.1 HV-DC bus configuration 54
5.2.2 LV-DC bus configuration 58
5.2.3 HVAC bus configuration 59
5.2.4 HVAC rectified bus configuration 61
5.2.5 Double bus configuration 62
5.3 Comparative analysis 63
5.4 Performance Indexes 64
5.5 Simulation results 66
5.5.1 Global Efficiency 66
5.5.2 Efficiency of energy transfer from RES to BSS 67
5.5.3 Efficiency of energy delivered from BSS to load 68
5.5.4Fraction of useful renewable energy performance index 69
5.6 Sensitivity of performance indexes to seasonal load variation 70
5.7 Conclusion 71

Chapter 6: Fuzzy Logic Based Management of a Stand-Alone Hybrid Generator 72

6.1 Introduction 72
6.2 System Configuration 72
6.3 Power Management Strategy Methodology 74
6.4 Fuzzy Logic Controller 76
6.4.1Background information 76
6.4.2 Fuzzy Logic Controller Design 78
6.5Simulation Results 82
6.5.1 Time Domain Performance Indexes 82
6.5.2 Performance of FL based management 83
6.5.3 Comparison between the FL based strategy and a conventional one based on a deterministic approach. 87
6.6 Conclusion 89

Part II: Sizing Step up Transformers for Grid Connected Wind Farms **90**

Chapter 7: A Probabilistic Approach to Size Step-Up Transformers for Grid Connected Wind Farms **91**

7.1 Introduction 91
7.2 Schematic of the Proposed Wind Farm 92
7.3 The Proposed Approach 94
7.3.1 Wind Farm Without ESS 95
7.3.2 Wind Farm Plant With ESS 98
7.4 Sizing Step-Up Transformers Analysis 100
7.4.1 Sizing Step-up transformers for Wind Farm plants without ESS 101
7.4.2 Sizing Step-up transformers for Wind Farm plants with ESS 104
7.5 Conclusion 108

References **109**

Nomenclature

List of Abbreviation

AC	Alternating Current
BSS	Battery Storage System
DC	Direct Current
DG	Distributed Generation
E	Electrolyser
ESS	Energy Storage System
FC	Fuel Cell
FL	Fuzzy Logic
GHG	Global Greenhouse Gas
LPF	Low Pass Filter
LPPP	Loss of Produced Power Probability
LPSP	Lost of Power Supply Probability
MPPT	Maximum Power Point Tracker
PI	Proportional Integral
PID	Proportional Integral Derivative
PV	Photovoltaic
PVG	Photovoltaic Generator
Pu	Per Unit
PWM	Pulse Width Modulation
RE	Renewable Energy
RES	Renewable Energy Sources
RMS	Root Mean Square
SOC	State of Charge
THD	Total Harmonic Distortion
WEG	Wind Energy Generator
WT	Wind Turbine

Chapter 1

Introduction

This chapter presents the background, objectives and the motivation of the thesis, continuing with a list of the main contributions and finishing with the outline of the thesis.

1.1 Background, Objectives and Motivation

As shown in Figure 1.1 electricity generation is still largely based on conventional energy sources, which however, sooner or later, are going to be depleted. This makes the future dangerously vulnerable, as fossil fuel demand will shortly exceed the production capacity of even the largest suppliers, and the nuclear power generation, once considered as an unlimited energy source, is today quite unpopular and worrying, especially after Chernobyl and Fukushima Daiichi nuclear power plants disasters in Ukraine and Japan, respectively. Moreover, the generation of electrical energy using conventional technologies over decades has severely affected the environment. As a result, the whole world is today engaged in a challenge to reduce the negative impact of the energy generation on our planet and find out how to generate the required amount of energy from clean energy sources.

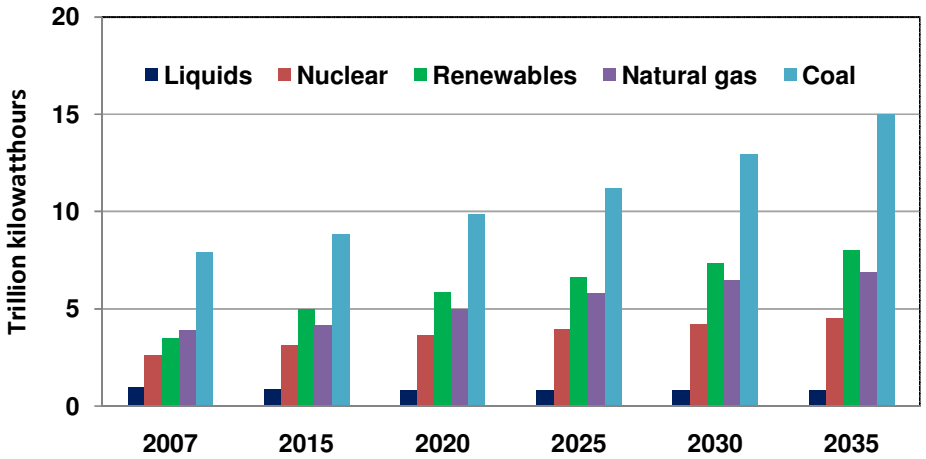

Figure 1.1. World net electricity generation by fuel, 2007-2035 [1]

The world electric power generation is expected to rapidly increase in the next two decades, Figure 1.2 shows the strong growth of the total electric power and total energy consumption in the in the past two decades and its projection over the next two decades.

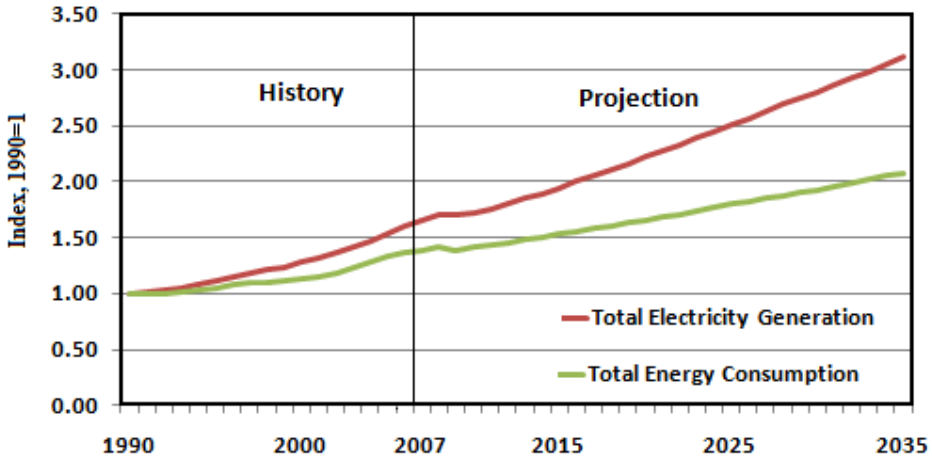

Figure 1.2. Growth in world electric power generation and total energy consumption, 1990-2035 [1]

The share of electrical energy over the total energetic demand is increasing and grows up faster than those of liquid fuels, natural gas, and coal in all end-use sectors except transportation. This increases the total energy consumption, the global warming and the worries about shortage of conventional fuels, powering a great interest about large scale generation from renewable energy sources (RES) as a viable solution to the energetic problem.

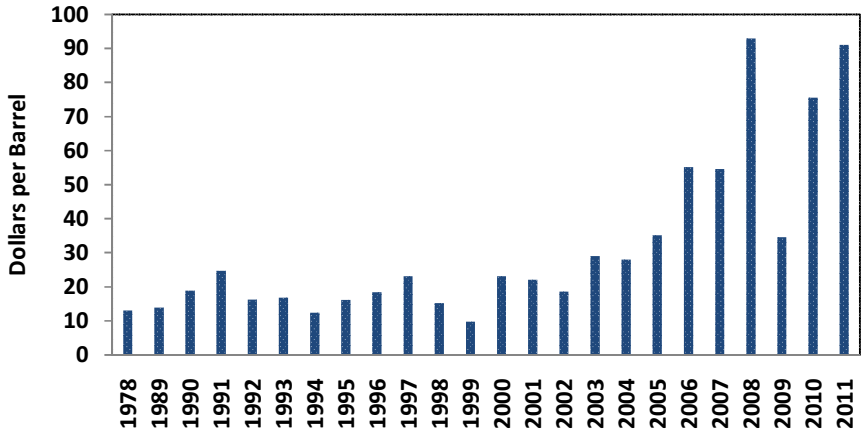

Figure 1.3. World crude oil prices based on the first week data of January in each year 1978-2011 [2]

Renewable energies is a fast-growing segment as depicted in Figure 1.1. The total electricity generation from RES increases by 3.0 percent annually, and the renewable share of world electricity generation will grow from 18 percent in 2007 to 23 percent in 2035. It is good practice to mention that almost 80 percent of the increase is in hydroelectric and wind power [1].

Among RE technologies, photovoltaic (PV) and wind turbines (WT) are indeed the most popular, although their diffusion has been hampered by high costs and technological problems. However, in the last two decades the efficiency and reliability of photovoltaic and wind generators have been remarkably improved and the capital costs lowered.

The solar energy that hits the earth's surface in one hour is about the same that is consumed by all human activities in one year. Electricity can be generated from sunlight through photovoltaic (PV) and solar thermal systems. PV energy will be discussed throughout this dissertation.

There are four primary applications for PV power systems as reported in [3]: off-grid domestic, off-grid non domestic, grid connected distributed and grid connected centralized. PV energy is one of the fast growing renewable energy technology. Figure 1.4 shows the cumulative installed grid-connected and off-grid PV power in the IEA-PVPS[1] countries, About 6.2 GW of PV capacity were installed in the IEA PVPS countries during 2009 while total PV capacity installed worldwide during 2009 is estimated to be a little over 7 GW [3].

Much the same amount was installed in the previous year which is considered a good indication to healthy growth rate of PV energy market despite the global economic slowdown.

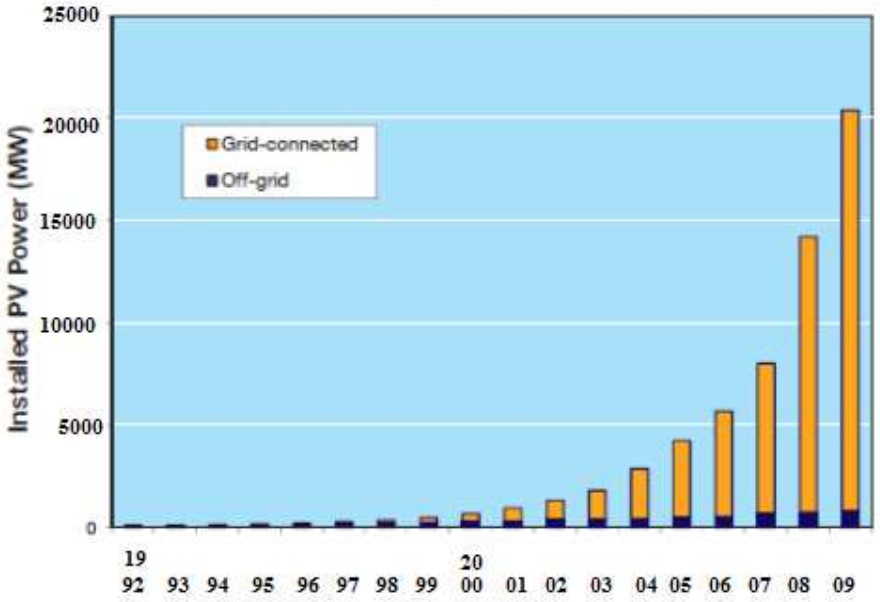

Figure 1.4. Cumulative installed grid-connected and off-grid PV power in the reporting countries [3]

In 2009 the average price of photovoltaic modules in the IEA PVPS countries was about 2.6 USD/W, a decrease of 35 % compared to the corresponding figure for 2008. Prices as low as 3.5 USD/W were reported for grid-connected systems in 2009 but typically prices were in the range 4 USD/W to 6 USD/W [3].

Wind energy is a clean energy source that increasingly contributes to reduce the dependency from fossil fuels, taking full advantage from a progressive cost reduction of wind generators in times in which the cost of traditional fuels instead increases [4]. According to the Figure 1.5 released by the Global Wind Energy Council (GWEC) in 2010 the wind energy generation has grown exponentially in the last two decades.

[1] IEA-PVPS : International Energy Agency – Photovoltaic Power Systems Programme. There are 19 countries participating in this program. The top three PV countries, Japan, Germany, and the U.S. Over 90% of the world total PV capacity is installed in the IEA-PVPS countries.

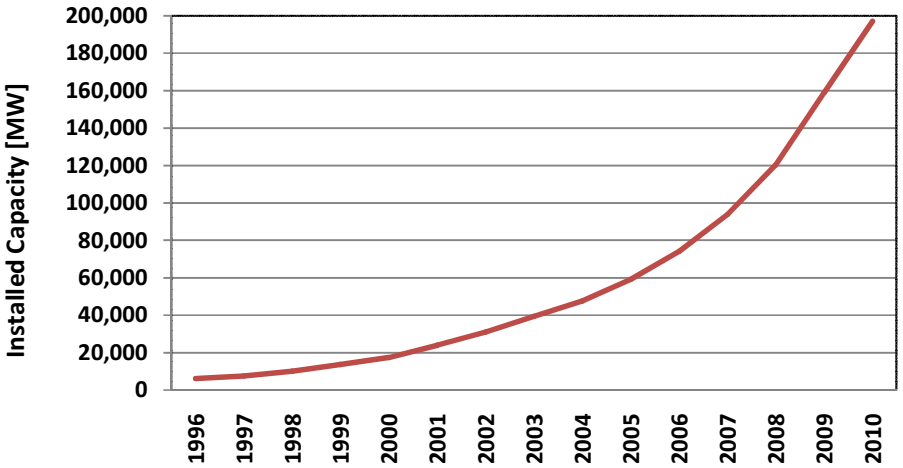

Figure 1.5. Growth of the world's wind installed capacity [5]

Fuel Cell technology is an attractive option to compensate the discontinuity of some renewable energy sources like solar irradiation and wind, thanks to a high efficiency, a fast load response, the modularity, and large fuel flexibility [6]. A FC is an electrochemical device that generates electricity directly from the chemical energy of a fuel, generally hydrogen or hydrocarbon. The yearly amount of annual patent applications related to the FC technology today exceeds 3500 [7], reflecting a rapid technological progress, leading to a massive introduction of FC systems into the market in a near future.

Hybrid generation stand-alone power system composed of wind energy generator (WEG) and Photovoltaic energy generator (PVG) with proper control methodology and configuration have great potential to provide higher quality and more reliable power to customers than a system based on a single resource due to the overlap of the availability of the two primary sources. In this context FC technology is an attractive option to compensate the discontinuity of solar irradiation and wind, thanks to a high efficiency, a fast load response and modularity [6].

The matter of finding out the optimal system configuration, for a of a hybrid wind/PV/FC DG system is first addressed along this work. Proper power electronic interfaces and power management techniques are examined and comprehensively discussed. In the second part of the thesis, a design technique is proposed to optimally select the step-up transformer on conventional wind farm plants and those with ESS. It is based on the evaluation of initial and operating costs. This work is very important as traditional method of sizing step up transformers leads to huge power losses and network stability problems.

1.2 Main Contribution

1. Dynamic modelling, control and validation of the main components of a hybrid wind/PV/FC DG system using Matlab/Simulink/SimPowSys^{TM}. These components include:

- PVG with maximum power point tracking (MPPT).
- WEG with maximum power point tracking (MPPT).
- FC and Electrolyser (E) with the required control strategies.
- Battery storage system (BSS) with the required control strategy.
- Power electronic interfacing equipments with control strategy.
- Accessories

The developed models are based on real commercial devices installed in lab. The models were validated using experimental and simulation studies.

2. An investigation, accomplished through simulations, about different requirements of stand-alone and grid-connected hybrid power systems in terms of power electronic interfacing devices, control methodologies and the capacity of the required storage system.

3. The identification of possible stand-alone hybrid power system architectures featuring different bus voltages. Among those architectures are:

- High voltage DC bus configuration (HV-DC),
- Low voltage DC bus configuration (LV-DC),
- High voltage AC bus configuration (HV-AC),
- High voltage AC rectified bus configuration (HV-AC rect.) and
- Double buses low and high voltage DC bus configuration (LV/HV-DC).

4. The above configurations are modelled and controlled using different control strategies.

5. The identification of the optimal configuration based on special performances indexes designed specially for this purpose.

6. The design of a power management strategy for a stand-alone hybrid system based on both conventional controller and fuzzy logic controller.

7. The design of a probabilistic methodology to size step up transformers for conventional grid connected wind farms plants and those with ESS on the basis of the statistical distribution of the wind energy in the selected site and the mathematical model of the plant.

1.3 Thesis Outlines

Chapter 1 presents the background, objectives, motivation and main contribution of this research.

Chapter 2 reviews the fundamental concepts and principles of the new and renewable energy sources utilized in this study. Some types of energy storage systems are also reviewed.

In chapter 3 the distribution generation (DG) system and topologies of the hybrid power systems are presented in addition to simulation studies to define the main features of the stand alone and

grid connected systems, it also introduces different architecture of stand-alone hybrid system. The input weather data for a specific site and daily load demand in cold season is also included with the real hybrid system components parameters utilized in the study.

In Chapter 4, the stand alone alternative energy hybrid system components are modelled and controlled.

In Chapter 5, the control of different configurations for a stand-alone hybrid generator and the comparison analysis between those configurations are presented.

In Chapter 6, a power management strategy for a stand-alone generator based on a fuzzy logic controller is developed.

In Chapter 7, a probabilistic approach to size step-up transformers for grid connected wind farms on the basis of statistical distribution of the wind energy is carried out.

Part I

Distributed Generation Systems Based on Hybrid Wind/Photovoltaic/Fuel Cell

Chapter 2

Fundamentals of Renewable Energy Sources and Energy Storage Systems

This chapter reviews the fundamental concepts and principles of renewable energy sources utilized in this study. Three types of energy storage systems will be reviewed as they are considered in this research.

2.1 Renewable Energy Sources

Sun is the source of all types of renewable energies, earth receives solar energy as radiation from the sun which makes the planet heated up and in consequence the wind, rain, rivers, and waves are generated. The biomass that is used to produce electricity and transportation fuel is originated from the sun as well.

The hydrogen which can be extracted from many organic compounds and water is considered a source of energy once separated as it doesn't occur naturally as a gas but combined with other elements.

Renewable energy sources (RES) can't be exhausted or run out and cause so little damage to environment. Photovoltaic, Wind and Fuel Cells energy conversion systems will be discussed in some details as they are the main energy sources utilized in this research.

2.1.1 Photovoltaic Energy

Before going into details of PV energy conversion system, it is good practice to define some important terminologies.

- Solar radiation: It is a collection of beam, diffusion and albedo radiations that come directly and indirectly from the sun [8].
- Solar constant: The solar radiation that falls on a unit area above the atmosphere at a vertical angle. It equals to 1367 W/m² [8].
- Irradiance: A measure of power density of sunlight (W/m^2).
- Air mass: It is defined as the ratio of the mass of atmosphere through which the solar radiation passes to the mass it would pass through if the sun were at the zenith.

2.1.1.1 General Description of a PV Cell

PV cells are used worldwide to convert sunlight into electricity and considered one of the technologies with the fastest growth rate. Due to many incentives PV power supplied to utility grid is increasing and become more visible [9].

The PV cell contains two layers of positive and negative charge semiconductor materials. As the sunlight strikes and enters the cell, some photons are absorbed by semiconductor atoms, freeing electrons that travel from the negative layer of the cell back to the positive layer. In consequence of this process the voltage is created. The flow of electrons through an external circuit produces electricity [10]. Figure 2.1 shows the basic solar cell structure.

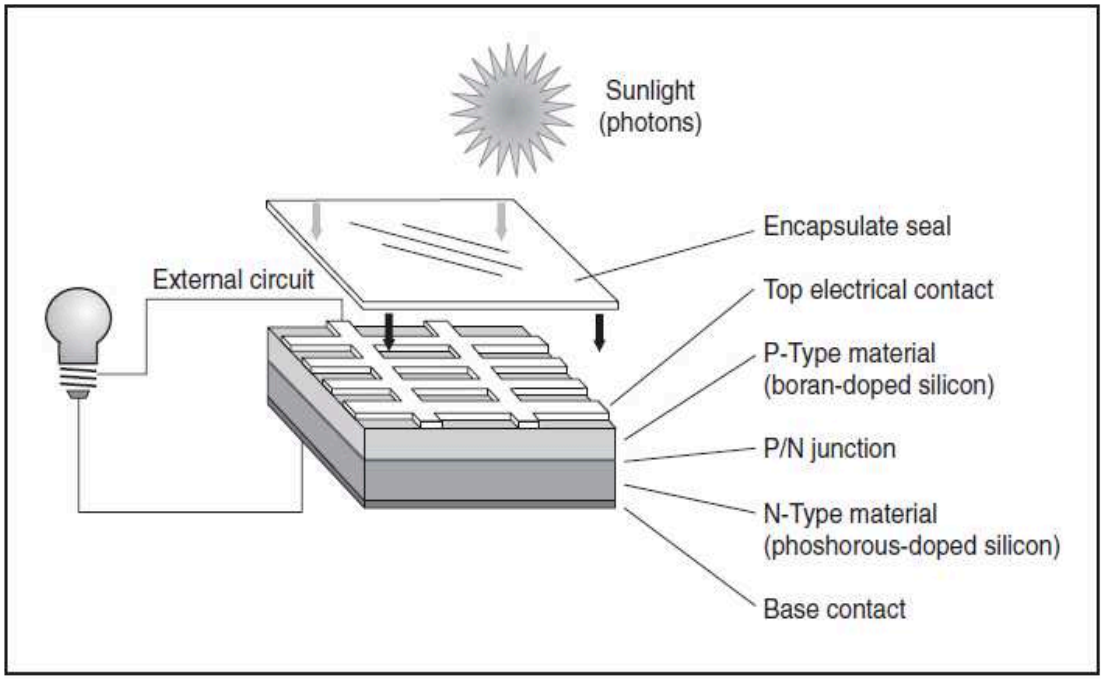

Figure 2.1. Basic solar cell structure [10]

There are no moving parts inside a PV module resulting in a life time exceeding 25 years.

There are different types of PV cell technologies [11]:

- Single crystalline silicon PV cell with efficiency range: 10 - 15%.
- Multi-crystalline silicon with efficiency range: 9% - 12%.
- Thin-film amorphous silicon with 10% efficiency.
- Thin-film copper indium diselenide with 12% efficiency.
- Thin-film cadmium telluride and dye-sensitised nano-structured materials with 9% efficiency.
- Novel technologies such as the thin-layer silicon with 8% efficiency.

2.1.1.2 I-U Characteristics of a PV Module

The electrical model of PV cell is simply a current source in parallel with a diode as shown in Figure 2.2; the current is proportional to the intensity of light that falls on the cell.

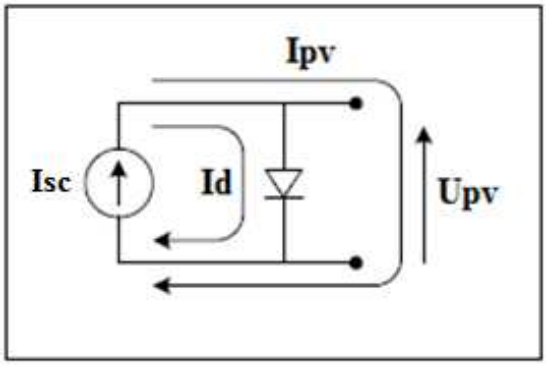

Figure 2.2. Electrical model and characteristics of a PV cell

Figure 2.3 shows the I-V characteristics of a PV cell. The open circuit voltage is obtained when the PV cell is not connected to any load. In such a working condition the voltage across the PV cell is maximum.

When a load is connected to the PV cell, current flows through the circuit and the voltage goes down. The current is maximum when the two terminals are directly connected with each other and the voltage is zero. The current in this case is called short circuit current. The point where the maximum power is obtained is called the maximum power point as shown in Figure 2.3.

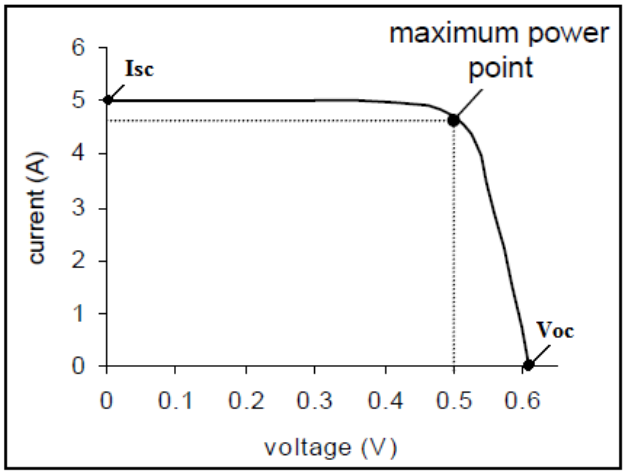

Figure 2.3. I-V characteristics of a typical PV cell

The amount of generated energy from PV cell mainly depends on its size and material. Solar radiation and temperature also affect the PV cell characteristics. Current is directly and highly affected by the amount of solar radiation while voltage is not highly affected.

Figure 2.4 shows the I-V characteristics of BP 585 high-efficiency mono-crystalline PV module at different irradiations at 25C° [12].

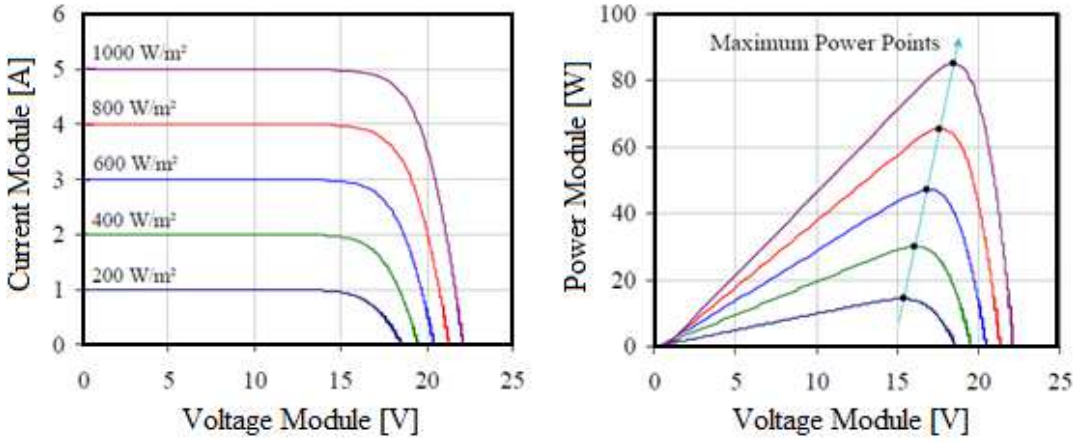

Figure 2.4. I-V and P-V characteristics of BP 585 high-efficiency mono-crystalline PV module at different irradiations and 25 ◦C.

On the other hand, the voltage is more affected by changes in the temperature of the PV cell than the current. Figure 2.5 shows the characteristics of BP 585 high-efficiency Mono-crystalline PV module at 1000 W/m^2 with different cell temperature [12]. It is clear that as the solar cell temperature increases the amount of open voltage decreases.

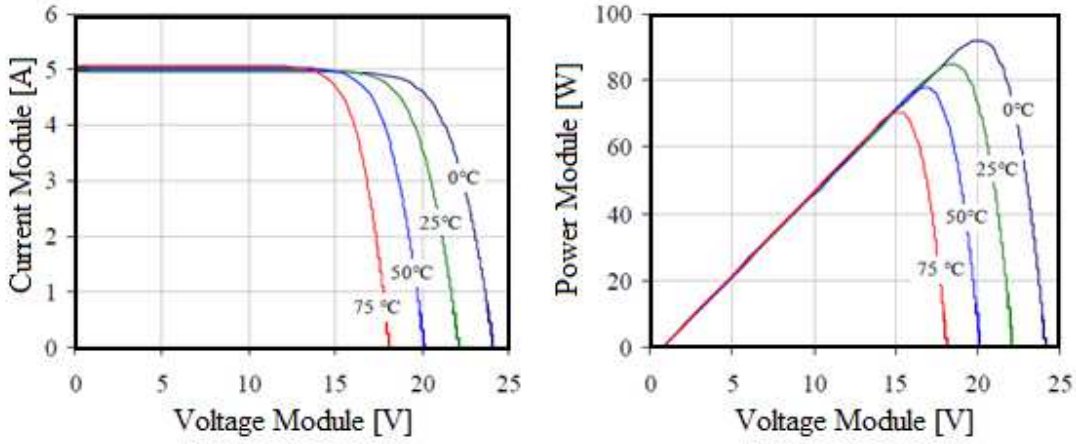

Figure 2.5. I-V and P-V characteristics of BP 585 high-efficiency mono-crystalline PV module at different temperatures and 1000W/m^2

As the power generated from a typical single PV cell is less than 2W at approximately 0.5V DC, a typical PV module is made up of around 36 or 72 cells connected in series. An array of PV modules is made up by connecting number of modules in series and in parallel in order to have the required capacity of power and voltages. Figure 2.6 shows the PV cell, module and array.

2.1.1.3 Maximum Power Point Tracker (MPPT)

The I-V characteristic is very sensitive to solar radiation and temperature. It is observed from I-V characteristics that at different values of temperature and solar radiation correspond different points of maximum power (MPP).

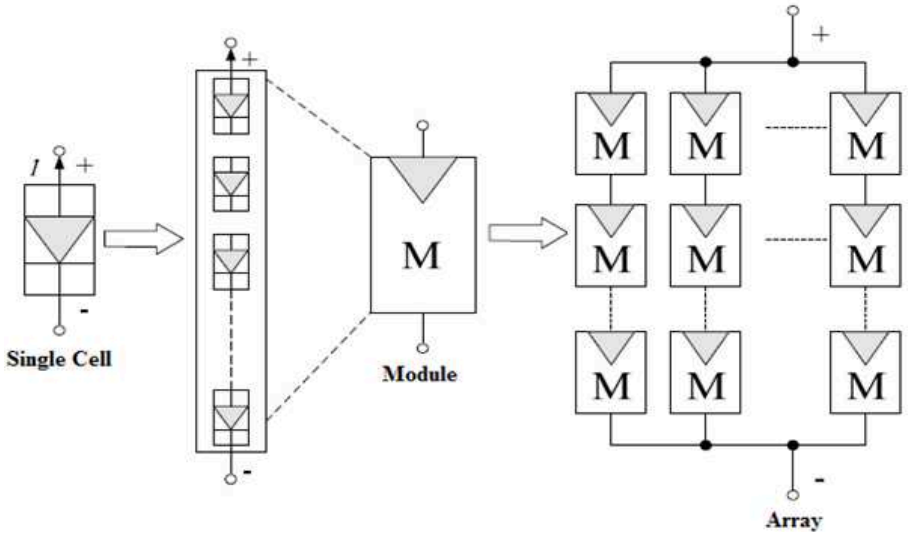

Figure 2.6. PV cell, module and array

It is essential to force a PV module to always work at the MPP corresponding to actual conditions of solar radiation and temperature, in order to obtain the best energetic efficiency. Working at MPP is essential in PV power generation, because the input energy is free while the capital investment is relatively high.

Various MPPT techniques can be found in literature [13]. Among these, the most important are:

- The perturbation and observation method (P&O).
- Incremental Conductance method.
- Current-Based MPPT.
- Voltage-Based MPPT.

The perturbation and observation method (P&O)

This method is widely used in MPPT because of its simple structure and the few measured parameters. The working principle is summarised as follows: The array terminal voltage is periodically perturbed (increased or decreased) and the gradient of the PV output power is analysed. If the perturbation produces an increment of the output power, a further perturbation with the same sign is exerted, otherwise the sign of the perturbation is changed [14].

The flow chart of a P&O MPPT algorithm is shown in Figure 2.7. The algorithm reads the values of PV module output current and voltage, then computes the gradient of the output power. The main disadvantage of this method is that as the voltage is perturbed every MPPT cycle even at constant or slowly weather conditions, the algorithm causes an oscillation of the working point

around the point of maximum power of the PV which causes some power loss, this could be reduced by reducing the perturbation step [14].

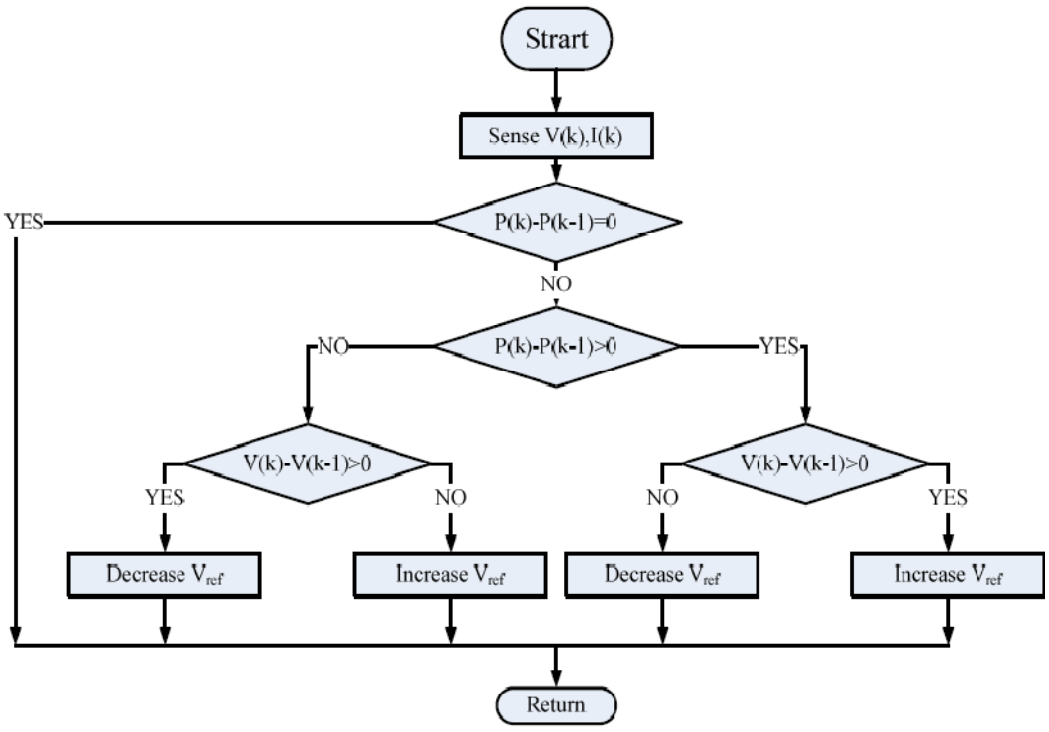

Figure 2.7. Flow chart of P&O MPPT algorithm

Incremental conductance MPPT algorithm

This method solves the problem of the perturbation and observation (P&O) method to track the fast varying weather conditions.

The basic idea is that at the MPP, the derivative of the power with respect to the voltage is zero because the MPP corresponds to the point of maximum of the power curve as shown in the right side of Figure 2.4, i.e. dP/dV = 0. In the same Figure we note that at the left side of the MPP the power is increasing with the voltage, i.e. dP/dV > 0, and it is decreasing to the right of the MPP, i.e. dP/dV < 0 [14].

These relations can be rewritten in terms of the array current and voltage using

$$dP/dV = d(lV)/dV = I + V\ dI/dV \qquad (2.1)$$

Hence by measuring the incremental and instantaneous array conductances (dI/dV and I/V, respectively) and making use of the above dP/dV relations, the PV array terminal voltage can be adjusted to reach the MPP. One disadvantage of this algorithm is the increased complexity when compared to the perturb and observe approach.

Current-Based Maximum Power Point Tracking CMPPT [13]

A linear relationship between the current at maximum power point (Imp) and the short circuit current (Isc) has been observed. This can be written in eq. (2.2).

$$I_{mp} = K_c * I_{sc} \quad (2.2)$$

Where:
I_{sc}: short circuit current
I_{mp}: current at maximum power point.
K_c: current factor control and assumed to be 0.9.

The main disadvantage of this method is the need to measure the short circuit current, which needs a high power resistor.

Voltage-Based Maximum Power Point Tracking (VMPPT) [13]

The idea of this method is similar to CMPPT, in which a linear relationship between the voltage at maximum power point (V_{mp}) and the open circuit voltage (V_{oc}). This can be written in eq. (2.3).

$$V_{mp} = K_v * V_{oc} \quad (2.3)$$

Where:

V_{oc}: open circuit voltage.
V_{mp}: voltage at maximum power point.
K_v: voltage factor control, and assumed to be 0.75.

A direct measurement of the open circuit voltage (V_{oc}) makes possible to generate a reference voltage according to a feed forward voltage control scheme to bring the solar PV module voltage to the point of maximum power. The main drawback of this method is that open circuit voltage should be measured very often since it depends on the temperature. To do this, the load must be disconnected from the PV module, this reduces the power generated.

The perturbation and observation method (P&O) and the Incremental Conductance method are the most common strategies used to achieve a maximum power point tracking in PV plants.

Incremental Conductance method has a good performance during the varying weather conditions, but, as it uses four sensors for measurements and making decision, a large amount of power will be lost specially if the system requires more conversion time [15]. The complexity and the cost of the system is higher than P&O method which uses only two sensors.

Power losses decrease if the sampling and execution speed of the perturbation and observation method is increased [15]. According to the previous presentation, perturbation and observation (P&O) method is selected in this research as a trade-off between accuracy, complexity and the cost of the control system.

2.1.2 Wind Energy System

Wind energy systems captures the kinetic energy of wind by means of aerodynamically designed blades and convert it into electrical energy or use it to do other work, such as pump water, grind grains, etc.

The generated low-speed, high-torque mechanical power is converted to electrical power using a gear-box and a standard fixed speed generator. Alternatively, the gear-box can be eliminated exploiting multi-pole generator systems. Between the grid and the generator a power converter can be inserted. The generated electrical power can be AC or DC, in the last case an AC/DC power converter is required.

The wind power generation has zero fuel cost and zero emissions. The natural variability of the wind speed and direction during the day and season is considered a major drawback, making difficult the integration of wind powered generators into conventional utility grids, especially in the case of grids that were not designed for fluctuations.

2.1.2.1 Wind turbine types

Two different turbine configurations are available as shown in Figure 2.8. The horizontal-axis turbine which is called Danish wind turbine and the vertical-axis configuration that looks like an egg beater and is called Darrieus rotor after its inventor.

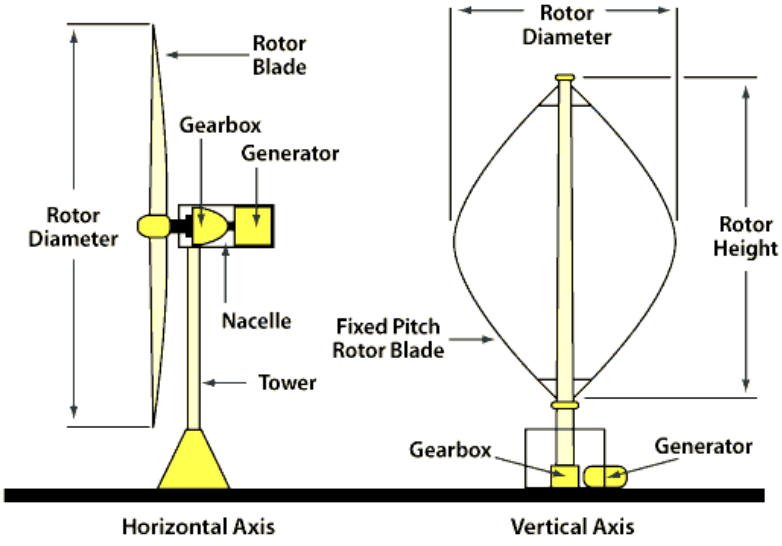

Figure 2.8. Horizontal-axis and vertical-axis wind turbines [16]

In the Danish turbine the axis of blade rotation is horizontal with respect to the ground and parallel to the wind stream. Most wind turbines are built today with the horizontal-axis design, which features cost-effective realization and installation and an easy control through adjustment of the blade pitch [17].

The advantages of vertical-axis Darrieus machine are [17]:

- It is unidirectional and requires no yaw mechanism to continuously orient itself toward the wind direction.
- Its vertical drive shaft simplifies the installation of the gearbox and the electrical generator on the ground, making the structure much simpler.
- Has a balanced structure compared with a horizontal-axis turbine.

The disadvantages of vertical-axis Darrieus machine are [17]:

- It requires guy wires attached to the top for support limiting its applications at offshore sites.
- Not widely used because of output power control problems at high winds.
- It is unable to effectively use higher wind speeds using a higher tower.

The wind turbines can be classified into three main class according to the size. Small turbines rating less than 10kW. They are mainly used to electrify single homes. Intermediate-sized systems, with a capacity between 10 and 250 kW. They can be used to electrify a village or groups of homes and buildings. Utility-scale turbines can generate several megawatts and usually are grouped together into power plants often called "wind farms," and connected to the electrical utility grid; their power is sold to utility customers. The number of blades is normally three.

2.1.2.2 Wind energy model

The mechanical power extracted from the rotor is equal to the difference between the upstream and downstream wind power as given in eq. (2.4) [17-19].

$$P_t = \frac{1}{2}\rho a\, C_p\, A_t\, V^3 \qquad (2.4)$$

A_t is swept area of the turbine, $\boldsymbol{\rho}_a$ is the air density, Cp is the power coefficient, V is the upstream speed of the wind approaching the rotor blades. Eq. (2.4) discloses that the power varies linearly with the density of the air sweeping the blades and with the cube of the wind speed. The blades cannot extract all of the upstream wind power, as some power is left in the downstream air that continues to move with reduced speed.

Cp is defined as shown in eq. (2.5) [17].

$$C_P = \frac{\left(1+\frac{V_0}{V}\right)\left[1-\left(\frac{V_0}{V}\right)^2\right]}{2} \qquad (2.5)$$

Being V_0 the downstream speed of the wind leaving the rotor blades. Cp is defined as a fraction of the upstream wind power which is captured by the rotor blades and has a theoretical maximum value of 0.59. The value of Cp depends on the ratio of the downstream to the upstream wind speeds (Vo/V). Figure 2.9 shown the relation between Cp and (Vo/V), it shows that Cp is a single-maximum-value function [17].

The rotor efficiency is defined as the fraction of available wind power extracted by the rotor and fed to the electrical generator. It has a single maximum point. In practical designs, maximum achievable Cp is between 0.4 and 0.5 for high-speed, two-blade turbines and between 0.2 and 0.4 for low-speed turbines with more blades [17].

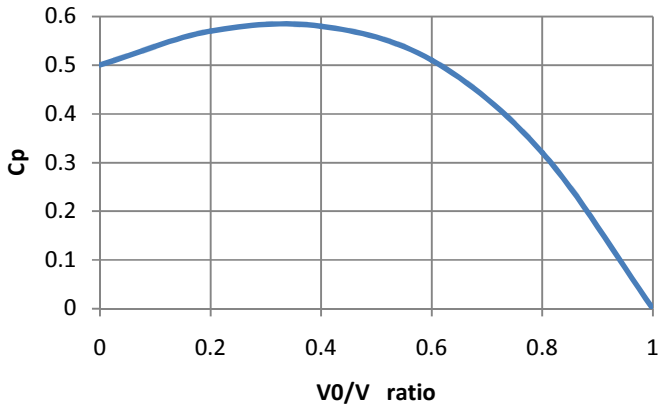

Figure 2.9. Rotor efficiency vs. Vo/V ratio

The maximum rotor efficiency Cp is achieved at a particular tip speed ratio (TSR,) which is defined as the ratio between the peripheral speed of the blades and the wind speed as defined in equation (2.6):

$$TSR = \frac{wR}{V} \qquad (2.6)$$

Where w, R, and V are: the turbine rotor speed in "rad/s", the length of a turbine blade (the radius of the turbine swept area) in "m", and the wind speed in "m/s", respectively. TSR is of vital importance in the design of wind turbine generators to extract as much power out of the wind as possible. Cp is often expressed as a function of the rotor TSR as shown in Figure 2.10 [17]. The optimum TSR depends on the number of the blades.

2.1.2.3 Wind energy control system

The generated power is proportional to the cube of the wind speed, so a small change in wind speed produces a higher power difference. This necessitates a control system to limit the converted mechanical power. The power control may be exerted by one of the three control systems [11, 20]:

- Stall control: The output power is regulated through purposely designed rotor blades. In this case, when the wind speed is too high, the shape of the blades generates some turbulences decreasing the aerodynamic efficiency of the wind turbine.
- Active stall: the blade angle is adjusted in order to create stall along the blades.
- Pitch control: the blades are turned out of the wind at higher wind speed.

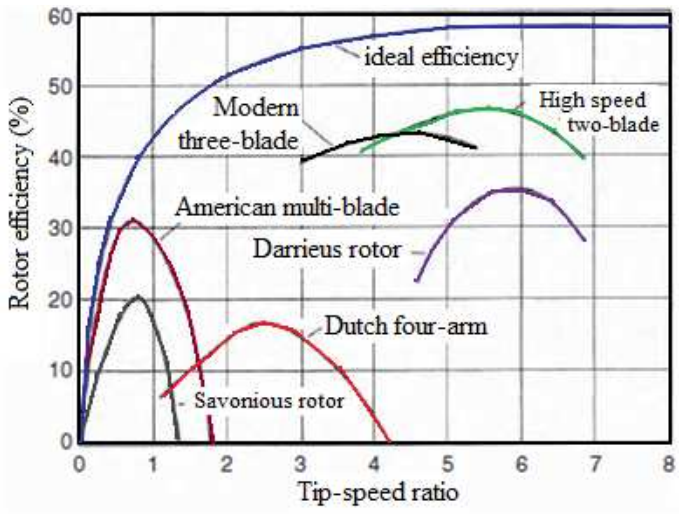

Figure 2.10 Rotor efficiency vs. TSR for rotors with different numbers of blades [17]

It is shown in Figure 2.11 that, according to active and pitch control approaches, when the wind speed exceeds the rated value, the power is held constant.

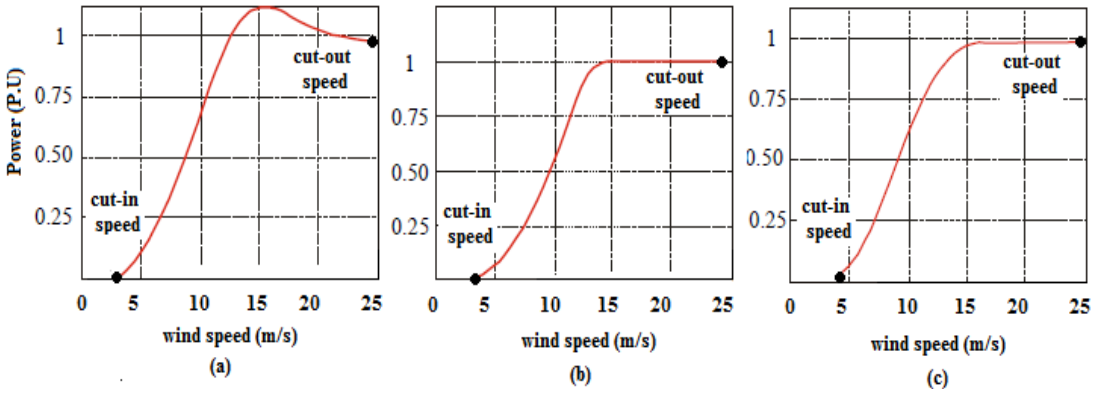

Figure 2.11. Power characteristics of fixed speed wind turbines. a) Stall control b) Active stall control c) Pitch control

For a stall controlled constant speed system, the output power will reach its peak value somewhat higher than its rated value and then decreases as wind speed increases.

2.1.3 Fuel Cells

The worldwide increased interest in FC technology makes relatively huge stationary power plants from 200W to 2 MW commercially available, with efficiencies ranging from 30 to 50%.

Fuel cell is an electrochemical static energy conversion device that produces DC electricity through the reaction of hydrogen and oxygen in the presence of an electrolyte, a positive electrode (cathode) and a negative electrode (anode). The electrolyte carries electrical charges from one electrode to the other. A catalyst is normally exploited to speed up the reaction at the electrodes.

2.1.3.1 Fuel Cell work principle

There are several kinds of fuel cells and each one operates a bit differently. The hydrogen atoms enter a FC at the anode where a chemical reaction strips them of their electrons as shown in eq. (2.7):

$$H_2 \rightarrow 2H^+ + 2e^- \qquad (2.7)$$

The hydrogen atoms are now ionized and carry a positive electrical charge. At cathode, the reaction shown in eq. (2.8) happens:

$$\frac{1}{2}O_2 + 2H^+ + 2e^- \rightarrow H_2O \qquad (2.8)$$

The negatively charged electrons provide the current through the wires; the overall reaction is shown in eq. (2.9).

$$\frac{1}{2}O_2 + H_2 \rightarrow H_2O + \text{Heat} \qquad (2.9)$$

Figure 2.12 shows a schematic diagram of an individual FC with the reactant/product gases and the ion conduction flow directions through the cell [21].

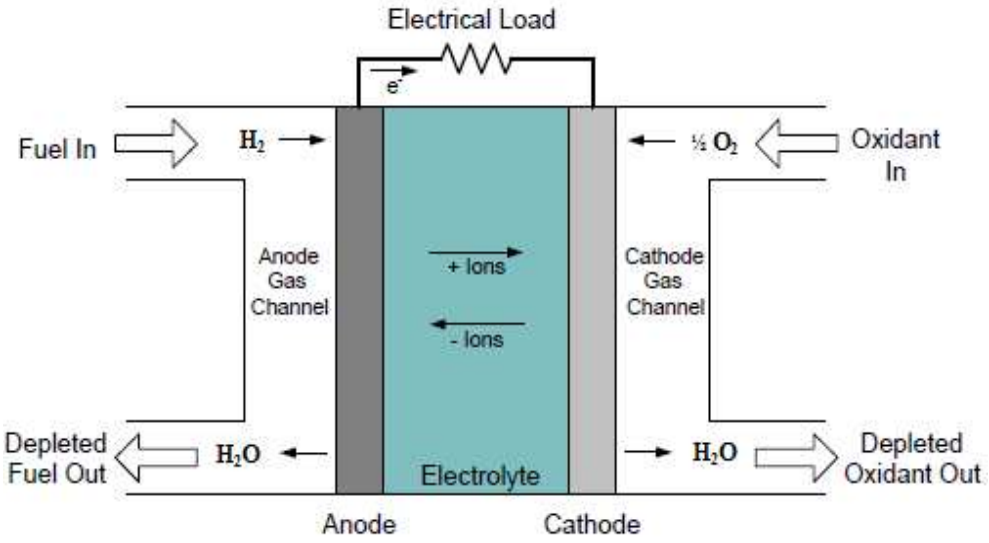

Figure 2.12. Schematic of an Individual FC

2.1.3.2 Fuel Cell types and characteristics

There are several different types of fuel cells, most often categorized by the type of electrolyte present.

- Polymer electrolyte membrane fuel cells (PEMFC),
- Solid oxide fuel cells (SOFC),
- Phosphoric acid fuel cells (PAFC),

- Molten carbonate fuel cells (MCFC).

The characteristics of different types of FC are summarized in Table 2.2 [21-22].

Table 2.2. Characteristics of Types of Fuel Cells

	PEMFC	PAFC	MCFC	SOFC
Electrolyte	Polymer Membrane	Phosphoric Acid	Molten Mixture	Ceramic
Operating Temperature	$\leq 80°C$	205°C	650°C	800-1000°C
Power Density	> 0.6 W/cm^2	0.2-0.3 W/cm^2	0.1- 0.2 W/cm^2	0.25- 0.35 W/cm^2
Charge Carrier	H^+	H^+	CO_3^-	O^-
Catalyst	Platinum	Platinum	Nickel	Perovskites

2.1.3.3 FC Polarization Curve

A single FC generates a small DC current and in order to have a reasonable amount of power, several fuel cells are usually assembled into a stack. Each individual FC produces a very small voltage; the theoretical potential of a cell at 80°C, 1 atm of pressure and under no load is V_0 = 1.16 V [23].

A typical polarization curve consists of three regions as shown in Figure 2.13. The first region represents the activation voltage drop due to the slowness of the chemical reactions taking place at electrode surfaces. The wideness of this region depends on the temperature, operating pressure, type of electrode, and catalyst used [21-23].

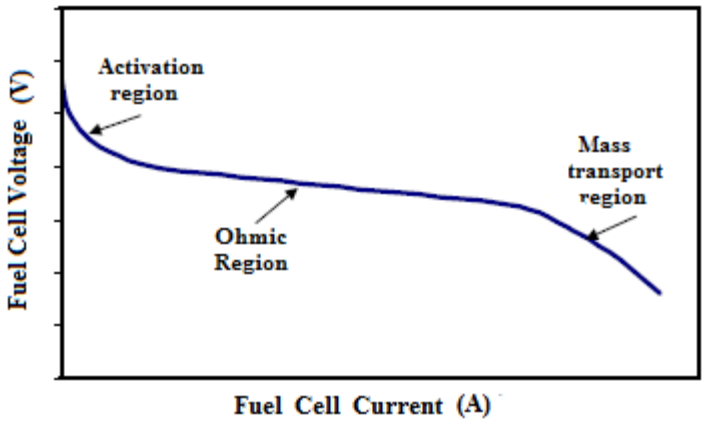

Figure 2.13 Typical fuel Cell Polarization Curve

The second region represents the resistive losses due the internal resistance of the fuel cell stack. Finally, the third region represents the mass transport losses resulting from the change in concentration of reactants as the fuel is used.

Hydrogen has some unique features that make it an ideal energy carrier [21, 22]:

- High conversion efficiency and zero or low emission.
- Water is the raw material for hydrogen production which is available and abundant.
- Hydrogen is considered a renewable fuel and can be stored as liquid, gas and solid.
- Hydrogen can be transported over large distances.
- FC feature a flexible modular structure and can be placed anywhere in the power system.

2.2 Energy Storage System (ESS)

Various types of energy storage system technologies are currently available they can be classified in terms of power capabilities, storage time, transient response time, cost and maturity to be applied in real application.

Energy storage systems enhance the distributed generation (DG) as they stabilize the output power despite of load and primary power fluctuations, especially for DG based on PV and wind systems.

The main performance parameters of ESS for DG are: capacity (Wh), specific energy (Wh/kg), energy density (Wh/m^3), specific power (W/kg), efficiency, recharge rate, self-discharge, lifetime, capital cost, and operating cost [24].

A fully exploitation of all the available energy from renewable energy sources can hardly been accomplished without a suitable energy storage system. Among several possible solutions, three types of energy storage system have been considered throughout this dissertation.

2.2.1 Lead Acid Battery Energy Storage System

The lead–acid battery is an electrochemical device with two electrodes reacting with a sulphuric acid electrolyte. The charge-discharge reaction shows that both electrodes are converted to lead sulphate during discharge [25].

$$\underset{Pb}{cathode} + 2H_2SO_4 + \underset{PbO_2}{anode} \underset{\longleftarrow}{\overset{discharge}{\longrightarrow}} \underset{PbSO_4}{cathode} + 2H_2O + \underset{PbSO_4}{anode} \quad (2.10)$$

During the charge reaction, the anode and cathode are restored to lead dioxide and metallic lead, respectively. The frequent changes in the electrodes limit the number of cycles which normally depends on the battery design and depth of charges.

The lead acid technology have a low-cost (300–600$/kW), high reliability, high efficiency and mature technology. It is suitable for rapid charge/discharge large storage systems, but the low energy density and limited life cycle are major disadvantages [26]. Table 2.2 summarizes the main parameters for lead acid batteries [24].

The voltage of each lead-acid single cell is a 2.12 to 2.15V. In order to produce higher voltage such as 12, 24 and 48V strings, some lead-acid cells are connected in series. These strings may be also connected in parallel to produce the required power.

Table 2.2. Typical lead acid parameters

Specific energy	20–35 Wh/kg
Energy density	50–90 Wh/L
Specific power	About 250 W/kg
Rated cell voltage	2 V
Electrical efficiency	About 80%, depending on recharge rate and temperature
Recharge rate	About 8 hours (possible to quick recharge 90%)
Self-discharge	1–2% per day
Lifetime	About 800 cycles, depending on the depth of cycle

Deep cycle batteries is an important type of lead acid batteries that is mostly used to store electricity in autonomous power systems (e.g. solar, mini- hydro), for emergency back-up and electric vehicles. Deep cycle batteries can be classified as following [24, 27]:

Flooded lead acid battery: These batteries have a conventional liquid electrolyte and have two sets of lead plates that are coated with chemicals. Standard types have removable caps so that the electrolyte can be diluted and the specific gravity measured, such batteries are supplied with distilled water as the battery is used.

Maintenance free lead acid batteries: These batteries evolved in two types of lead acid batteries: Small sealed lead–acid (SLA) battery, also known under the brand name Gel Cell, and the large valve-regulated lead–acid (VRLA) battery. Those types are developed by transforming liquid electrolyte into moistened separators and sealing the enclosure. Special valves are normally equipped to allow gas venting for safety purposes [24].

A VRLA battery requires a low maintenance and is more tightly packaged if compared with a flooded lead-acid battery. However, VRLA batteries are high-priced, less robust and feature a shorter life time than flooded lead-acid batteries [24].

VRLA batteries are normally utilized as standby power supplies in telecommunication applications and uninterruptible power supplies. As SLA and VRLA batteries are sealed, they are designed to work at low overvoltage potential and avoiding any excess charging which would cause gassing and water depletion. This limitation is not included to flooded lead–acid batteries, which have wider margin to work at over-voltage and excess charging [24].

SLA batteries are favored for mobile application for safety and ease of maintenance while VRLA batteries have better cost and performance characteristics for stationary applications.

Different types of rechargeable electrochemical batteries exist which work according to the same principle but with different performances. Table 2.3 shows a comparison between lead-acid batteries and Nickel–cadmium, Nickel–metal hydride, Zebra, Lithium ion and Zinc–air technologies.

Table 2.3. Lead acid batteries compared with other technologies

	Specific Energy Wh/kg	Energy Density Wh/L	Specific Power W/kg	Rated Cell Voltage(V)
Lead–acid	30	75	250	2.0
Nickel–cadmium	50	80	150	1.2
Nickel–metal hydride	65	150	200	1.2
Zebra	100	150	150	High voltage integrated stack
Lithium ion	90	150	300	3.6
Zinc–air	230	270	105	1.65

2.2.2 Fuel cell - Electrolyser (FC/E-ESS)

The combination of a FC energy source and an electrolyser (E) can form another type of energy storage system. The surplus electrical energy can be stored in the form of hydrogen through the electrolysis process which is considered clean and efficient, while the FC transform the stored hydrogen into electric power when a deficit of available power is detected. As the conversion efficiency is less than one (>70%), the amount of energy required to produce hydrogen is always greater than the energy that can be released by hydrogen utilization.

Water-electrolysis is an expensive process as it needs electrical energy, however it is particularly suitable to be used in conjunction with PV and wind energy. Operations of PV/electrolyser pilot plants led to a 93% coupling efficiency, without power tracking electronics [28].

The basic methods for water electrolysis can be classified as following [29].

- Alkaline electrolysis,
- Acidic electrolysis: it is commercially available.
- High temperature electrolysis: (700 – 1000°C) steam electrolysis, far from maturity.
- Thermochemical electrolysis,
- Photochemical electrolysis,
- Photoelectrochemical electrolysis.

The Alkaline electrolysis is the most common and established technology and it will be discussed in this chapter.

The electrolyte used in conventional alkaline water electrolysers is aqueous potassium hydroxide (KOH) and the typical operating temperatures and pressures are 70–100°C and 1–30 bars, respectively [29].

The electrolyser consists of several electrolytic cells connected in parallel. Two different cell designs exist: monopolar and bipolar as shown in Figure 2.14 part (a). In monopolar cells the electrodes are either negative or positive, while bipolar cells have electrodes that are negative on one side and positive on the other side normally separated by an electrical insulator [29].

A bipolar electrolyser is more compact than a monopolar system and can operate at higher pressure (up to 30 bars) which greatly reduces the compression work required to store the hydrogen produced by the electrolyser. Monopolar systems operate at atmospheric pressure [29].

Another advantage of the compactness of the bipolar cell design is that it gives shorter current paths in the electrical wires and electrodes compared to the monopolar cell design which reduces the internal ohmic losses of the electrolyte, and therefore increases the electrolyser efficiency [29].

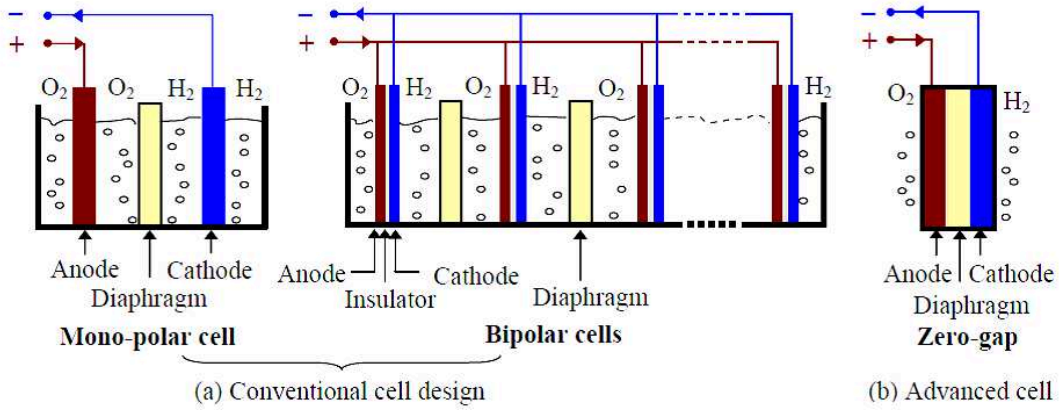

Figure 2.14. Principle of alkaline water electrolyser cell designs [29]

The compactness and high pressures of the bipolar electrolyzes require relatively sophisticated and complex system designs, and consequently higher manufacturing costs than monopolar electrolysers. Most alkaline electrolysers manufactured today are bipolar [29].

Advanced alkaline electrolysers are currently being developed. The overall aim of this advanced technology is to reduce the practical cell voltage to reduce the unit cost as well as increase the current density and thereby reduce the investment cost [30].

In zero-gap cell design shown in Figure 2.14 part b, the electrode materials are pressed on either side of the diaphragm so that the hydrogen and oxygen gases are forced to leave the electrodes at the rear. Most manufacturers are already adopting this design. The investment cost of this type is approximately 500$/kW [12, 31].

The decomposition of water into hydrogen and oxygen occurs when a DC electric current flows between two electrodes separated by a KOH electrolyte. The bad ionic conductivity of the water is the reason behind using a conductive electrolyte. The electrochemical half cell reactions and the overall reaction of water electrolysis is given by following equations.

Anodic half reaction: $2OH^- \Rightarrow ½\ O + H_2O + 2e^-$ (2.11a)

Cathodic half reaction: $2H_2O + 2e^- \Rightarrow H_2 + 2OH^-$ (2.11b)

The overall reaction: $H_2O_{(L)}$ + electrical energy $\Rightarrow H_{2(gas)} + ½\ O_{2(gas)}$ (2.11c)

Figure 2.15 shows a plot of the voltage V for an alkaline water electrolyser cell versus the current density *I*/*A* (current per electrode area) at a high and low operation temperature is shown in Figure 2.15 [32].

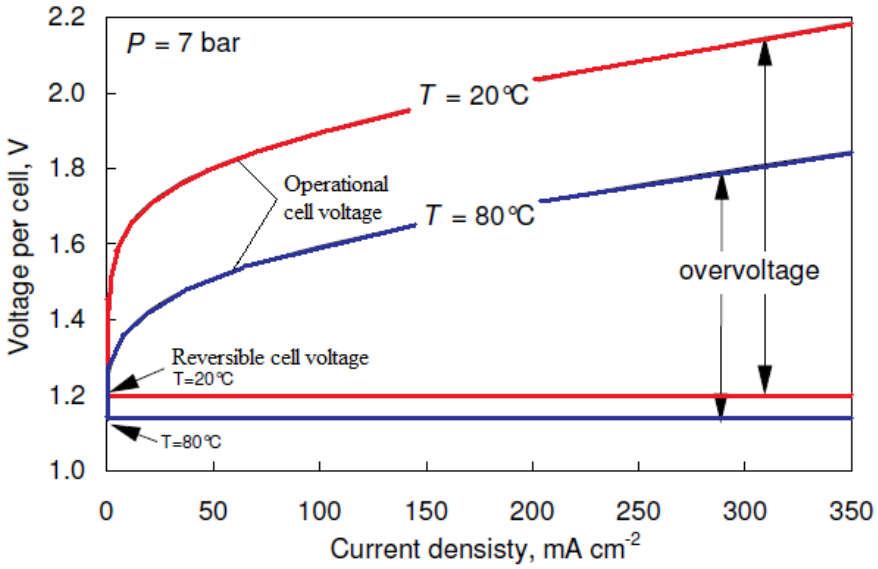

Figure 2.15. I-V curves for an electrolyser cell at high and low temperatures

Hydrogen can be stored as gas or liquid, or under the form of hydrides. Main hydrogen storing technologies include:

- Large underground hydrogen storage systems in caverns, aquifers, depleted petroleum, and natural gas fields. They are likely to be technologically and economically feasible [33]. The Hydrogen in these cases has a gaseous form at a pressure ranging from 80 to 160 bars.
- Above ground pressurized gas storage systems. Hydrogen is stored in standard pressure cylinders of 50L and 200 bars, high-pressure containers at higher pressure over 200bars and low pressure spherical containers more than 30,000m^3 at pressure ranging from 12 to16 bars [34].
- Vehicular pressurized hydrogen tanks. Composite material has been developed that allow higher pressure more than 200 bars and used in prototype automobiles and buses [35].
- Liquid hydrogen storage. This process is costly and seems not to be feasible in ordinary application; it is usually used in application where high storage density is absolutely essential

as aerospace applications. Hydrogen liquefaction is an energy consuming process as it consumes about one third of the energy in liquefied hydrogen [34].

- Metal hydride storage: Hydrogen can form metal hydrides with some metals and alloys.

2.2.3 Vanadium Redox Flow Battery (VRB- ESS)

Flow batteries are a special class of batteries where a large amount of electrolyte is stored in external tanks and driven through a galvanic cell by pump. It stores and generates electricity through oxidation and reduction of a Vanadium electrolyte that's why it is often called Redox flow batteries.

The two electrolytes are separated by a semi-permeable membrane (PEM) and stored in tanks from which they are pumped through PVC pumps to a cell stack. Each electrolyte contains a redox-pair based on vanadium dissolved in sulphuric acid [36].

The PEM permits ion flow, but prevents mixing of the liquids. Electrical contact is made through inert conductors in the liquids. As the ions flow across the membrane, an electrical current is induced in the conductors. Figure 2.16 shows a schematic of the VRB working principle.

Each cell provides 1.26 V at 25 °C, in real systems there are cell stacks, consisting of many cells, each containing two half-cells separated by PEM, The electrolyte is usually pumped through these cells in parallel [36].

The chemical reaction determines the cell potential of the total flow battery, when the battery is being discharged; the following half-reactions take place [36]:

The negative cell reaction:	$V^{2+} \rightarrow V^{3+} + 1e^-$	(2.12a)
The positive cell reaction:	$VO_2^+ + 2H^+ + 1e^- \rightarrow VO^{2+} + H_2O$	(2.12b)
The global reaction:	$V^{2+} + VO_2^+ + 2H^+ \rightarrow V^{3+} + VO^{2+} + H_2O$	(2.12c)

When the vanadium redox flow battery is being charged, the electrochemical processes take place the other way round as shown in the following equations:

Negative cell reaction:	$V^{3+} + 1e^- \rightarrow V^{2+}$	(2.13a)
Positive cell reaction:	$VO^{2+} + H_2O \rightarrow VO_2^+ + 2H^+ + 1e^-$	(2.13b)
Global reaction:	$V^{3+} + VO^{2+} + H_2O \rightarrow V^{2+} + VO_2^+ + 2H^+$	(2.13c)

Advantages of the vanadium redox flow battery include [36, 38, 39]:

- A virtually unlimited capacity. The capacity can be increased simply by using larger storage tanks, as the amount of stored energy depends only on the tank size (the capacity can also be increased by using electrolytes with higher concentration of the electroactive vanadium species).
- Can be left completely discharged for a long time and can be quickly recharged by replacing the electrolyte if no power is available to charge it.

- Very little environmental impact and no health risks.
- Long lifetime, low materials price, low maintenance requirements, and fast response to rapid changes, and a very flexible design.
- Can be designed for high power applications as well for high-capacity electricity storage, for instance for grid-connected electricity storage at wind farms.

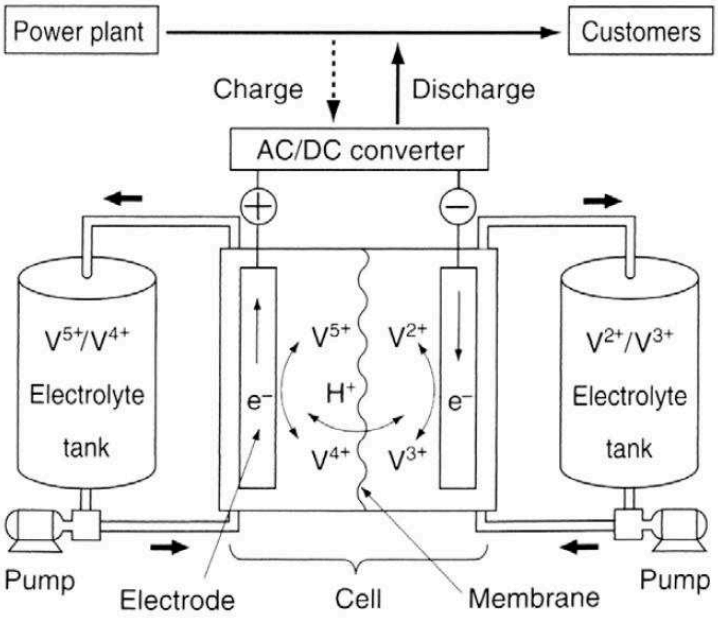

Figure 2.16. Schematic of a VRB system [37]

- Has round-trip efficiencies of 65% - 75%.
- VRB-ESS is very suitable in large scale applications helping to level the production of highly variable generation sources such as wind or solar power, can be used as uninterruptible power supply and to replace lead-acid batteries and even diesel generators.
- The VRB-ESS deals with power fluctuation, support reactive power and effectively improve the power quality and stability of grid connected wind farms.
- The VRB-ESS is a promising renewable energy storage technology that may improve a powerful rise on environmentally friendly energy production like PV and wind energy.
- VRB-ESS has entered the commercialization phase of development and leading manufacturers have demonstrated full-scale grid connected systems in Japan, South Africa, and North America.

Disadvantages of the vanadium redox flow battery [36]:

- Lower energy density (25Wh/kg) if compared with other rechargeable batteries, such as lead-acid (30 - 40 Wh/kg) or lithium-ion battery (80 - 200 Wh/kg).
- The system is complex compared with standard storage batteries
- Higher complexity of the system in comparison, especially the hydraulic system.

Chapter 3

Stand-Alone Hybrid Distributed Generation System

This chapter first defines the concept of distributed generation, then introduces and compares different topologies for hybrid power systems. Stand-alone and grid connected hybrid power systems are defined with the aid of simulations to show the key differences between the two systems.

Some different configurations for stand-alone hybrid power systems are presented and their components examined in detail.

3.1 Distributed Generation System

According to the Distributed Generation (DG) concept the electric power generation is decentralized through the introduction of several modular electric generators located close to the end users. It differs fundamentally from the traditional model of central generation where large power stations are located far from end-users and connected to load sites through very long transmission lines [40].

DG devices can be strategically placed in power systems for grid reinforcement, reducing power losses and on-peak operating costs, improving voltage profiles and load factors, deferring or eliminating system upgrades, and improving system integrity, reliability, and efficiency [41].

Figure 3.1 illustrates a comparison between the conventional centralized generation concept and the distributed generation one.

Many combinations of clean and renewable DG technologies and storage devices can be assembled to form a standalone or a grid-connected hybrid system. Common combinations are shown in Figure 3.2.

DG based on alternative energy sources has been increased in the last decade and penetrated the energy generation market due to the huge rising up in energy consumption, environmental issues as well as due to the predicted depletion of the conventional energy sources.

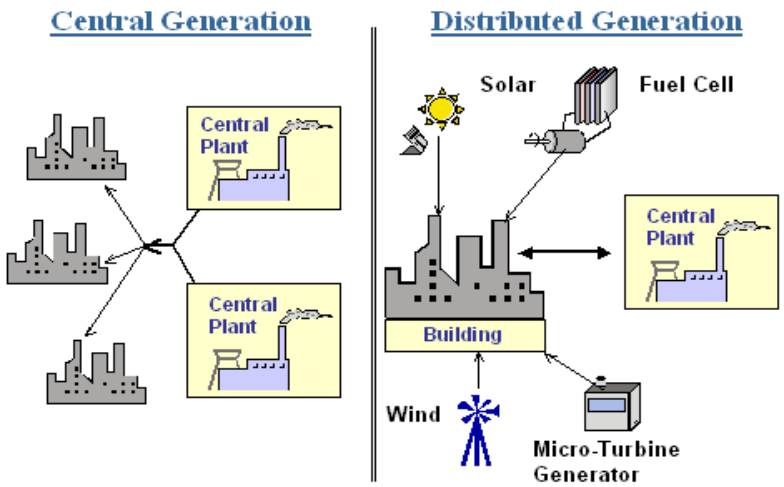

Figure 3.1. Central power generation plant versus the distributed generation plant

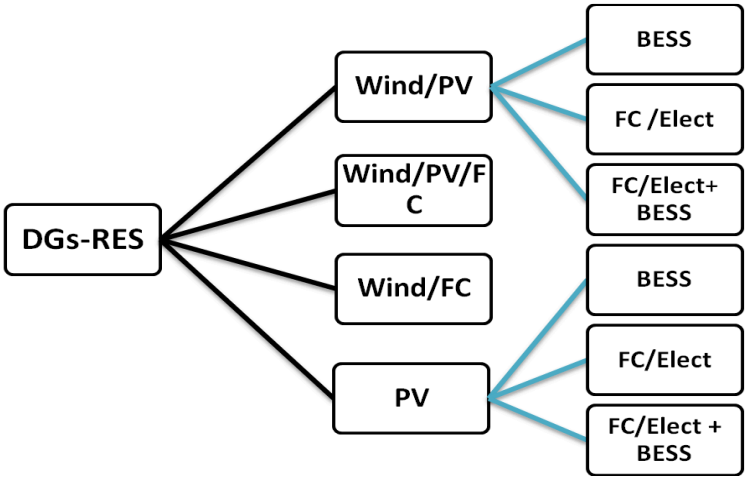

Figure 3.2. Common DGs combinations based on RES

3.2 Hybrid Power Systems

In hybrid power systems, a number of power generators and energy storage systems are combined together to meet a specific energy demand profile. In this research only renewable energy sources are considered as solar irradiation and wind while the FC technology is exploited to compensate the discontinuity of renewable energy sources.

An hybrid generation system composed of a WEG and a PVG, in theory features a load supply continuity higher than simple PV or wind generators, due to the overlap of the availability of the two primary sources. However, a fully exploitation of all the available energy can hardly been accomplished without a suitable energy storage system.

Along this chapter different stand-alone hybrid system plant architectures are presented, analysed and discussed in details. All the considered architectures encompass three basic components,

namely: PVG, a WEG and a battery storage system (BSS). This chapter also includes a general comparison between stand-alone and grid connected systems.

3.3 Topologies of Hybrid Power Systems

Hybrid power systems encompass different types of renewable power generators, which can be DC or AC coupled.

3.3.1 DC Bus Coupled Topology

A DC coupled hybrid power system is a system where different power sources are connected to a main DC bus. If present, AC power sources, are connected to the DC bus through suitable AC/DC power converters. The DC bus is in turn connected to the utility grid trough a DC/AC inverter. The size of this inverter should be accurately selected in order to cover the peak load demand. An insufficient rating of the DC/AC inverter is the main obstacle to expand the system by increasing the size or the number of generators [42].

3.3.2 AC Bus Coupled Topology

An AC coupled hybrid power system is a system where different power sources are directly connected to an AC grid or to the AC user loads. Table 3.1 summaries the advantages and disadvantages of each coupling scheme [41].

Table 3.1. Comparison between DC and AC Bus Coupled Topologies

Coupling Scheme	Advantage	Disadvantage
DC	1. Synchronism is not needed. 2. Less transmission losses. 3. Single-wired connection	1.Voltage compatibility problems 2. Corrosion concerns with the DC electrodes. 3. Non-standard connection requires high costs in installing and maintenance. 4. If the DC/AC inverter is out of service, the whole system fails to supply AC power.
AC	1. Can be isolated from the system easily in case of one of the sources fails. 2. Easy to connect to grid. 3. Standard interfacing and modular structure. 3. Easy multi-voltage and multi-terminal matching. 4. Well established scale economy.	1. Synchronism required. 2. Power factor and harmonic distortion Correction is needed. 3. Higher transmission losses. (specially for long distances)

Each inverter according to the AC coupled scheme can provide power to the grid or the loads separately and concurrently with other inverters, unlike the DC coupled configuration [43]. This feature offers some flexibility to load demand management. In fact, the peak demand can be fulfilled by operating in parallel the generators and storage systems, while in case of low demand some inverters may be set in stand-by.

3.4 Stand-alone Hybrid Systems versus Grid Connected Systems

An hybrid energy system is called a grid-connected system if it is connected to the grid and is called stand-alone if it is not connected to the main utility grid and works independently.

An hybrid system in stand-alone applications requires a suitable energy storage system to handle fluctuations of the input power, especially if the generation is totally based on RES. This system is considered as a micro-grid as it has its own generation sources and loads [44].

The micro-grid can supply an utility grid or local loads. In the first case it is called grid-connected hybrid system. The storage system capacity can be smaller as the grid compensates the deficiency and absorb the surplus power.

Figures 3.3 and 3.4 show some results of a comparative study between stand-alone and grid-connected systems. Simulations are based on dynamic models designed on MatLab/Simulink/SimPowSys^{TM}. Details of models and simulations are introduced in the next chapters.

As shown in Figure 3.3 any power unbalance is compensated from the BSS, while in Figure 3.4 the grid utility behaves like a BSS.

In grid-connected hybrid power systems, some important requirements, such as voltage, frequency and harmonic content, are imposed by regulations [45].

DG systems can also be used as active filters or to generate reactive power in order to control the voltage of the utility grid.

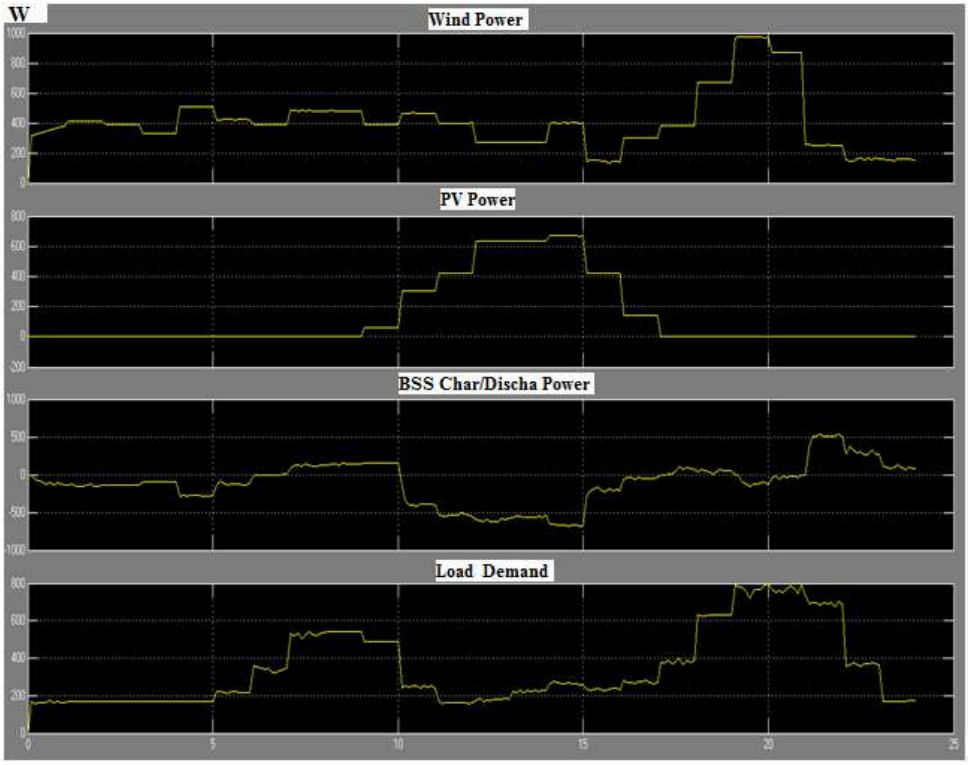

Figure 3.3. Simulation results of PVG/WEG/BSS hybrid generator

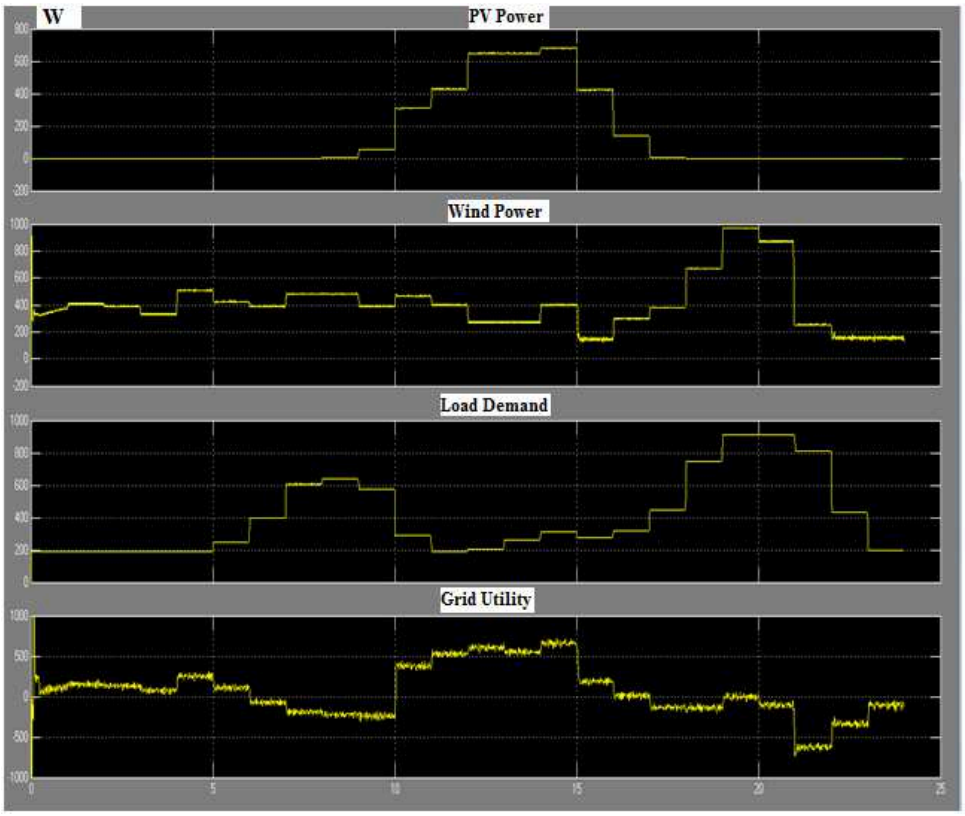

Figure 3.4 Simulation results of PVG/WEG grid connected hybrid generator

3.5 Stand-Alone Hybrid System Plant Architectures

Some different bus voltage configurations can be considered to design a stand-alone power system. Among them the following analysed in this dissertation:

- High voltage DC bus configuration (HVDC),
- Low voltage DC bus configuration (LVDC),
- High voltage AC bus configuration (HVAC),
- High voltage AC rectified bus configuration (HVAC rect.),
- Double buses low and high voltage DC bus configuration (LV/HV-DC).

3.5.1 High Voltage DC Bus Configuration (HVDC)

In this configuration, the power generated from the different sources is delivered to the load through a high voltage DC bus. This configuration requires the installation of an ad hoc network operating in DC.

Figure 3.5 shows a schematic of a stand-alone hybrid system including WEG, PVG and BSS devices. The number of conversion stages is relatively low; this reduces the power conversion losses as well as the cost. All the components shown in Figure 3.5 are studied in chapter 4 and 5.

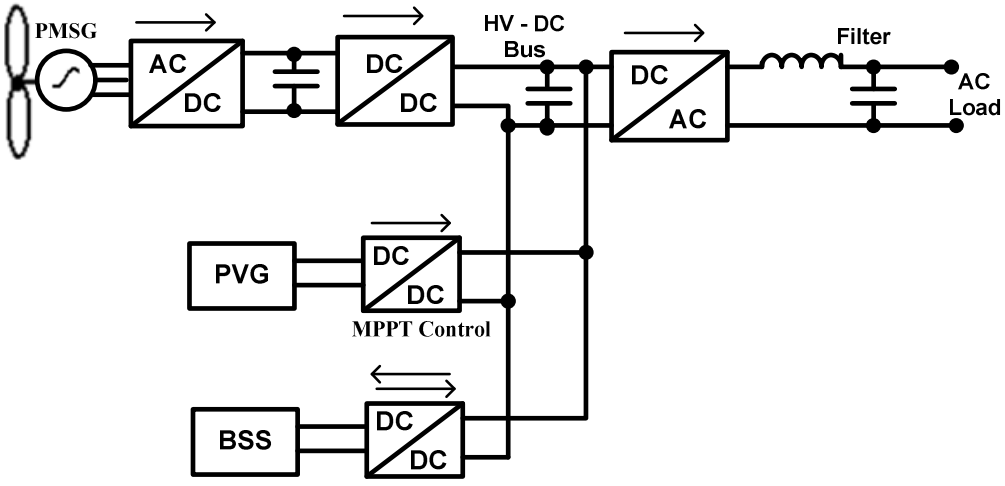

Figure 3.5. Schematic of HVDC bus hybrid system

3.5.2 Low Voltage DC Bus Configuration (LV-DC)

Figure 3.6 shows a schematic diagram of a standalone hybrid system comprising WEG, PVG and BSS systems. The generated power is delivered to the load via a low voltage DC bus (36-100)V. In a preliminary simulation study, the low DC bus voltage is rated at 96V. In this configuration, the BSS is attached directly to the low voltage DC bus; this allows to store energy without conversion losses.

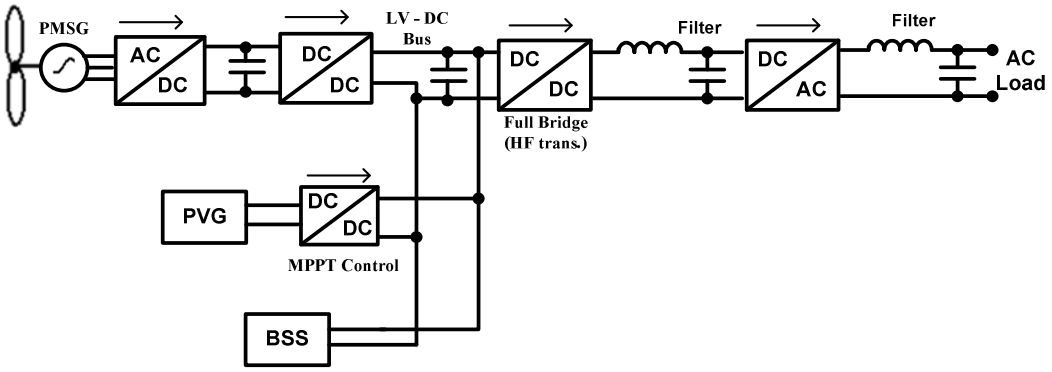

Figure 3.6. Schematic of LVDC bus configuration

3.5.3 High voltage AC Bus configuration (HVAC)

Figure 3.7 shows a schematic diagram of the traditional stand-alone hybrid system including WEG, PVG and BSS systems. The generated power is delivered to the load through an AC bus.

The great advantage of this configuration is that it can likely use existing infrastructures and facilities. This allows an easily allocation of different elements of the system even at considerable distance. In this context, the possibility of achieving 'plug and play' modules designed to be directly connected to the AC single phase domestic network is an interesting perspective.

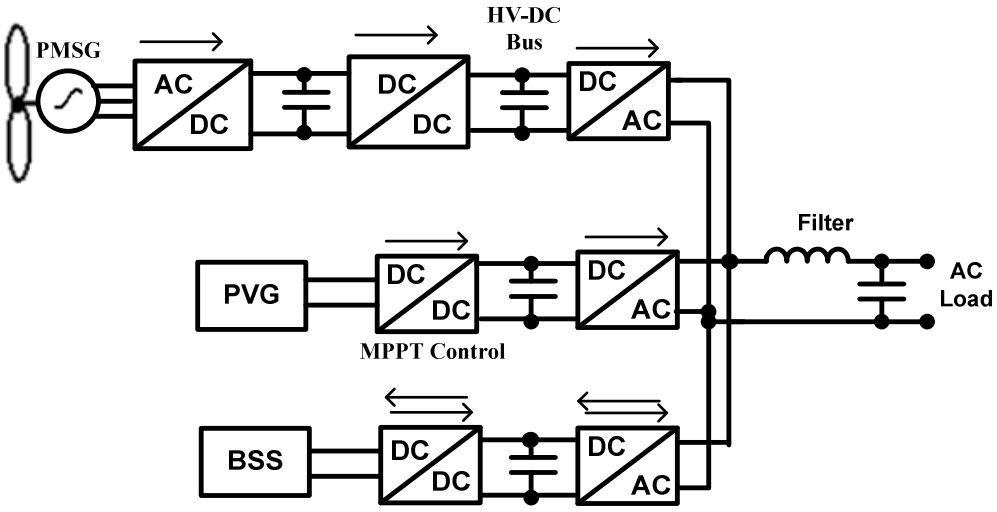

Figure 3.7. Schematic of HVAC bus configuration

3.5.4 High Voltage AC-rectified Bus Configuration (HVAC-Rect.)

Figure 3.8 shows the schematic diagram of a stand-alone hybrid system, where the generated power is delivered to the load via an $AC_{rect.}$/AC converter. Each generator is equipped to directly provide power to the bus featuring an AC rectified voltage. According to such an approach the inverters operate in square wave mode with a high efficiency.

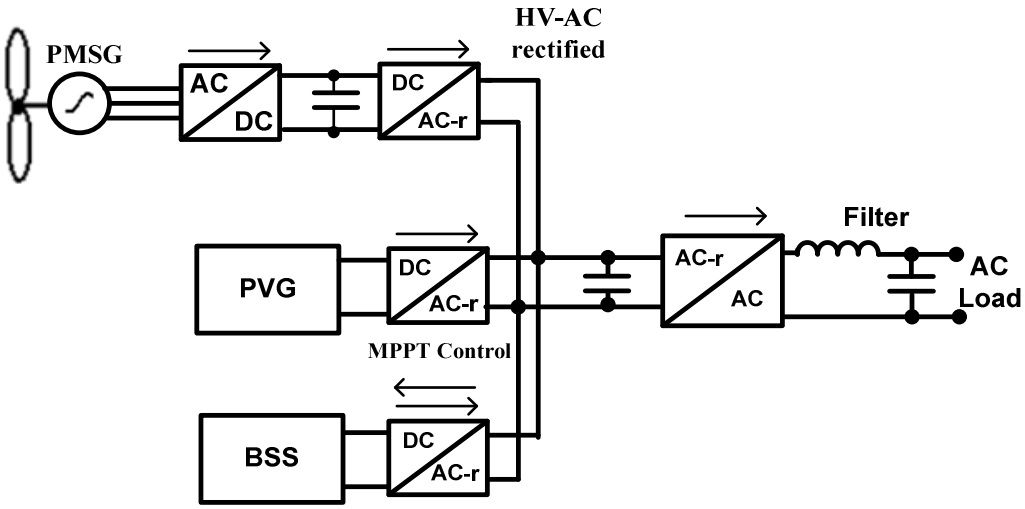

Figure 3.8. Schematic of HVAC-Rect.

3.5.5 Double Bus Low and High DC Voltage (LV/HV-DC)

Figure 3.9 shows the schematic diagram of a stand-alone hybrid system featuring a sophisticated double DC bus configuration. A low voltage DC bus is used to store energy, while a high voltage DC bus is exploited to deliver power to the grid.

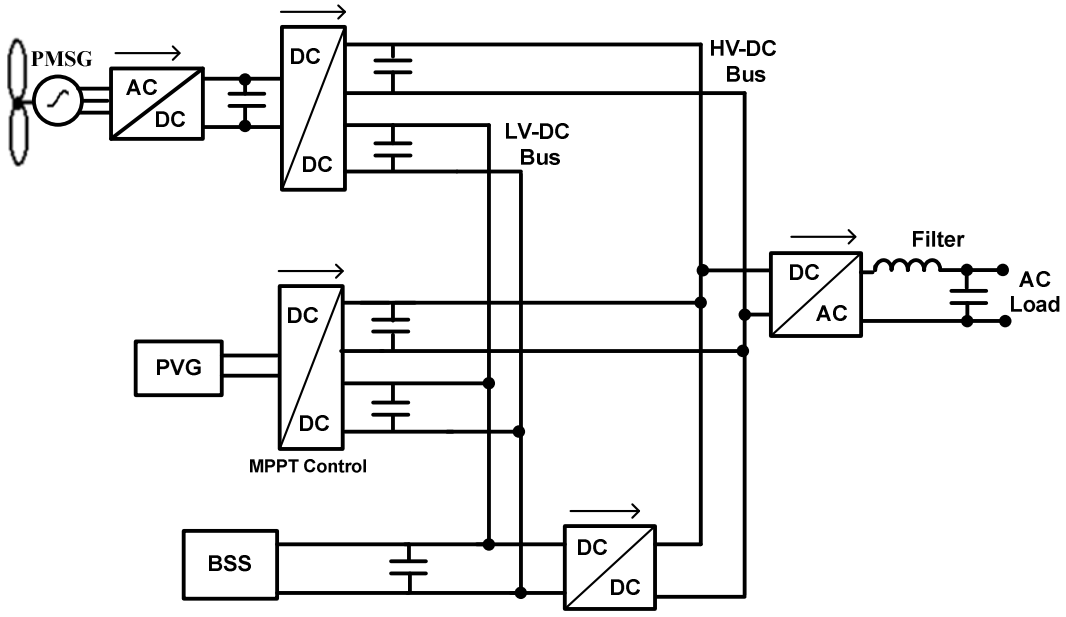

Figure 3.9. Schematic of LV/HV- DC bus

The low DC bus voltage is rated at 96V and the high DC bus voltage at (380-400) V. This configuration requires dedicated power lines.

The BSS is directly connected to the low voltage DC bus which allows to store energy with zero conversion losses.

3.6 Hybrid System Input Data

The average power demand profile for one home in Italy in the cold season is shown in Figure 3.10. This load profile is obtained from European load profiles included in reference [46].

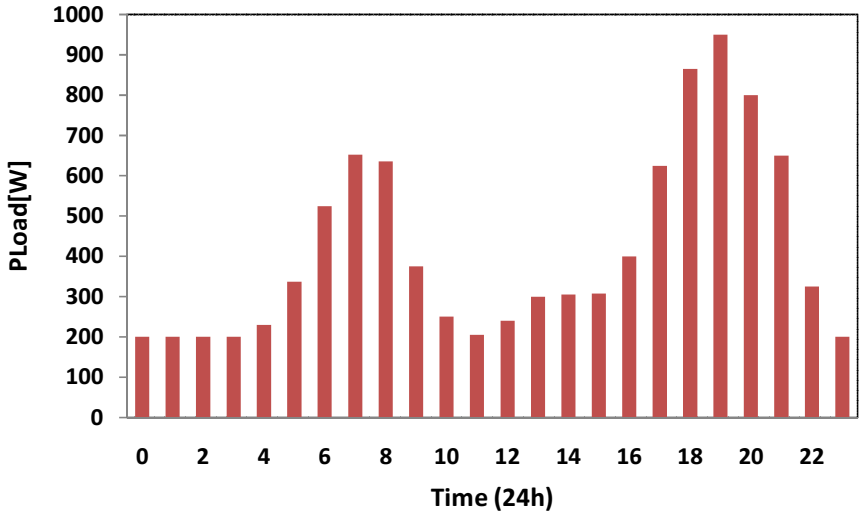

Figure 3.10. A hourly average load demand of a typical home in Italy- cold season.

The weather data represent the typical day profile in December (winter) as recorded at the CNR/ITAE-Italy/Messina. The hourly average wind speed, hourly solar irradiance and hourly air temperature data at the same site on the same day are shown in Figures 3.11, 3.12 and 3.13.

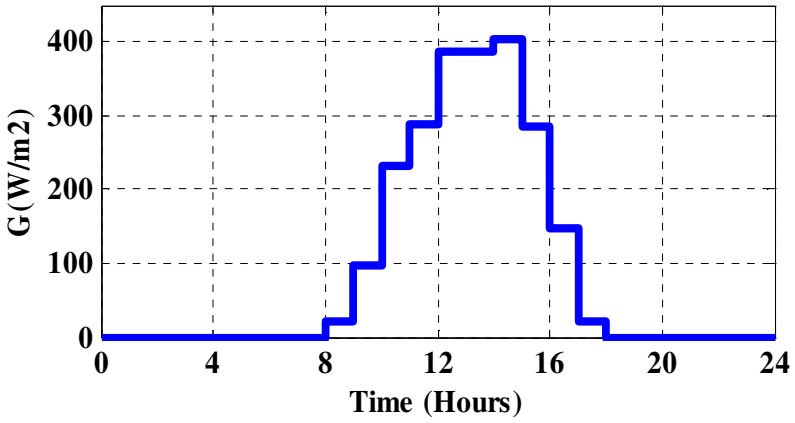

Figure 3.11. Irradiance data in Messina - Sicily for a typical day in December (winter)

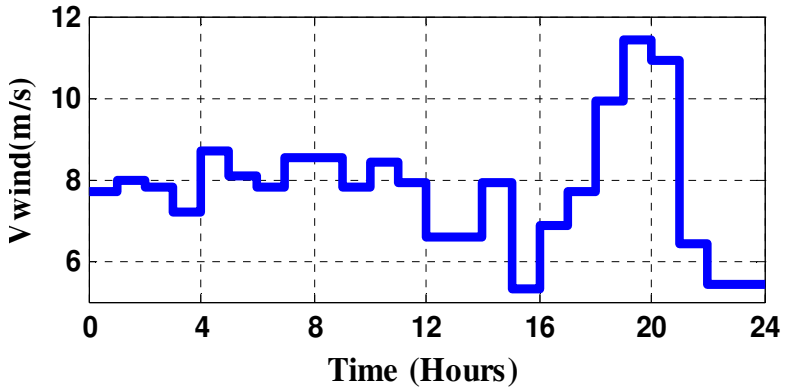

Figure 3.12. Average wind speed in Messina - Sicily for a typical day in December (winter)

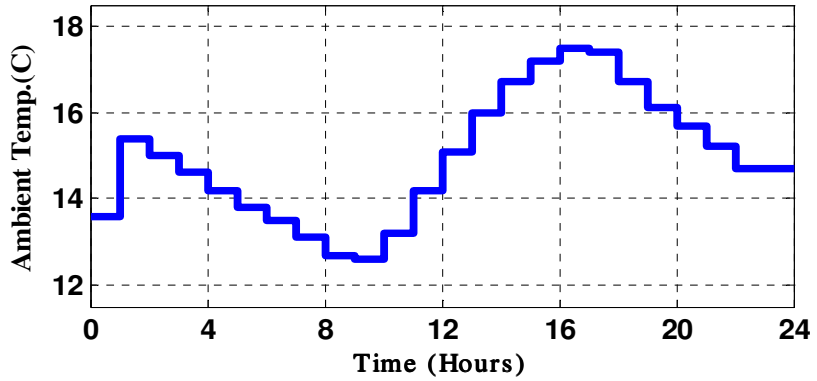

Figure 3.13. Temperature data in Messina - Sicily for a typical day in December (winter)

3.7 Hybrid system components

Throughout this thesis different configurations of stand-alone hybrid system are modelled using MatLab/Simulink/SimPowSys™. The models of the components of the hybrid system are based on real devices installed in the Lab, specifically:

A TN-1.5 Tozzi Nord wind turbine of 1.5kW. Due to its vertical axis assembly, with three helical blades, this micro turbine is able to harness wind power from every direction, achieving more consistent power generation and a low level of acoustic emissions. The wind turbine is fitted with a permanent magnet synchronous generator (PMSG) built especially for this type of application [47]. The system is connected to the utility network through a specific power converter providing a stable 230V 50Hz voltage. In the following it is supposed to consider only the mechanical and electromechanical parts of the system.

A Solyndra® 1.88kWp solar array based on the amorphous silicon (a-Si) technology. The installed system consists of 3 paralleled strings each one encompassing 4 series connected modules. Each module (SL001-157) is rated at 157Wp and 92.5V open circuit voltage [48].

Figure 3.14 shows the Solyndra PV arrays and TN-1.5 Tozzi Nord mini wind turbine installed in the lab.

Figure 3.14 Solyndra PV arrays and TN-1.5 Tozzi Nord mini wind turbine installed in the lab

The BSS rated at 4.6kWh is of the lead acid type, featuring a 96V no load voltage. The commercial name is 'EnerSys -G16EPX (16Ah)'. The BSS consists of 3 strings connected in parallel, each string in turn consisting of 8 batteries connected in series to obtain 96V and 4.6kWh. Main parameters of these components are given in Tables 3.2.

Table 3.2: PVG and WEG main data

PVG	
Module model	Solyndra® - SL001-157
Module unit	157Wp at STC
Module open circuit voltage	92.5 V
Module number	3 × 4 = 12
Power rating	1.88kWp
WEG	
Model	TN-1.5 Tozzi Nord
Rated power	1.5kW
Cut in/Cut out speed	4m/s & 20m/s
Generator type and ratings	1.5kW PMSG @ 50 Hz
BSS	
Battery (lead acid)	4.6kWh at 96 V

In the following, while the size of PVG and WEG are those of the systems installed in the Lab, the size of the lead acid BSS is selected on the basis of weather data and load profiles to ensure specific goals.

The Loss of Power Supply Probability (LPSP) index is used to size the lead acid battery system. MatlabTM software is exploited for this purpose.

The probabilistic index LPSP estimates the probability that the output power is insufficient to supply a given load in a stand-alone configuration. This index is directly assessing the reliability of the system, taking into account the load demand profile, the availability of PV and wind energy, the size of the storage system and its charge and discharge efficiency. It can be used to determine the minimum size of the storage system that ensures an acceptable continuity of load power supply [49]. Typically, values of this index below or equal to 0.0003 are considered sufficient. This corresponds to about one day of lack of load power in ten years [49].

In the following chapters, some simulations are performed based on a system using a fuel cell and electrolyser energy storage system (FC-E-ESS) as a main energy storage system .

The FC system considered is a Nexta™ power module 1.2kW PEM fuel cell stack [50] and a Von Hoerner electrolyser rated at 2.25kW. The rated voltage is in the of 30-100 V range, depending on the generated power [51]. Main parameters of the FC stack and electrolyser are given in Tables 3.3.

Table 3.3. FC stack and electrolyzer main data

FC Stack	
Model	Nexta™ (PEMFC)
Rated power	1.2 kW
Operating voltage	22-50V
Temperature range	3°C - 40°C
Range of inlet supply pressure	70 – 1720 kPa(g)
Electrolyzer	
Model	Von Hoerner
Rated power	2.25kW
Voltage range	30-100V
Battery (lead acid)	1kWh at 96 V

Figure 3.15 shows a picture of the PEM Fuel cell stack Nexta™ unit installed in the lab.

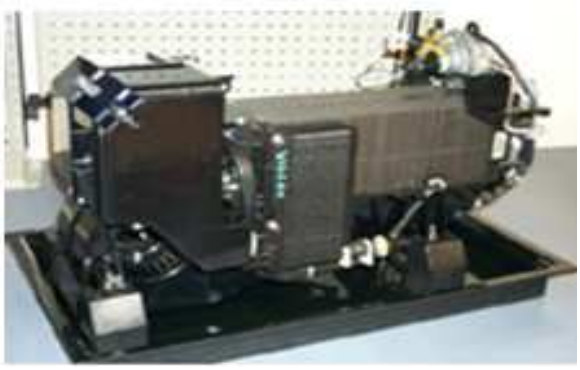

Figure 3.15 Nexta™ PEM Fuel cell stack.

Chapter 4

Modelling and Control of the Stand-Alone Hybrid System components

In this chapter, models and control strategies for: the Photovoltaic energy Generator (PVG), the wind energy generator (WEG), Fuel cells (FC), the Electrolyser (E), the Battery storage system (BSS) and the dump load are developed.

4.1 Modelling and control of PVG

A PV cell converts the energy of photons into electric energy in the form of direct current. An accurate mathematical model of PV cells is a very important tool to study and analyse the dynamic of plants including arrays of PV modules and other systems, such as power electronic converters.

Figure 4.1(a) illustrates a PV cell model using the one-diode equivalent circuit with five parameters [52]. In this work, assuming that the parallel resistance is sufficiently high, a simplified model is used featuring four parameters as shown in Figure 4. 1(b)

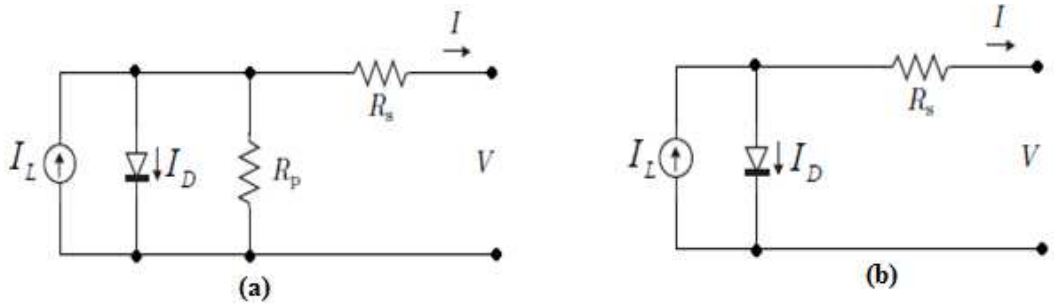

Figure 4. 1 One-diode photovoltaic cell equivalent circuit model. (a) Five parameter model, (b) Simplified four parameter model

The relationship between current and terminal voltage is illustrated in equation (4.1) [53].

$$I = I_L - I_o[exp\ (V + Rs\ I/V_t a) - 1] \quad (4.1)$$

And

$$V_t = N_s \mathrm{k} T/q \quad (4.2)$$

Where:

a: the ideality factor,
I: output current of the array(A),
$I_{L:}$ light current of array (A),
$I_{0:}$ diode reverse saturation current (A),
k: Boltzmann's constant (J/°K),
Ns: number of series connected PV cells,
q: electron's charge,
R_s: equivalent series resistance of the array (Ω),
T: PV cell temperature at STC in Kelvin (°K),
V: output voltage of the array (V),
V_t : thermal voltage of the array (V).

Equations (4.3) and (4.4) are used to calculate the series resistance at reference condition [54]. The reference condition is taken as standard test condition (STD) with a radiant power of 1000 W/m^2, a sunlight spectrum of AM = 1.5 and a cell temperature of 25°C.

$$R_s = [\alpha_{ref} \ln(1 - \frac{I_{mp,ref}}{I_{sc,ref}}) + V_{oc,ref} - V_{mp,ref}]/I_{mp,ref} \quad (4.3)$$

$$\alpha_{ref} = \frac{2V_{mp,ref} - V_{oc,ref}}{\frac{I_{sc,ref}}{I_{sc,ref} - I_{mp,ref}} + \ln\left(1 - \frac{I_{mp,ref}}{I_{sc,ref}}\right)} \quad (4.4)$$

Where:

$V_{mp,ref}$ = maximum power point voltage at the STD, V;
$V_{oc,ref}$ = open circuit voltage at STD, V;
$I_{mp,ref}$ = maximum power point current STD, A;
$I_{sc,ref}$ = short circuit current at STD, A;
α_{ref} = thermal voltage timing completion factor at STD, V.

The open circuit voltage shows a linear dependence with the temperature as shown in equation (4.5).

$$V_{oc}(T) = V_{oc} + k_v\ (T_{cell} - T_{stc}) \quad (4.5)$$

Where K_v is the voltage coefficient temperature, V/ C°.

The cell temperature can be derived using an empirical equation (4.6) which depends on rated operating conditions temperature (NOCT), NOCT is the temperature of the cell at 800 W/m^2 irradiance and 20 C° of ambient temperature [54,55].

$$T_{cell} = T_{ambient} - \frac{NOCT - 20}{0.8} G \quad (4.6)$$

Where G is the current irradiance at ambient temperature. The short circuit current has a linear dependence with the temperature but with less effect than open circuit voltage [55].

$$I_{sc}(T) = I_{sc}\ (1 + \frac{k_i}{100}(T_{cell} - T_{stc})) \quad (4.7)$$

Where k_i is the current coefficient temperature, A/ °C.

Using the above equations, Solyndra® PV modules have been modelled. Figure 4.3 shows the I-V characteristics of the considered Solyndra® PV array at different temperatures.

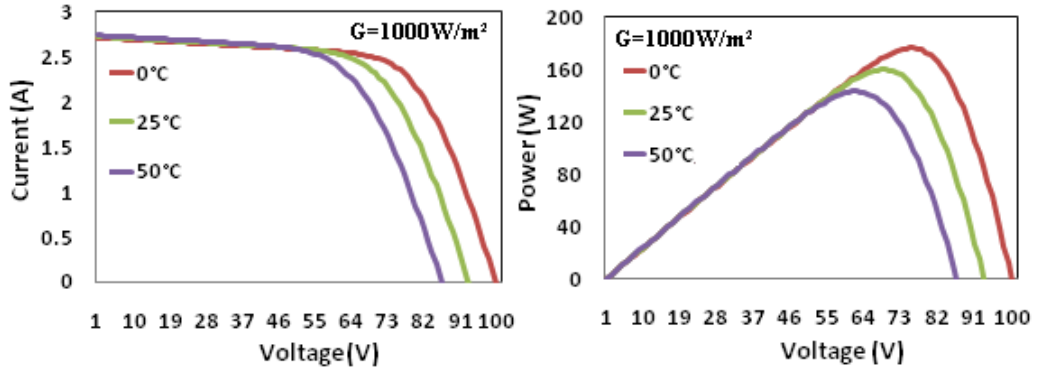

Figure 4.3 I-V characteristics of the Solyndra® solar array model at different temperatures and constant solar radiation

Figure 4.4 show the I-V characteristics of the Solyndra® solar array under different solar radiation values and 25C° cell temperature.

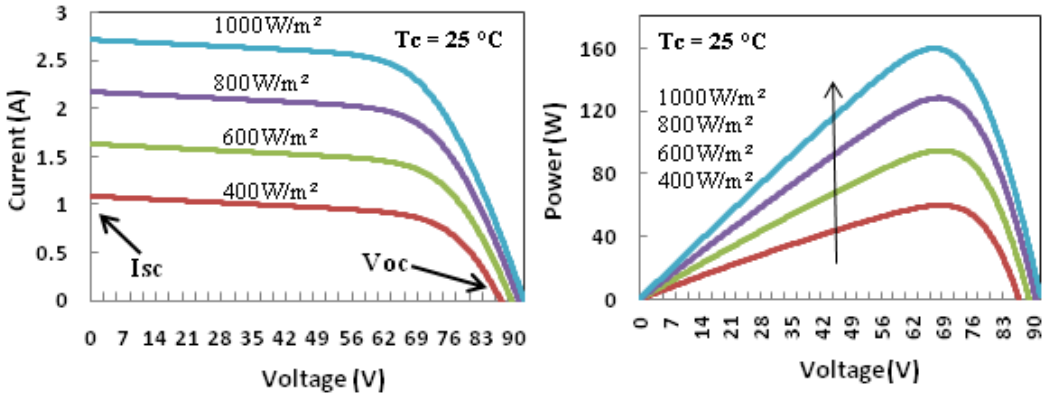

Figure 4.4. I-V characteristics of the Solyndra® solar array at different solar radiation values and constant cell temperature (25C°)

Maximum Power Point Tracking (MPPT) Control

The perturbation and observation (P&O) MPPT algorithm is here used as a trade-off between accuracy, complexity and the cost of the control system.

As shown in Figure 4.5, the duty cycle of the DC/DC converter interfacing the PV array and the DC bus is continuously adjusted in order to track the maximum power point.

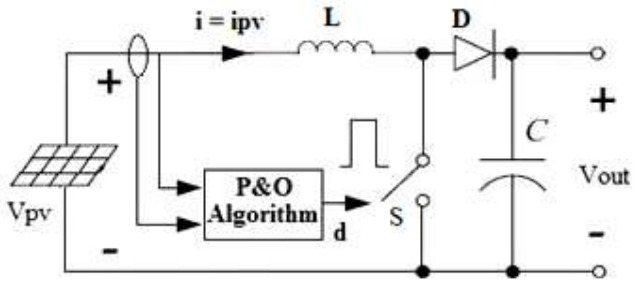

Figure 4.5. DC/DC boost converter topology controlled by MPPT algorithm

Figure 4.6 shows the power improvement deriving from the activation of the P&O MPPT algorithm in a system based on the Solyndra® solar array .

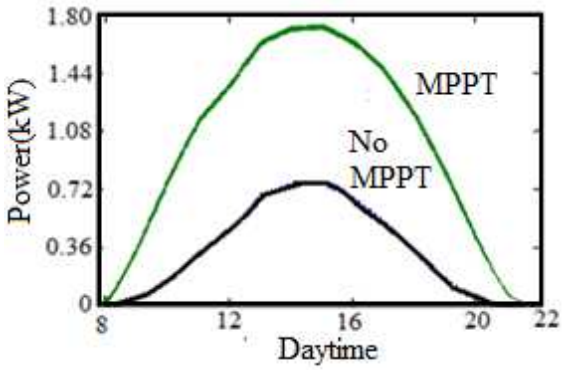

Figure 4. 6 PV generated power with/without MPPT

4.2 Modelling and control of WEG

A TN-1.5 Tozzi Nord 1.5kW wind turbine has been modelled. The output power of a WEG is obtained through equation (4.8) [56].

$$P_t = \frac{1}{2}\rho a\, C_p\, A_t\, V_w{}^3 \qquad (4.8)$$

Where:

P_t: wind turbine power (W),
$\boldsymbol{\rho}_a$: air density (kg/m^3),
C_p: wind power coefficient,
A_t: swept area of the turbine (m^2),
V_w: wind speed (m/s),

Figure 4.7 illustrates the relationship between the power coefficient (Cp) and the wind speed [57]. This coefficient is defined as the aerodynamic efficiency of the wind turbine as a function of tip speed ratio (TSR). This curve makes easier the calculation of the maximum power that can be extracted from wind turbine at various wind speeds.

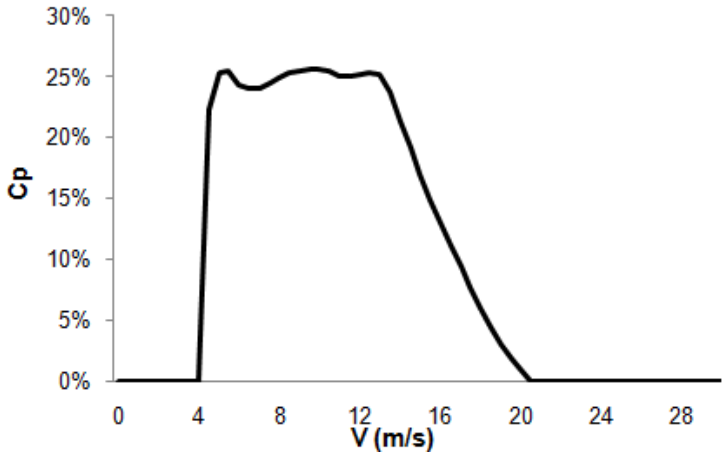

Figure 4.7. Power coefficient versus different wind speeds

Figure 4.8 shows the wind turbine output power at different wind speed levels. Main parameters of the wind turbine, namely: cut-in, cut-off and rated wind speed respectively are: 4m/s, 20m/s and 13m/s.

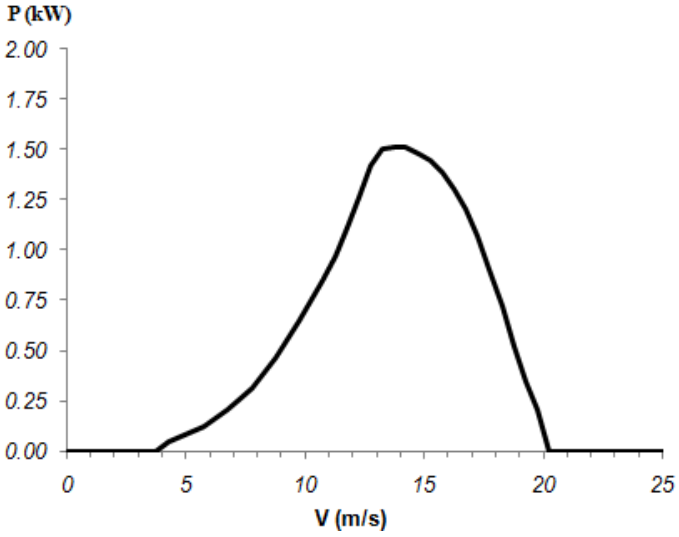

Figure 4.8. Wind turbine output power characteristic

It can be observed that the output power is kept constant at higher wind speed, even though the wind turbine has the potential to produce more power. This is done to protect the electrical system and to prevent the over speeding of the rotor.

The wind turbine shaft torque on the can be computed from the wind power as in equation (4.9), in which the rotational speed of the blades (Ω) is that obtained from the mechanical model of the PMSG. .

$$T_t = P_t/\Omega = \frac{1}{2}\rho a C_p A_t V_w^3/\Omega \qquad (4.9)$$

The generated torque (T_t) is used as an input for the model of the electrical generator. The mechanical section of the electrical generator is described by the following equation (4.10) [58]:

$$\frac{d}{dt}\omega_r = \frac{1}{J}(T_e - F\omega_r - T_t) \quad (4.10)$$

Where:

ω_r : angular speed $d\theta/dt$ (rad.s^{-1}),
θ : Rotor angular position (rad),
J: combined inertia of rotor and load (kg.m^2),
Te: electromagnetic torque (N.m),
F: combined viscous friction of rotor and load (N.m.s.rad^{-1}),
T_t : shaft torque (N.m).

The built in SimPowerSys™ block model of a permanent magnet synchronous machine has been used to carry out the model of the power generator driven by the wind turbine. The electrical model of the permanent magnet generator in the synchronous reference frame (dq) is given in equations (4.11), (4.12) and (4.13) [59].

$$\frac{d}{dt}i_d = \frac{1}{L_d}v_d - \frac{R}{L_d}i_d + \frac{L_q}{L_d}pw_r i_q \quad (4.11)$$

$$\frac{d}{dt}i_q = \frac{1}{L_q}v_q - \frac{R}{L_q}i_q - \frac{L_d}{L_q}pw_r i_d - \frac{\lambda pw_r}{L_q} \quad (4.12)$$

$$T_e = 1.5\ p\ [\lambda i_q + (L_d - L_q)i_d i_q] \quad (4.13)$$

Where:

iq, id : q and d axis currents (A),
Lq, Ld: q and d axis inductances (H),
p : number of pole pairs,
R: resistance of the stator windings (Ω),
Vq, Vd: q and d axis voltages (V),
λ: the amplitude of the flux induced by the permanent magnets of the rotor (Wb),

Figure 4.9 shows a schematic diagram of the WEG model.

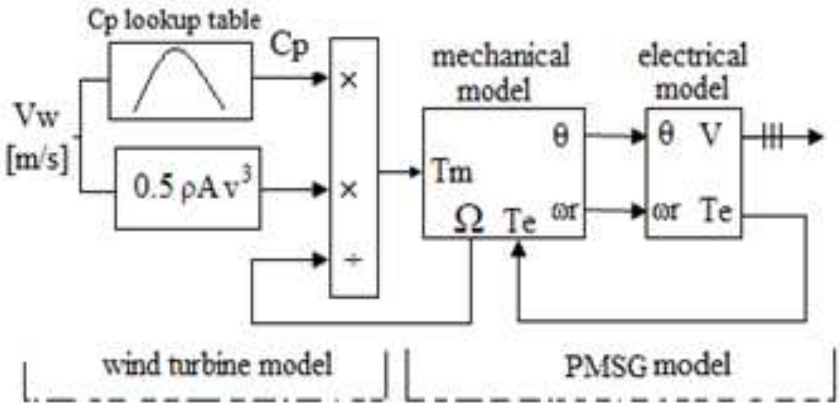

Figure 4.9. Schematic diagram of WEG model

Figure 4.10 deals with a simulation computing the power generated by the WEG at different wind speeds.

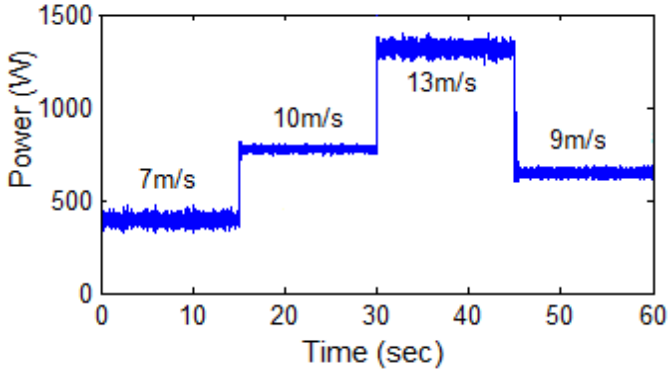

Figure 4. 10. Output power of the WEG model at different wind speeds

4.3 Modelling and control of Fuel cell

A 1.2kW Nexta™ power module PEM fuel cell stack is used. The PEM fuel cell model is based on a SimPowerSys™ block model [60]. This model is built using the relationship between output voltage and partial pressure of hydrogen, oxygen and water. Figure 4.11 shows the equivalent circuit of the fuel cell stack.

The fuel cell parameters used in this model are as follows:

R= Universal gas constant, 8.3145 J/ (mol K)
F = Faradays's constant, 96485 A s/mol,
z = Number of moving electrons,
E_n = Nernst voltage,
i_0 = Exchange current and
α = Charge transfer coefficient.
T = Temperature of operation
P_{Fuel} = Absolute supply pressure of fuel (atm.)

P_{air} = Absolute supply pressure of air (atm.)
$V_{lpm(fuel)}$ = Fuel flow rate (l/min)
$V_{lpm(air)}$ = Air flow rate (l/min)
x = Percentage of hydrogen in the fuel (%)
y = Percentage of oxygen in the oxidant (%)
P_{H2} = Partial pressure of hydrogen inside the stack
P_{O2} = Partial pressure of oxygen inside the stack
P_{H2O} = Partial pressure of water vapour inside the stack
w = Percentage of water vapor in the oxidant (%)
Rin : internal resistance of the fuel cell stack.
k = Boltzmann's constant, J/^{0}K
h = Planck's constant = J s
ΔG = Size of the activation barrier.

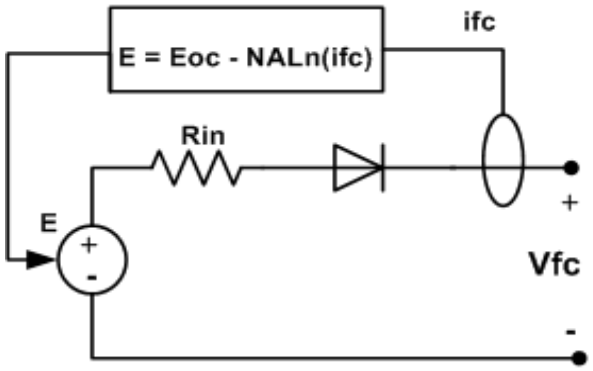

Figure 4.11. Equivalent circuit of the fuel cell stack

The fuel cell stack voltage is given by:

$$V_{fc} = E_{oc} - NA \ln i_{fc} - i_{fc} R_{in} \quad (4.14)$$

Where

$$E_{oc} = N(E_n - A \ln i_0) \quad (4.15)$$

$$A = RT/2\alpha F \quad (4.16)$$

Now the Nernst voltage can be expressed as:

$$E_n = 1.229 + (T - 298)(-44.43/zF) + RT \ln(P_{H2}\sqrt{P_{o2}}/zF) \quad (4.17)$$

$$i_0 = zF(P_{H2} + P_{O2}) e^{\frac{\Delta G}{RT}}/Rh \quad (4.18)$$

Figures 4.12 shows a comparison between the model and experimental V-I and P-I characteristics of the considered FC system.

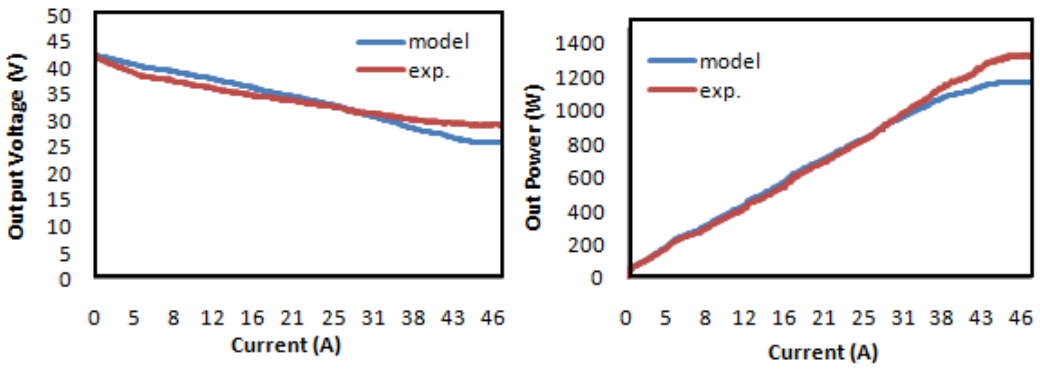

Figure 4. 12. Estimated and experimental I-V and P-I characteristics of the FC system

Figure 4.13 shows a schematic of the FC control system.

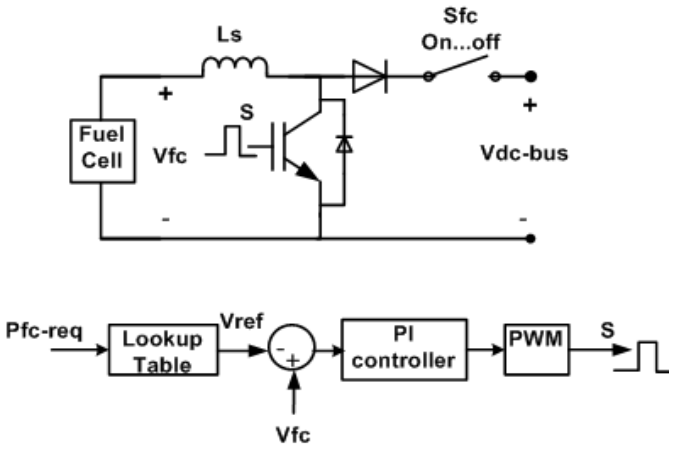

Figure 4.13 Control scheme of connecting FC with the DC bus

The reference voltage (V_{ref}), is determined by a look up table defined on the basis of experimental tests on the FC stack. The required FC power ($P_{fc\text{-}req}$) is determined from the power management controller. The fuel cell voltage is processed by a step up DC/DC converter, that is controlled through a PI controller.

4.4 Modelling and control of the electrolyser, H_2 storage tank, Compressor and Dump load.

Hydrogen and oxygen can be obtained by forcing a direct current to flow between two electrodes separated by an aqueous electrolyte [61]. The total reaction of water decomposition is shown in equation (4.19) provided that a sufficient voltage is applied between the two electrodes [60]:

$$H_2O_{liquid} + \ electrical\ energy \rightarrow H_{2(gas)} + \tfrac{1}{2}O_{2(gas)} \qquad (4.19)$$

Main parameters of the electrolyser model are shown below:

F: Faraday constant (C/kmol),

I: electrolyser current (A),
nc : number of series connected electrolyser cells
η_F: Faraday efficiency
$\dot{n}_{H2}$: produced hydrogen moles per second (mol/s)

According to Faraday's law [62], the ideal hydrogen production rate of an electrolyser stack is given by equation (4.20):

$$\dot{n}_{H2} = n_c I_e / 2F \qquad (4.20)$$

Due to the involved parasitic current losses, the actual production rate becomes as in equation (4.21) [61,62].

$$\dot{n}_{H2} = \eta_F \, n_c I_e / 2F \qquad (4.21)$$

This efficiency is defined as the ratio between the actual amount of hydrogen that can be produced from the electrolyser to the real amount. The current efficiency will increase as the current density grows because the percentage of the parasitic current over the total current decreases. A higher temperature will result in a lower resistance, which leads to a higher parasitic current and a lower current efficiency. Assuming that the working temperature of the electrolyser is 40°C, the Faraday efficiency may be computed as shown in equation (4.22) [61].

$$\eta_F = 96.5 e^{(0.09/Ie - 75.5/I_e^2)} \qquad (4.22)$$

Figure 4.15 shows the electrolyser model designed in Simulink.

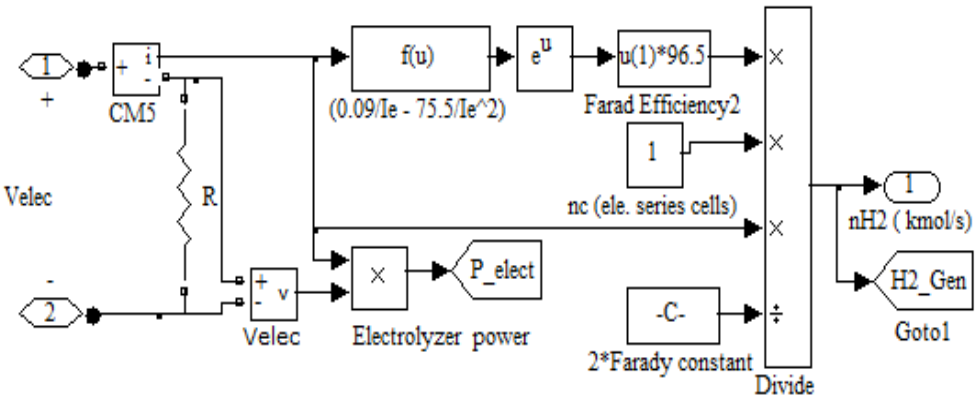

Figure 4. 15. Simulink electrolyser model

A 2.25kW Von Hoerner electrolyser is considered in this study. The rated voltage is in the 30-100 V range, depending on the power.

The electrolyser is connected with the DC bus through a DC buck converter, the electrolyser can be considered as a voltage-sensitive nonlinear DC load [63]. The electrolyser control system acts on the buck converter in order to control the generation of H_2. Figure 4.16 shows the DC/DC buck converter.

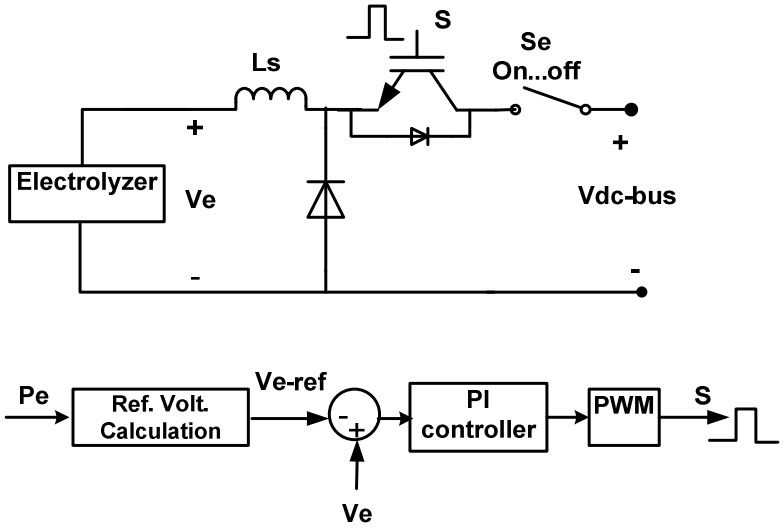

Figure 4.16. Electrolyser control scheme

The produced hydrogen is stored in a suitable tank. Once the maximum allowable pressure is reached, the hydrogen stops flowing into the storage tank. In this model, it is assumed that the storage tank temperature is constant and that all the auxiliary power requirements are ignored. The storage process is modelled according to equation (4.23) [64]:

$$P_t \widehat{=} P_{ti} = z\ N_{H2} R T_t / M_{H2}\ V_t \qquad (4.23)$$

Where:

P_t: Internal pressure of the tank (kPa),
P_{ti} : Initial internal pressure of the tank (kPa),
z: Hydrogen compressibility factor,
M_{H2}: Hydrogen molar mass (kg/ kmol),
N_{H2}: Hydrogen moles delivered per second to the storage tank (kmol/s),
T_t: Temperature of the tank (°K)
V_t: Volume of the tank (m^3).

Figure 4.17 shows the storage tank model designed in Simulink.

The model of the compressor is based on a two stage polytropic compression process with inter-cooling [65]. The polytropic work of stage 1 and stage 2 to compress H_2 gas from P1 to P2 is obtained from the following equation (4.24).

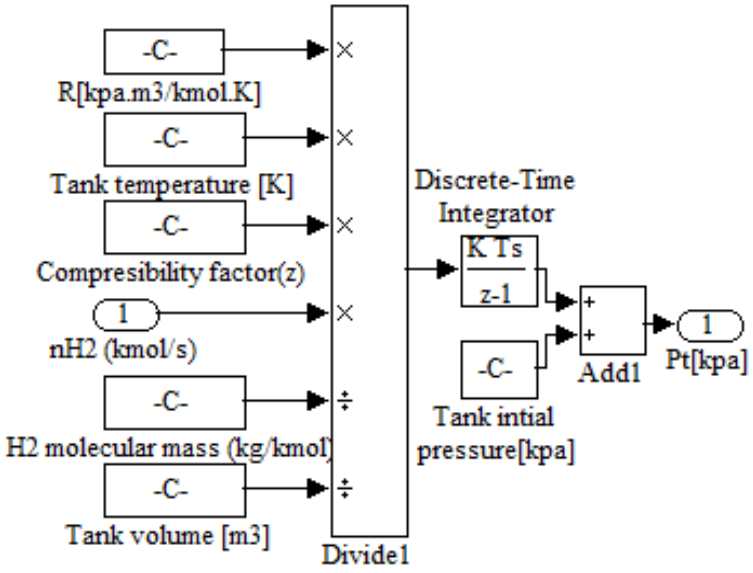

Figure 4. 17. Simulink model of the hydrogen storage system

$$W_{s1} + W_{s2} = \frac{nRT1}{n-1}\left(\left(\frac{P_x}{P_1}\right)^{\frac{n-1}{n}} + \left(\frac{P_2}{P_x}\right)^{\frac{n-1}{n}} - 2\right) \quad (4.24)$$

Then the total work is

$$W_{total} = \dot{n}_{gas}(W_{s1} + W_{s2})/\eta_{comp} \quad (4.25)$$

The dump load consists of a power converter and a bank of resistors [66]. The dump load rated power is chosen to be a 30% greater than PVG and WEG rated output power, so that the stand-alone power system can be controlled even in the case of no load and full storage system [67]. The dump load is connected to the DC bus.

4.5 Modelling and control of BSS and DC bus

The lead acid type EnerSys -G16EPX (16Ah) BSS features 4.6kWh at 96V. Main parameters used in the model are:

A: the exponential zone amplitude (V),
B: the exponential zone time constant inverse (Ah^{-1}),
E_{batt} : no load voltage (V),
E_0 : battery constant voltage (V),
I_{batt} : battery charging and discharging current (A),
K : polarisation voltage (V),
Q: battery capacity (Ah),
R_{in} : internal resistance of the battery (Ω) and
V_{batt} : terminal voltage of the battery (V).

The built-in SimPowerSys™ block model of lead acid battery is used to model the considered BSS [68] It basically consists in a constant resistance connected in series with a controlled voltage source, as shown in Figure 4.18. The controlled voltage source is defined by the following equations [69].

$$E_{batt} = E_0 - K\frac{Q}{Q-it} + Ae^{-B.it} \quad (4.26)$$

$$V_{batt} = E_{batt} - R_{in} . I_{batt} \quad (4.27)$$

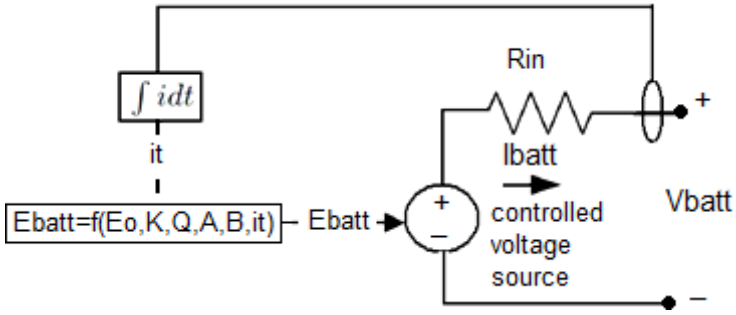

Figure 4.20. Equivalent electrical circuit of the lead battery

Chapter 5

Possible Configurations for a Stand-Alone Hybrid Generator

Stand-alone architectures presented in Chapter 3 are discussed in details in this chapter. An efficiency comparison is accomplished on the basis of suitable performance indexes.

5.1 Introduction

The stand-alone hybrid system plant discussed in this chapter is composed of three main elements, namely: PVG, WEG, and BSS. These elements can be connected together according to different configurations and approaches in order to provide energy to load or storage system, such as: DC-coupling, AC-coupling, or even more sophisticated multiple bus coupling.

In chapter 3 different stand-alone architectures are presented. In each architecture the amount of energy conversion steps that are required to deliver power to storage system and load is different and depends on the internal structure of the plant. Therefore, finding the optimum structure of a plant is significant task that is greatly affecting the efficiency and performance.

There is no general solution to find the optimum structure, neither suitable design tools have been developed to compare different candidate structures which makes the selection procedure of the internal structure of the stand-alone hybrid system plants is left to the skills and specific purpose of the designer.

The optimum configuration is identified among different structures on the basis of environmental conditions and load diagrams through a procedure computing the Loss of Power Supply Probability index (LPSP) [70] for standalone plants, and the Loss of Produced Power Probability index (LPPP) for grid connected plants [71].

In this thesis a more effective comparison approach has been followed based on specific control strategies of each structure, real distribution of solar radiation, wind speed and load as well as taking into account the efficiency of each power converter. To do this dynamic models of each architecture are designed using MatLab/Simulink/SimPowerSys™ as well as different performance indexes are presented.

5.2 Bus Voltage Configurations for a Stand-Alone Hybrid Generator

Five possible bus configurations have been selected to build a stand-alone hybrid generator, namely:

- High voltage DC bus (HV-DC),

- Low voltage DC bus (LV-DC),
- High voltage AC bus (HV-AC),
- High voltage AC rectified bus (HV-AC rect.),
- Double bus (LV/HV-DC).

Schematics of each configuration have been presented in Chapter 3.

5.2.1 HV-DC bus configuration

The main elements of the stand-alone hybrid system can be connected through a high DC bus (380 - 420V) and connected to the AC bus by a centralized inverter. This requires the installation of a dedicated DC power line, but, on the other hand, the number of conversion steps is reduced resulting in lower costs and an increased efficiency. The selected level of the DC bus voltage plays an important role in obtaining the best possible efficiency according to the prevalent power stream inside the plant.

In this approach two conversion steps are needed to convey power by PVG system to the ESS, namely: a first DC/DC conversion is required to conveniently boost the voltage and bidirectional DC/DC converter is needed to store the energy in the ESS. Four conversion steps are required to store energy from PVG and then deliver it to load.

System configuration

Figure 3.5 shows the schematic of a stand-alone hybrid system based on HV-DC bus and Figure 5.1 shows the MatLab/Simulink/SimPowSys™ simulation model.

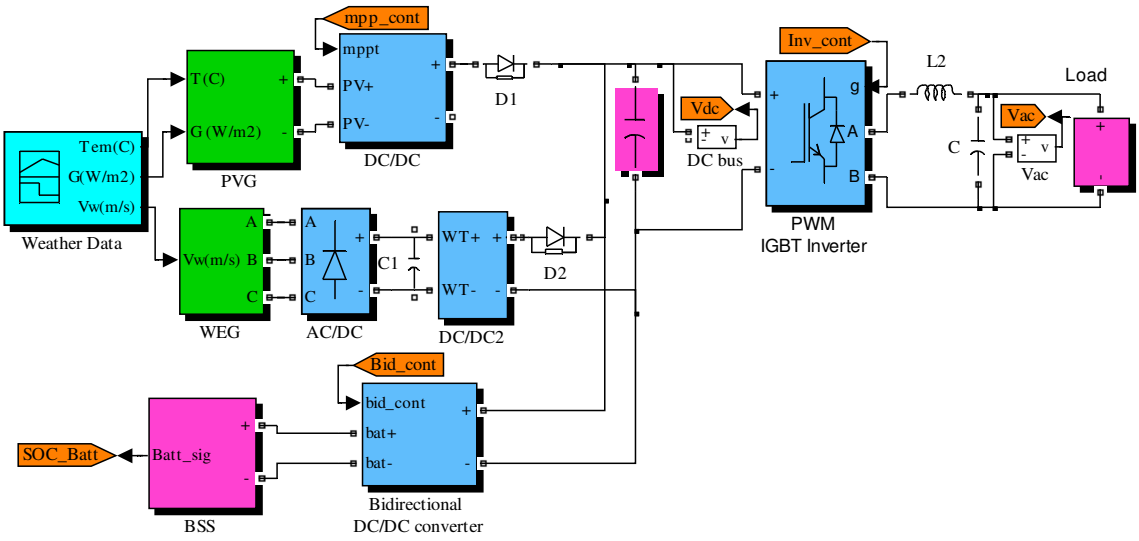

Figure 5.1. Schematic of HV-DC bus configuration

According to this configuration, the generated power is delivered to the load through a high voltage DC bus.

As shown in Figure 5.1, the number of power conversions required to store energy, or to deliver power to the load is quite low; this reduces the power losses as well as the cost.

The DC bus voltage is selected to be in the 380 - 420V range in order to ensure a 230Vrms and 50 Hertz sinusoidal waveform at the load connection point.

The Control Methodology

WEG and PVG are individually controlled to always generate the maximum possible power. A diode is connected at the output of each generator to make the power flow unidirectional [72].

A DC/DC boost converter is connected to the output of the PVG to obtain the DC bus voltage. A boost converter is selected because the rated output voltage of the Solyndra® PV array (370V) is lower than the DC bus voltage. The output of the converter is directly connected to the DC bus, where a bulk capacitor is present.

A schematic of the DC/DC boost converter is shown in Figure 5.2. It is controlled in such a way to obtain the required output voltage, while forcing the PV array to work at the MPP.

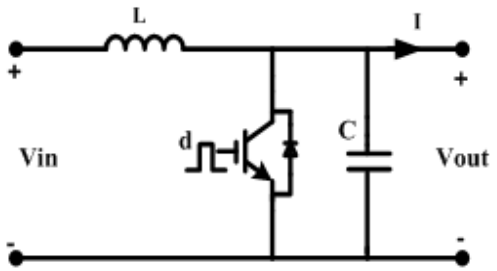

Figure 5.2. DC/DC Boost converter

The WEG is connected to a three phase diodes bridge in order to convert the generated variable amplitude, variable frequency three phase voltage to a DC voltage. A DC/DC boost converter is then tasked to generate the DC bus voltage, while holding the WEG at the MPP as presented in Chapter 4.

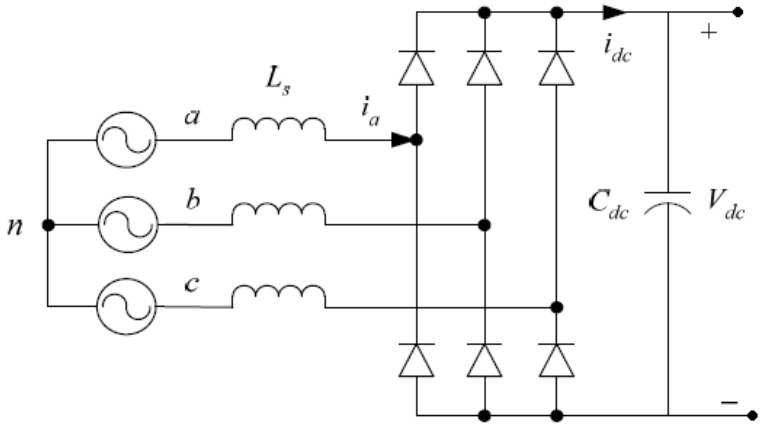

Figure 5.3. Three-phase uncontrolled full diode bridge rectifier

The BSS is connected to the DC bus via a DC/DC bidirectional buck-boost converter, such that shown in Figure 5.4.

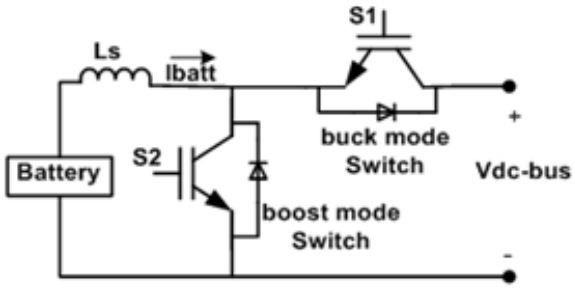

Figure 5.4. Bidirectional DC/DC converter

The inverter output voltage is rated at 230Vrms, 50 Hertz. Therefore, in order to allow a direct inversion, the DC bus voltage (V_{dc}) is set between 380 and 420V, as the peak value of the output AC voltage is 325 V. The high voltage DC bus (HV-DC) includes a large capacitor acting as a decoupling interface between the different components of the hybrid system. The DC bus voltage is controlled acting on the DC bus capacitor current.

The BSS may assume three different states, namely: charge, discharge and idle which play a major role in regulating the HV-DC bus voltage. In fact, the DC bus voltage increases when the BSS is discharging, while decreases, or remains constant, if the BSS assumes the other two states. As shown in Table 5.1, the BSS state is selected by the control algorithm on the basis of the actual DC bus voltage and an estimation of the state of charge (SOC) to not overcharge/over discharge the BSS.

The three BSS states correspond to three different modes of operation of the buck-boost bidirectional converter, that are selected by acting on the duty cycle of the two switches (S1, S2). The DC/DC bidirectional converter works in buck mode to charge the BSS and in boost mode to discharge it. Opening both the two switches the BSS is put in the idle mode, this happens whenever the BSS is overcharged, or has no sufficient charge to deliver power to the DC bus.

Table 5.1 : BSS control strategy

	SOC condition	**V_{bus} condition**
Charging mode (buck mode)	$0.4 \geq SOC < 0.95$	$V_{bus} > V_{max}$
Discharging mode (boost mode)	$0.4 < SOC \leq 0.95$	$V_{bus} < V_{min}$
Idle mode	$SOC < 0.35$	$V_{bus} < V_{min}$
	$SOC > 0.95$	$V_{bus} > V_{max}$

The control scheme of the DC/DC bidirectional converter is depicted in Figure 5.5. The DC bus voltage (Vdc-bus) is sensed and compared to the reference voltage (V_{ref}). The error is processed by the PI voltage controller to generate the BSS reference current (Ibat_ref). The last is then compared with the actual battery current. The current error is finally exploited to determine the duty cycles of the two switches. Parameters of the two PI regulators are shown in Table 5.2.

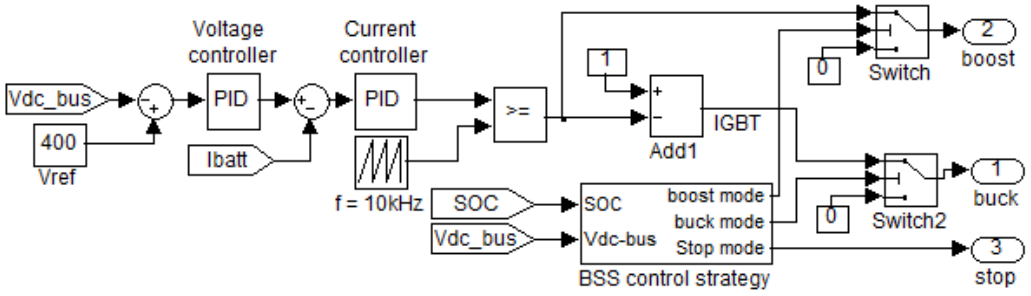

Figure 5.5. Control scheme of the DC/DC bidirectional converter

A single phase full bridge inverter, as that sketched in Figure 5.6 is used to obtain the required AC voltage. The inverter is controlled using the unipolar PWM technique, moreover, a low pass filter (LPF) is connected at the output of the inverter to cancel undesired harmonics. LPF inductance and capacitance are respectively set at 1.5mH and 200µF.

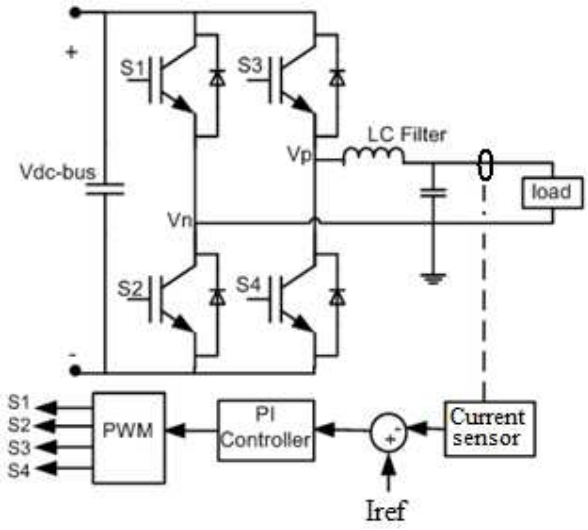

Figure 5.6. Single phase DC/AC full bridge topology with control circuit

Table 5.2: Controllers Parameters

	DC-DC Bidirectional converter	
	Voltage controller	Current controller
Kp	0.5	1
Ki	10	500

5.2.2 LV-DC bus configuration

The main elements of the stand-alone hybrid system can be connected through a low DC bus (24 - 96V) and accomplish a direct power delivery to the ESS. The low voltage DC bus can be boosted to high voltage using different methods in order to be connected to the AC bus by a centralized inverter. The selected level of the DC bus voltage plays an important role in obtaining the best possible efficiency according to the prevalent power stream inside the plant.

In this approach one conversion step is needed to convey power by PVG system to the ESS, namely: a first DC/DC conversion is required to store the energy in the ESS, while two conversion steps are required to transfer power from the WEG to BSS. Three and four conversion steps are necessary to achieve a complete cycle of energy storage and delivery to the load in PVG and WEG, respectively.

The high voltage DC bus (HVDC) is more suitable when a relevant amount of energy needs to be stored, while the low voltage DC bus (LVDC) is more advantageous if the prevalent power stream is that from the generators to the load.

System Configuration

Figure 3.6 shows the schematic of a stand-alone hybrid system based on the LV-DC bus configuration and Figure 5.7 shows the MatLab/Simulink/SimPowSys^{TM} simulation model.

Control methodology

WEG and PVG are controlled using the same methods and strategies used in the HVDC bus configuration.

A buck DC/DC converter is connected to the PVG to control the output voltage, while accomplishing the MPPT. A buck converter is used because the output voltage of the PV array is higher than the DC bus voltage (90 to 100V). The Buck inductance is set at 10mH.

The BSS is connected directly to the low DC bus voltage; this allows to store energy with zero conversion losses.

Different converter topologies were considered [73] to boost the bus voltage up to 380-420V in order to obtain the 230Vrms, 50Hz AC voltage. It has been found that a full-bridge DC/DC converter as shown in Figure 5.8 is more efficient and cost effective than Flyback, Boost, C'uk, Push-Pull and Half-Bridge topologies.

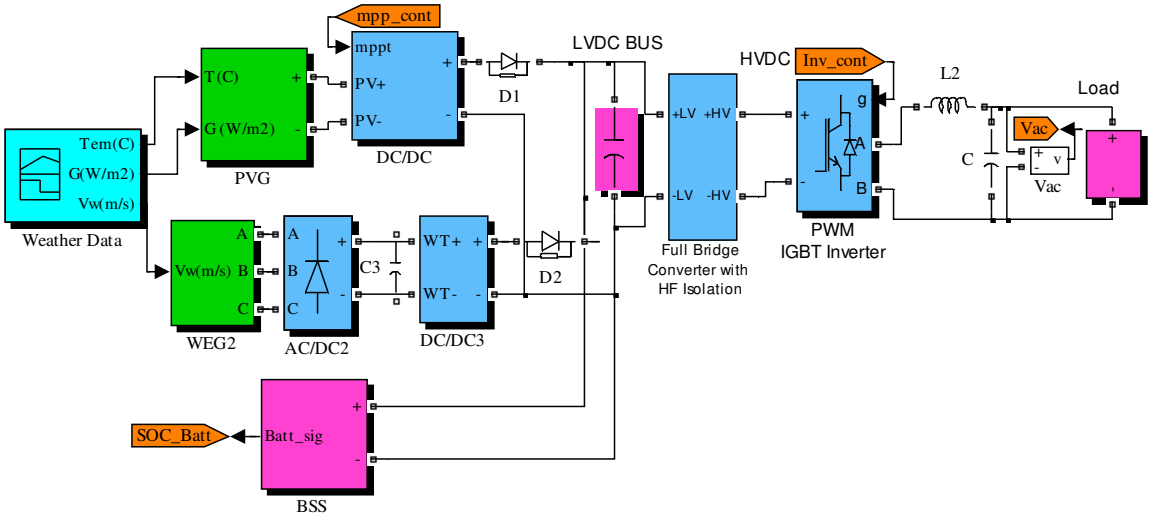

Figure 5.7. Schematic of LV-DC bus configuration

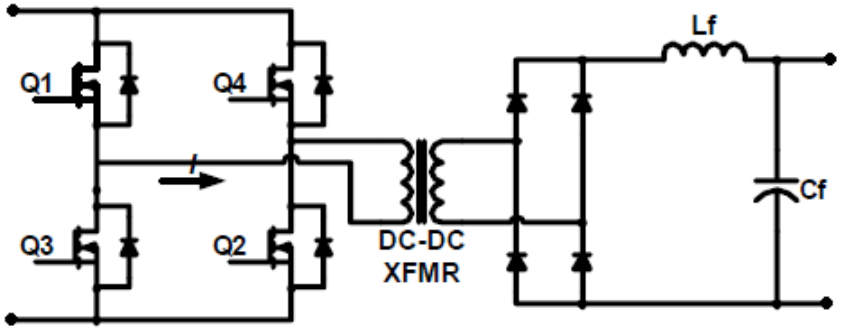

Figure 5.8. Full bridge DC/DC converter with HF isolation

A high frequency transformer is used to step up the voltage after inverting the low DC voltage to AC voltage; it minimizes hysteresis losses which consequently improves the efficiency to approximately 98%. The high frequency transformer is also much smaller and lighter than standard transformers [73].

An inverter is finally exploited to obtain the AC voltage. The topology and control methodology are the same of the HVDC configuration.

5.2.3 HVAC bus configuration

The main advantage of this configuration is that it can use existing infrastructures and power lines [74,75]. This allows an easy allocation of the different elements of the system even at considerable distance. In this context, of particular interest is the possibility of design 'plug and play' modules to be directly connected to the AC single phase domestic network.

The disadvantage of this configuration may come from the fact that each element must be equipped with a dedicated inverter which consequently increases the number of power converters,

the conversion steps and the power losses as well. In case of grid connected applications, each inverter must be qualified to autonomously achieve the synchronization and the anti islanding protection.

In this approach four conversion steps needed to convey power by PVG system to the ESS, that is: a first DC/DC conversion is required to conveniently boost the voltage, a DC/AC conversion is then necessary to deliver the energy to the AC bus, an AC/DC conversion and finally a bidirectional DC/DC conversion is needed to store the energy in the ESS. Alternatively, a direct power delivery to the AC load is accomplished with only two conversion steps.

Other possible option is to eliminate the DC/DC boost converter using PV strings with a suitably high output voltage, accordingly reducing the conversion steps and in theory improving the efficiency. However, such a single stage AC bus configuration is burdened a poor efficiency of the Maximum Power Point Tracking (MPPT) as the working point of PV modules can only be controlled through the inverter, in a less efficient way if compared with the conventional approach where the DC/DC converter accomplishes the MPPT.

System Configuration

Figure 3.7 shows the schematic of a stand-alone hybrid system based on the HV-AC bus configuration and Figure 5.9 shows the MatLab/Simulink/SimPowSys™ simulation model.

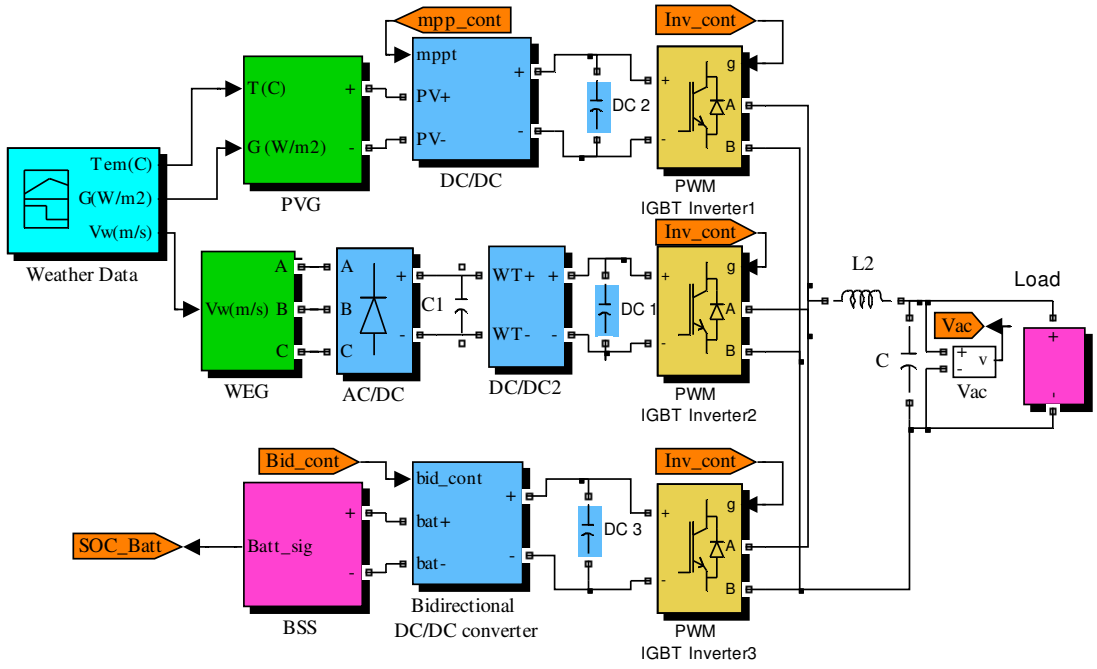

Figure 5.9. Schematic of HVAC bus configuration

Control Methodology

As shown in Figures 3.7 and 5.9 each element is equipped with an inverter, which consequently increases the cost and conversion losses. The DC input voltage of each inverter must be in the 380 to 420V range in order to obtain a $230V_{rms}$ and 50 Hertz output voltage.

A DC/DC boost converter is connected to the PVG to accomplish the MPPT and to increase the voltage up to the level required for the inversion.

A three phase diode bridge and a DC/DC boost converter process the three phase, variable amplitude, variable frequency AC voltage generated by the WEG in order to obtain a stable DC voltage suitable for inversion.

The BSS is connected to the inverter through a DC/DC bidirectional converter as that shown in Figure 5.4.

5.2.4 HVAC rectified bus configuration

System Configuration

The HVDC configuration can be modified in order to operate the inverter in unfolder mode. The generated power is delivered to the load via an AC rectified voltage bus. Each energy source is equipped with a DC/DC converter controlled in such a way to obtain an output voltage featuring an AC rectified voltage waveform. According to such an approach the inverter operates in square wave mode with very low switching losses, while the losses of the other power converters are almost unchanged if compared with a conventional DC/DC conversion. In fact a conversion step is virtually eliminated, as the voltage inversion can be accomplished at efficiency close to 98%, while the efficiency of the other power converters is unchanged.

Figure 3.8 shows the schematic of a stand-alone hybrid system based on HVAC rectified bus and Figure 5.10 shows the MatLab/Simulink/SimPowSys™ simulation model.

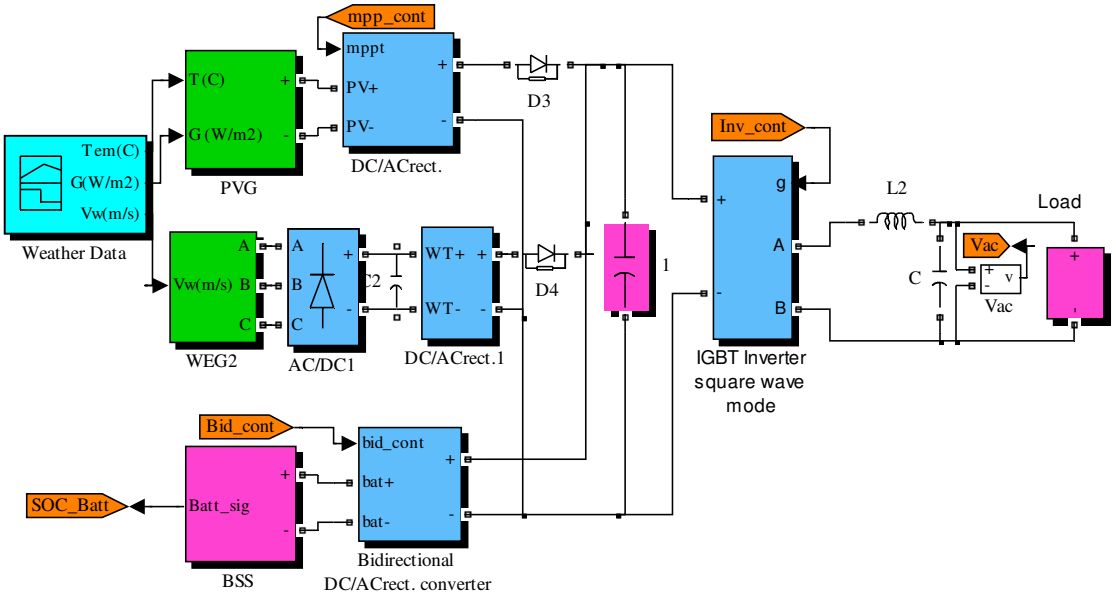

Figure 5.10. Schematic of HVACrect. bus configuration

Control Methodology

The cascade connection of a three phase diode bridge and a DC/DC step up converter is connected to the WEG. The DC/DC reference output voltage features an AC rectified waveform.

The BSS is connected with the DC bus via DC/ACrect. bidirectional converter which is controlled by a specific control strategy to an AC rectified output voltage waveform

A square wave operated inverter is finally used to invert the rectified AC voltage and to obtain the output voltage.

5.2.5 Double Bus configuration

System Configuration

Figure 3.9 shows the schematic of a stand-alone hybrid system based on double buses LV/HV-DC configuration and Figure 5.11 shows the MatLab/Simulink/SimPowSysTM simulation model.

The BSS is directly connected to the low voltage DC bus which allows storing energy with zero conversion losses. This configuration requires dedicated DC power lines.

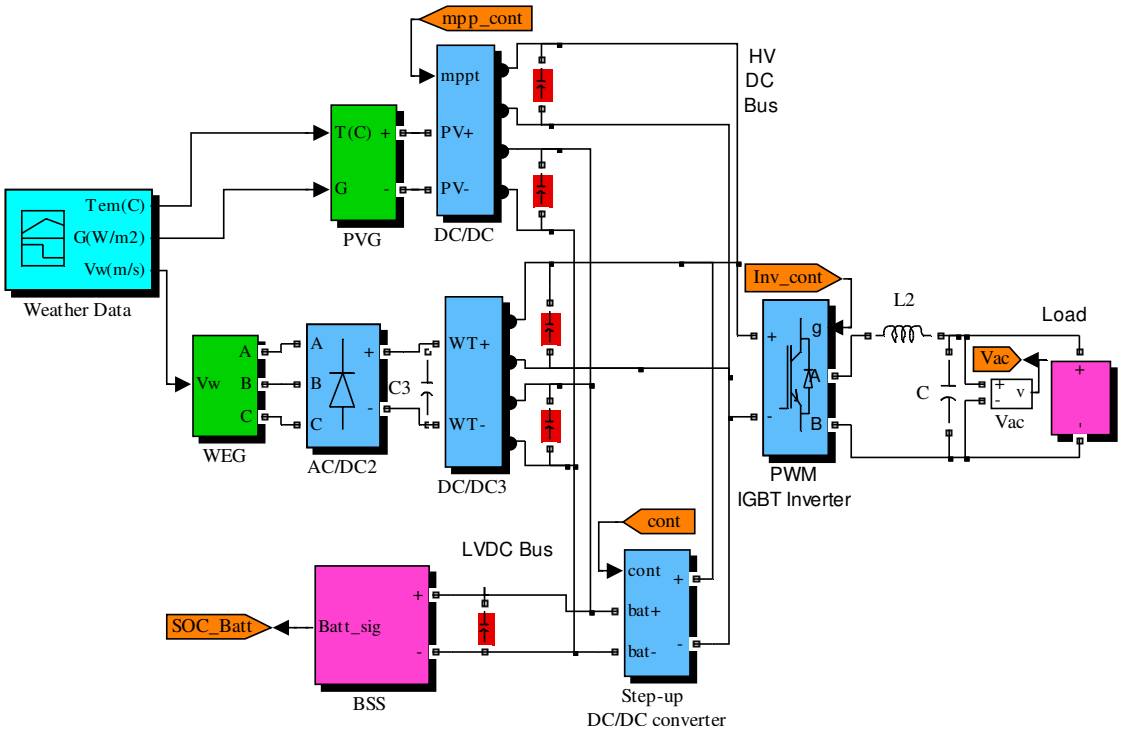

Figure 5.11. Schematic of LV/HV-DC bus hybrid system

Control Methodology

In this sophisticated configuration that features a double DC bus connection, a low voltage DC bus is used to straightforwardly store energy, while a high voltage DC bus is exploited to directly deliver power to the grid. While achieving the advantages of both LVDC and HVDC configurations, this architecture requires an extra DC power bus and more sophisticated multi-output power converters. On the other hand, it makes possible to store energy with a single conversion step, and to deliver power to the grid with two conversions steps. A full cycle of energy storage and delivery to the grid therefore encompasses three conversion steps. The inverter is controlled using a conventional PWM technique.

5.3 Comparative analysis

Determining the optimum configuration among possible solutions is necessary in order to obtain the maximum possible efficiency and the maximum possible continuity of load supply. On the other hand, no standard techniques are available for the selection of the optimum configuration of hybrid power system plants that in practice relies on the experience and the skill of the designer.

The traditional AC bus coupling is preferable when initial cost is a critical factor, while if the efficiency is the most important parameter, the choice among HVDC, LVDC and LV/HV-DC bus coupling must be accomplished case by case on the basis of the prevalent power streams occurring inside the plant., under this point of view, an interesting comparison can be made in terms of required conversion steps.

According to Table 5.3 the HVDC, LV/HVDC, HVAC and HVAC-rect. bus configurations are very effective in directly delivering power to the load. The LV/HVDC and LVDC are very suitable for plants including ESS, while HVAC is encountering high conversion losses for plants including ESS. The HVDC and HVAC-rect. buses are in the middle between the first and second group.

Table 5.3: Conversion steps

	HVDC	LVDC	HVAC	HVAC-rect.	LV/HV-DC
PV→AC load	2	3	2	1+1*	2
WT→AC load	3	4	3	2+1*	3
PV→ESS	2	1	4	2	1
WT→ESS	3	2	5	3	2
PV→ESS→AC load	4	3	6	3+1*	3
WT→ESS→AC load	5	4	7	4+1*	4
*1** = un folder mode voltage inversion					

The conversion steps analysis gives only a first quick comparison among the above considered configurations, however, it is insufficient to allow the detection of the most favourable configuration for a specific plant design. Table 5.3 shows the conversion steps required according to each architecture to store energy or to delivery power to the AC load or utility grid. A more effective comparison should be made on the basis of specific control strategies, real distribution of

solar radiation, wind speed and load as well as taking into account the efficiency of each power converter. To do this a dynamic models of each architecture of the above presented configurations are designed in MatLab/Simulink/SimPowerSys™ as presented in this chapter.

5.4 Performance Indexes

The comparison has been accomplished on the basis of four performance indexes:

- Global efficiency
- Efficiency in transferring energy from RES to BSS,
- Efficiency in transferring energy from BSS to load,
- Fraction of useful renewable energy.

The global efficiency (η_{global}) of an hybrid RES power plant is defined as follows:

$$\eta_{global} = E_{out} / E_{in} \quad (5.1a)$$

$$E_{conv.\_losses} = E_{in} - E_{out} \quad (5.1b)$$

$$\eta_{global} = 1 - E_{conv.\_losses}/E_{in} \quad (5.1c)$$

Where $E_{conv.\_losses}$ is the total energy conversion losses, E_{in} is the input energy from all the different energy sources which are PVG, WEG and BSS in this study.

The calculation of global efficiency based on daily input weather data and load using dynamic MatLab/Simulink/SimPowerSys™ models of the above mentioned configurations.

A typical day is divided into 24 intervals each one hour long. The energy conversion losses in one interval are computed based on a typical efficiency curve of each power converter using equation (5.2).

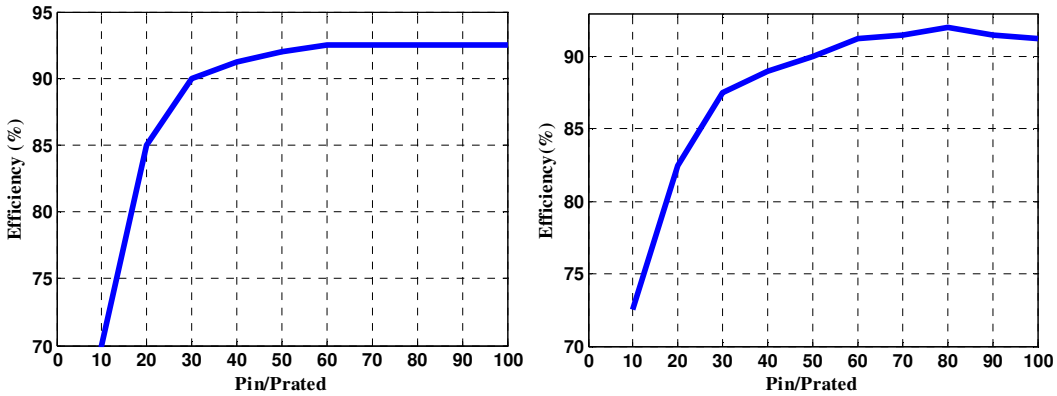

Figure 5.12. Typical efficiency of a 2kW DC/DC converter (left) and of a 2kW rectifier (right)

$$E_{conv-losses} = P_{in-conv}(1 - \eta_{typical-conv}) * \Delta t \quad (5.2)$$

Where $P_{in\text{-}conv}$ is the input power of a converter, $\eta_{typical\text{-}conv}$ is the typical efficiency of the converter at measured $P_{in\text{-}conv}$. Each amount of produced and consumed energy has been normalized in reference to the total energy consumed by the load. The typical efficiency curves of models' power converters are shown in Figures 5.12 and 5.13.

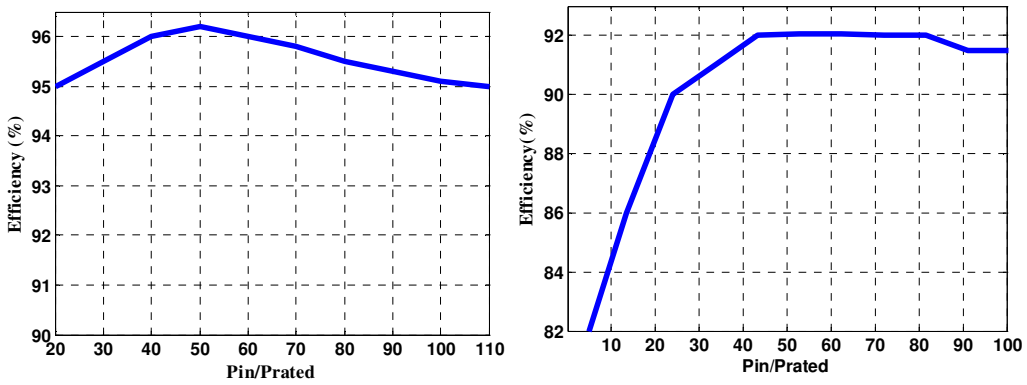

Figure 5.13. Typical efficiency of a 5kW PWM inverter (left) and of a 5kW full bridge DC/DC converter (right)

The flow chart shown in Figure 5.14 illustrates the global efficiency calculation procedure.

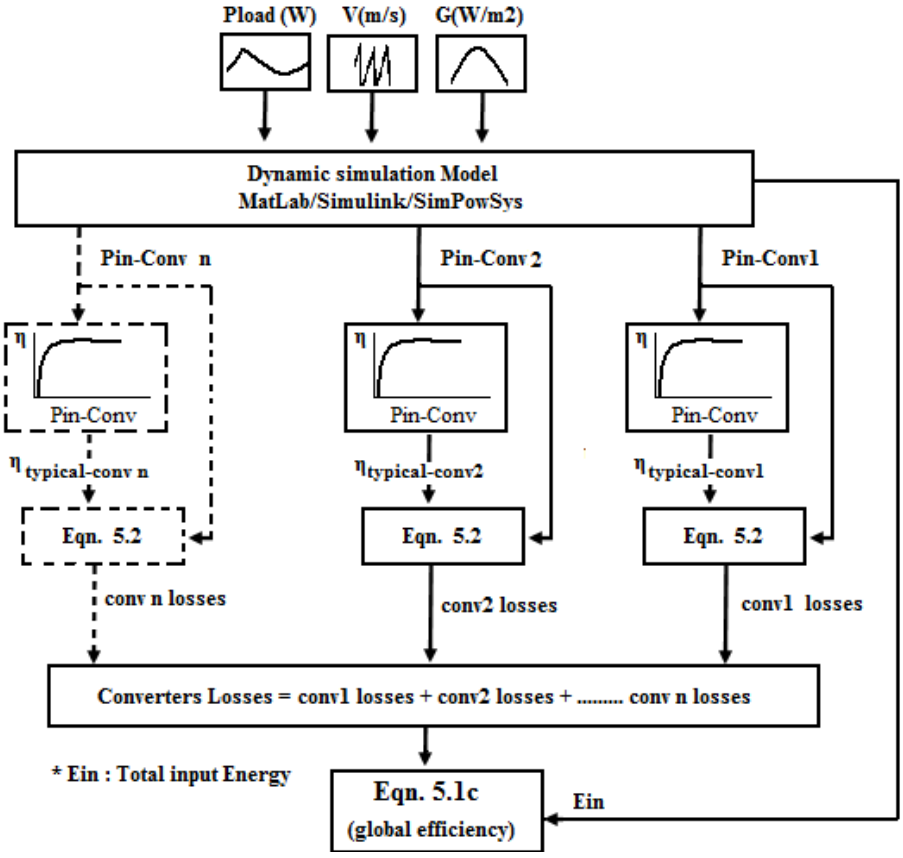

Figure 5.14. flow chart of global efficiency calculation in each configurations

The process starts immediately after running the dynamic simulation model. The daily load profile, wind speed distribution and solar radiation of a specific day are the input data of the simulation model. Each 0.1 second the input power of each converter is scanned and is entered to converter's efficiency lookup table for calculating the efficiency of the converter at a specific point. The converters losses can be easily calculated after identifying equation 5.2 parameters. The final step calculates the global efficiency as defined in equation 5.1c.

The efficiency in transferring energy from RES to BSS ($\eta_{RES-->BSS}$) is defined as the efficiency of excess energy delivered to BSS from the RES (PVG, WEG). This index is particularly significant in evaluating conversion losses of the energy delivered from RES to BSS. This index is measured by simulation based on the typical efficiency curves of models' power converters shown in Figures 5.12 and 5.13.

The efficiency in transferring energy from BSS to load ($\eta_{BSS-->Load}$) is defined as the efficiency of energy delivered from BSS to cover the deficiency of load. This index is particularly significant in evaluating conversion losses of the energy delivered from BSS to load. This index is measured by simulation based on the typical efficiency curves of models' power converters shown in Figures 5.12 and 5.13.

The solar fraction is normally used as a comparison index which is defined as the portion of energy consumed by the end use that is ultimately provided by the photovoltaic array [76]. This concept has been adapted to fit the case of an hybrid system including a wind turbine. Therefore the useful renewable energy fraction (RE-Fraction) is defined as the fraction of the end-use energy supplied by PVG and WEG. It is computed as shown in equation (5.3):

$$RE - Fraction = Useful\ Ren.Energy/Load\ Energy = (Input\ Ren.Energy - E_{conv.\_losses})/Load\ Energy \quad (5.3)$$

This performance index is significant in determining how well the system is utilising the available renewable energy.

5.5 Simulation results

Simulations have been accomplished using MatLab/Simulink/SimPowSys^{TM} dynamic models presented in the previous chapters. The average residential load demand profile for one home in Italy in the cold season shown in Figure 3.3 is considered in this study. The average wind speed, solar irradiance and air temperature data used are those of a typical day of December recorded at CNR/ITAE-Italy /Messina as shown in Figures 3.4, 3.5 and 3.6.

5.5.1 Global Efficiency

Figure 5.15 shows the global efficiency of each configuration.

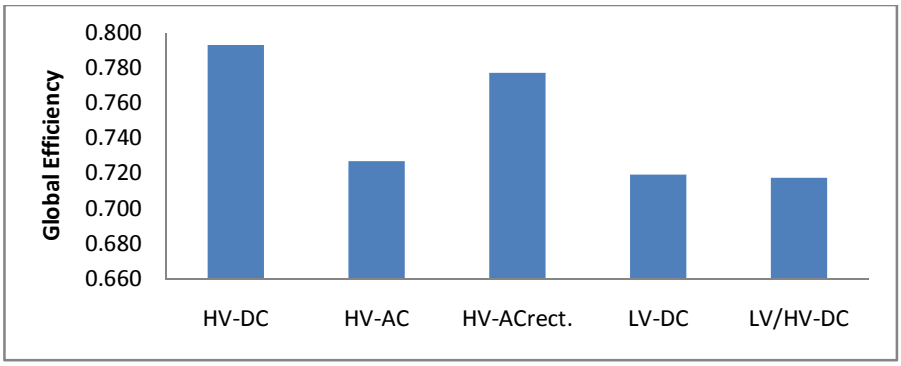

Figure 5.15. Global efficiency of different bus voltage configurations

It is clear that the HVDC bus configuration obtains the highest global efficiency and HVAC rect. bus configuration comes in the next.

The global efficiency doesn't depend only on the number of conversion steps as generally known. In fact other conditions may play significant roles in determining the effectiveness of energy flow from different energy sources and load such as the control strategy and the efficiency of power converters.

5.5.2 Efficiency of energy transfer from RES to BSS ($\eta_{RES-->BSS}$)

Figures 5.16 and 5.17 show the maximum and average $\eta_{RES-->BSS}$ index, respectively. It is clear that HVDC, LVDC and LV/HV-DC achieve the highest levels of efficiency. These results are well in accord with the results shown in Table 5.3.

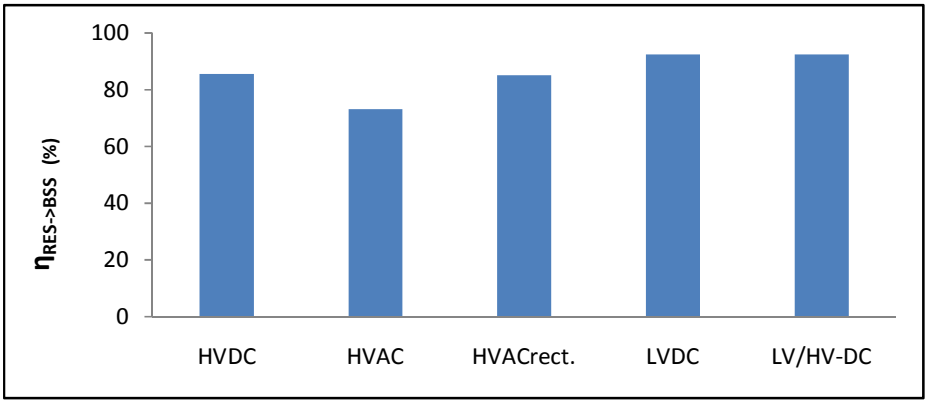

Figure 5.16. Maximum $\eta_{RES-->BSS}$ index of five bus voltage configurations

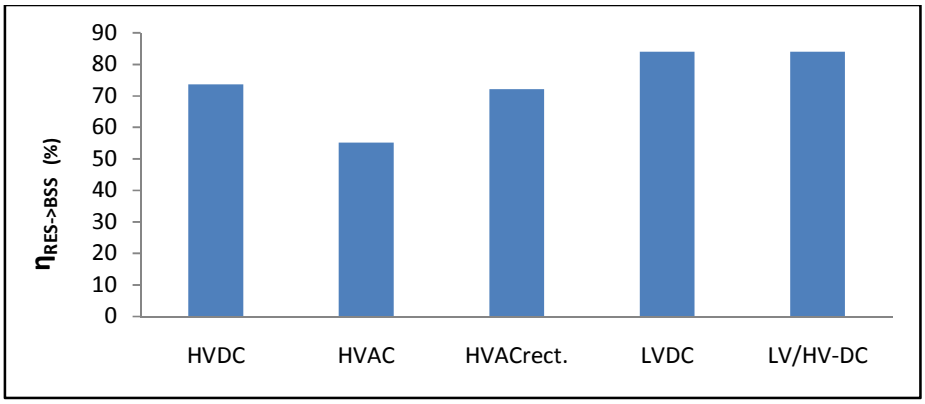

Figure 5.17. Average $\eta_{RES-->BSS}$ index of five bus voltage configurations

5.5.3 Efficiency of energy delivered from BSS to load ($\eta_{BSS-->Load}$)

Figures 5.18 and 5.19 show the maximum and average $\eta_{BSS-->Load}$ index of each architecture of a stand-alone hybrid power system, it is clear that the efficiency of energy delivery from BSS to load are very satisfactory in all configurations but HVDC, HVAC and LV/HVDC are the best.

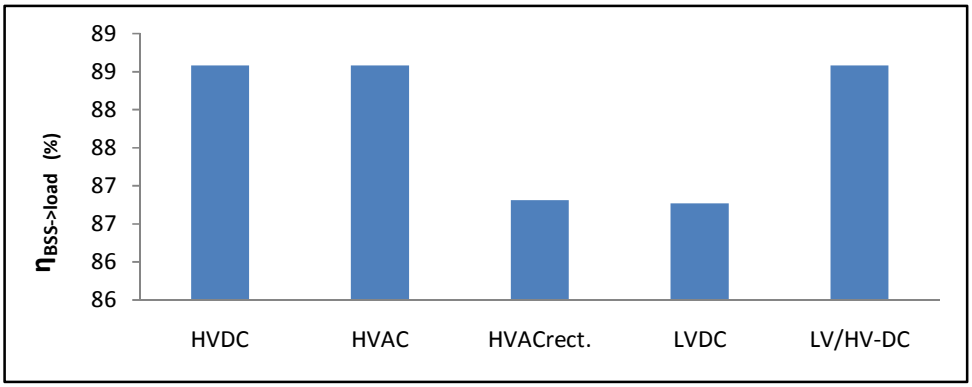

Figure 5.18. Maximum $\eta_{BSS-->Load}$ index of five bus voltage configurations

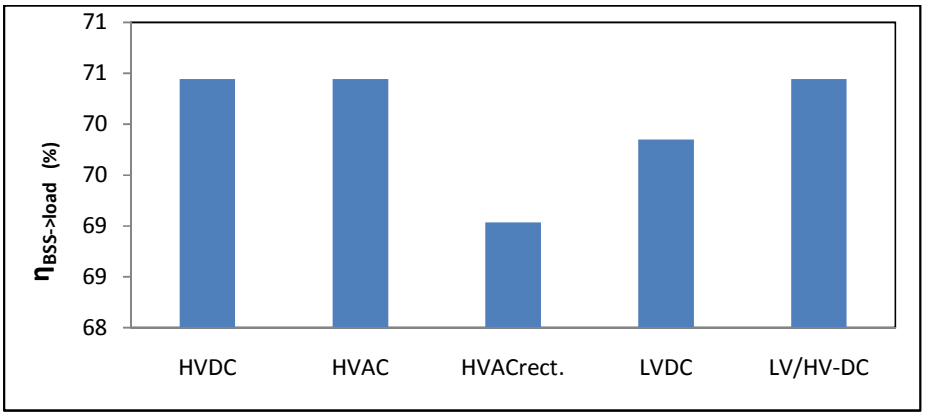

Figure 5.19. Average $\eta_{BSS-->Load}$ index of five bus voltage configurations

5.5.4 Fraction of useful renewable energy performance index

Figure 5.20 shows RE-Fraction achieved by the considered five configurations.

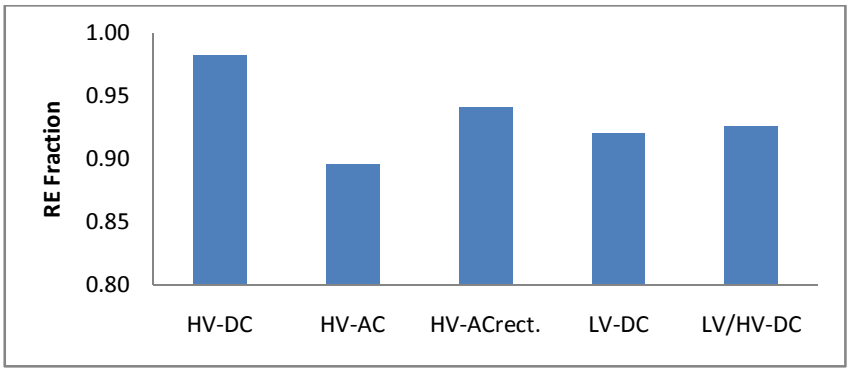

Figure 5.20. RE-Fraction of different bus voltage configurations

The maximum RE-Fraction is obtained by the HV-DC bus configuration and the HV-AC rect. bus configuration comes in the next. The LV-DC and LV/HV-DC have similar scores. Table 5.4 shows the deviation of performance indexes from those of the HV-DC bus configuration.

Table 5.4
Percentage deviation of performance indexes from those of the HV-DC bus configuration

	HV-AC	HV-ACrect.	LV-DC	LV/HV-DC
Global efficiency (%)	-8.3	-2.0	-9.3	-9.5
$\eta_{RES-->BSS}$ (%)	-14.5	-4.6	8.1	8.1
$\eta_{BSS-->Load}$ (%)	0	-2	-2.1	0
RE-Fraction (%)	-8.3	-4.2	-6.3	-5.3

As shown in Table 5.4 the HV-DC bus configuration is the best in terms of global efficiency as the percentage difference from HV-DC is negative in all configurations. HV-ACrect. bus configuration is more comparable to HV-DC. In contrast, the LV/HV-DC, HV-AC and LV-DC configurations achieve the highest negative difference from HV-DC.

The LV/DC and LV/HV-DC configurations are particularly efficient in storing energy while HVAC and HVACrect. aren't effective in storing energy. The HVDC bus is in between the two groups.

The five configurations show roughly the same efficiency when transferring energy from the BSS to the load ($\eta_{BSS-->Load}$).

The HV-DC bus configuration draws maximum RE-Fraction which indicates the best utilization of the available renewable energy sources.

5.6 Sensitivity of performance indexes to seasonal load variations

The sensitivity to seasonal load variations is investigated for each configuration. For this purpose, the simulation runs with three seasonal load profiles [77], namely: 0 or base load profile, 0.27 and -0.27 profiles, obtained multiplying the base profile respectively by a factor 1.27 and 0.73.

Figure 5.21 illustrates global efficiency of the five configurations over seasonal load variation. HVDC and HVACrect. configurations are less sensible to load variation.

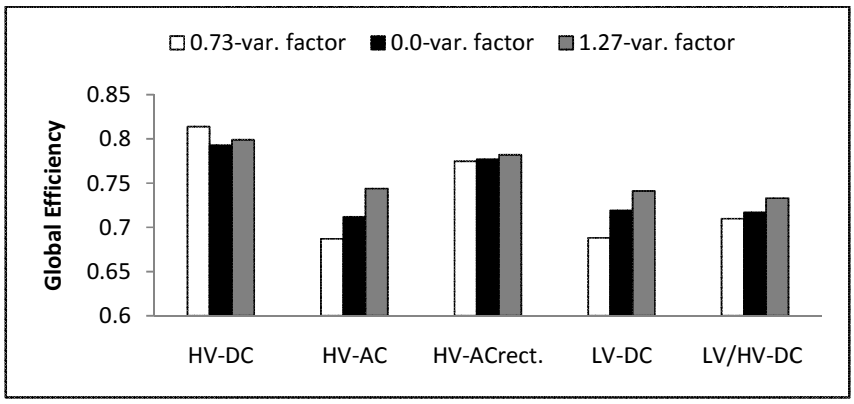

Figure 5.21. Global efficiency of different configurations with seasonal load variation

The global efficiency in LV/HV-DC, HVAC and LVDC configurations is sensible to load variations as if the load demand increases the efficiency improves.

Figure 5.22 deals with RE-Fraction of the five configurations over three load profiles. HV-DC configuration draws the maximum renewable energy fraction, while HVAC and LVDC are the lowest. The RE-Fraction is sensible to load variation as in all the configurations an increase in the load demand leads to a reduction of the renewable energy fraction.

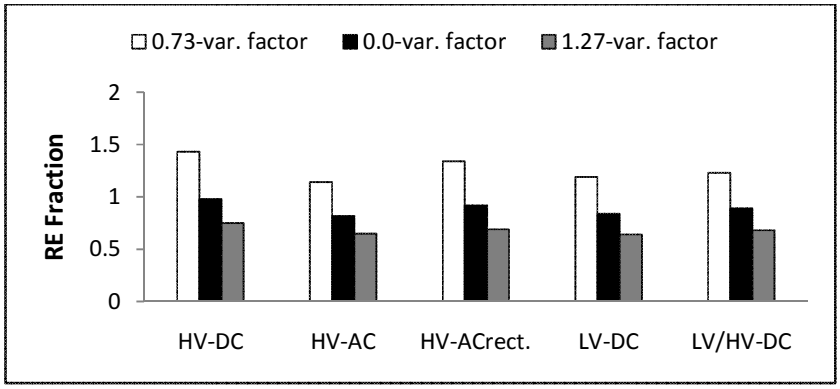

Figure 5.22. RE-Fraction of five configurations with seasonal load variation

5.7 Conclusion

1. Five architectures for a stand-alone hybrid system encompassing PVG, WEG and BSS are studied and analysed and suitable dynamic models have been built.

2. Some performance indexes, namely: the global efficiency, the efficiency in transferring energy from RES to BSS, the efficiency in transferring energy from BSS to load and the fraction of useful renewable energy have been selected to evaluate the five considered configurations.

3. On the basis of these indexes it is found that (at least for the specific case considered):

- The HVDC bus configuration features the highest global efficiency 79.3%, while the HVAC-rect. configuration is comparable to the HVDC configuration scoring 77.7%. Finally, HVAC, LVDC and LV/HV-DC configurations show lower levels of efficiency: 72.7%, 71.9%, 71.7% respectively. Under the global efficiency point of view HVDC and HV-ACrect. bus configurations are less sensible to load variation than LV/HV-DC, HVAC and LVDC.
- The LVDC and LV/HV-DC configurations are particularly efficient in storing energy ($\eta_{RES-->BSS}$) while HVAC is less efficient. The HVDC and HVACrect. bus configurations are in between the first and the second group.
- In case of energy delivery to load from BSS ($\eta_{BSS-->Load}$), all configurations obtain a quite similar efficiency.
- The HVDC bus configuration draws the maximum RE-Fraction, which indicates the best utilization of available renewable energy sources. The HVAC-rect. bus configuration is 4.2% worse than HVDC while the HVAC, LVDC and LV/HV-DC are respectively 8.3%, 6.3% and 5.3% less efficient than HVDC. In general, the RE-Fraction is sensible to load variations in all configurations.

4. Based on the above discussions and understandings for the considered case study the HVDC bus configuration is the most effective among the five different configurations, based on the following reasons:

- HVDC obtains the highest global efficiency and fraction of useful renewable energy performance indexes.
- HVDC obtains the highest value of $\eta_{BSS-->load}$ index (efficiency of energy delivered from BSS).
- HVDC bus is in the middle between the best and worst value of $\eta_{RES-->BSS}$ index (efficiency of energy delivery from RES to BSS).

Chapter 6

Fuzzy Logic Based Management of a Stand-Alone Hybrid Generator

The high voltage DC bus (HV-DC) configuration is found to be the best according to the performance indexes discussed in chapter 5, therefore further investigations are performed about this configuration. A fuzzy logic controller (FLC) is designed to manage the power flows in a stand-alone hybrid generation plant based on HV-DC configuration.

6.1 Introduction

The overall control strategy for power management in a hybrid generation plant using a Fuzzy logic controller (FLC) is discussed in this chapter. The plant works in island mode and is based on the high voltage DC bus configuration (HV-DC), it is composed of: a wind energy generator (WEG), a PV energy generator (PVG) and a fuel cell/electrolyser energy storage system (FC/E-ESS).

The performance of the proposed strategy are evaluated by simulation in different operating conditions based on performance indexes that will be discussed in this chapter. Moreover the efficiency of the developed FLC is compared to that of a more conventional controller taking into account the fuel cell H_2 consumption, the amount of H_2 generated from the Electrolyser and the final battery state of charge (SOC).

Based on the component models and control methodologies given in the previous chapters, a simulation system test-bed for the proposed hybrid alternative energy system has been developed in MatLab/Simulink/SimPowSys^{TM}.

6.2 System Configuration

A hybrid generation system composed of a WEG and a PVG, in theory features a load supply continuity higher than simple PVGs or WEGs, due to the overlap of the availability of the two primary sources. However, a fully exploitation of all the available energy can hardly been accomplished without a suitable energy storage system. Among several possible solutions a FC/E-ESS is considered coupled to an additional Lead Acid battery bank.

Figure 6.1 shows the schematic diagram of the considered standalone hybrid system. The three main elements: WEG, PVG and FC/E-ESS are controlled by three independent control systems,

also accounting for the MPPT. Details about MPPT algorithms and control methodologies of each component are presented in chapters 4 and 5.

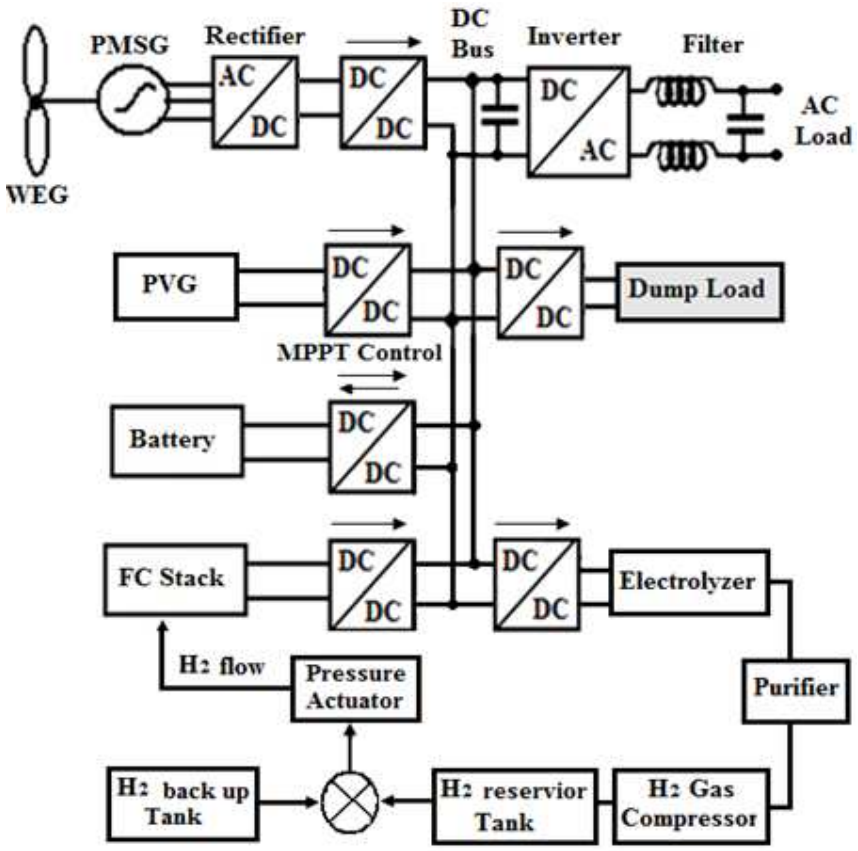

Figure 6.1. Schematic of the hybrid generation system

In this study FC/E-EES is the main energy storage system while the Lead Acid batteries are used to compensate the low dynamic of the FC system. In the considered plant, the main task of the batteries is to hold the DC bus voltage within the rated range in case of sudden load variations, therefore the capacity of the batteries is relatively small.

Suitable mathematical models of all the elements of the system have been previously carried out, a detailed description of the models can be found in chapter 4. The power controllers of the all components presented in Figure 6.1 are discussed in details in chapters 4 and 5.

Figure 6.2 shows the overall diagram of the simulation model in MATLAB/Simulink/ SimPowSys™.

Details about parameters of the four main subsystems of the considered plant are given in Table 3.1 and 3.2 in Chapter 3.

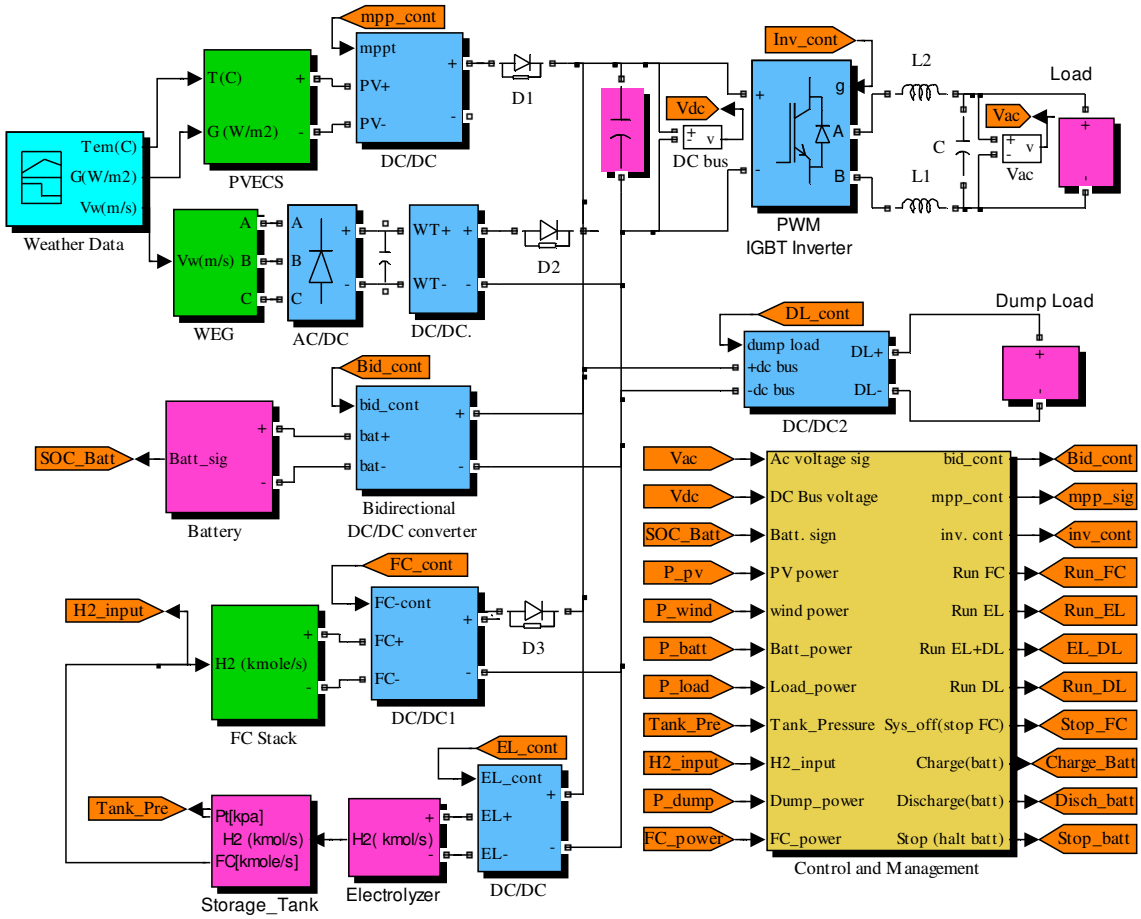

Figure 6.2. Simulation model for the proposed hybrid alternative energy system in MATLAB/Simulink/SimPowSys™

6.3 Power Management Strategy Methodology

A stand alone hybrid power generator must be suitably controlled in order to obtain the maximum possible efficiency and the maximum possible continuity of load supply. Specifically, the power exchange among WEG, PVG, FC/E-ESS and the load must be tightly regulated in order to ensure that the captured energy is delivered to the load as much as possible. To do this a system management unit computes the references for the control systems of the three main elements of the system on the basis of measurements of the power generated from WEG, PVG and FC/E-ESS, the DC bus voltage, the amount of H_2 in the storage tank and the battery SOC.

The definition of an optimal management strategy for a quite complex system as the considered hybrid generator can hardly be accomplished with a traditional method, therefore, a FL approach is instead proposed in this study.

FL controller approach is more suitable than conventional one especially in complex system like that under investigation in this research. The FL is the way to make machines more intelligent enabling them to reason in a fuzzy manner like humans emerged as a tool to deal with uncertain,

imprecise or qualitative decision-making problems [78] and it is a convenient way to map an input space to an output space.

The basic concept underlying FL is that of a linguistic variable. In effect, much of FL may be viewed as a methodology for computing with words rather than numbers; this avoids the need for a detailed model of the controlled system or of the control strategy. The most important features of FL are [79, 80]:

- It is flexible, and conceptually easy to understand.
- It is tolerant versus data imprecision and able to cope with models including non linear functions of random complexity.
- It can be integrated with conventional control techniques, to improve their performance while making easier their implementation.

Figure 6.3 shows a flow diagram of the proposed power management strategy. It starts from the evaluation of P_{net} the difference between the whole generated power and the load power demand as:

$$P_{net} = P_{pv} + P_w - P_{load} \quad (6.1)$$

Where P_{pv} and P_w are respectively the power generated from PVG and WEG, P_{load} is the load power. The value of P_{net} determines the plant operational mode. If $P_{net} > 0$, there is an excess of generated power while if $P_{net} < 0$, the generated power is insufficient.

The excess power is supplied to the electrolyser if the battery is fully charged and if the H_2 reservoir tank is not full. However, if the excess power is greater than the electrolyser rated power, part of the energy is transmitted to the dump load. If the reservoir tank is full then the excess power is totally delivered to the dump load. If a lack of power is detected and enough hydrogen is available in the reservoir tank, the FC stack is turned on. The lack of power is classified into small, normal and high in order to determine the most suitable strategy to compensate the shortage.

The FC/E-ESS is operated alone if the lack of power is lower than its rated power. However, if the lack of power is small enough only the battery is used. If the lack of power is high, the battery is tasked to support the FC/E-ESS, as in the case of a sudden load variation in order to compensate the low dynamic of the stack.

The management strategy shown in Figure 6.3 has been implemented exploiting a FL approach as illustrated in the next section.

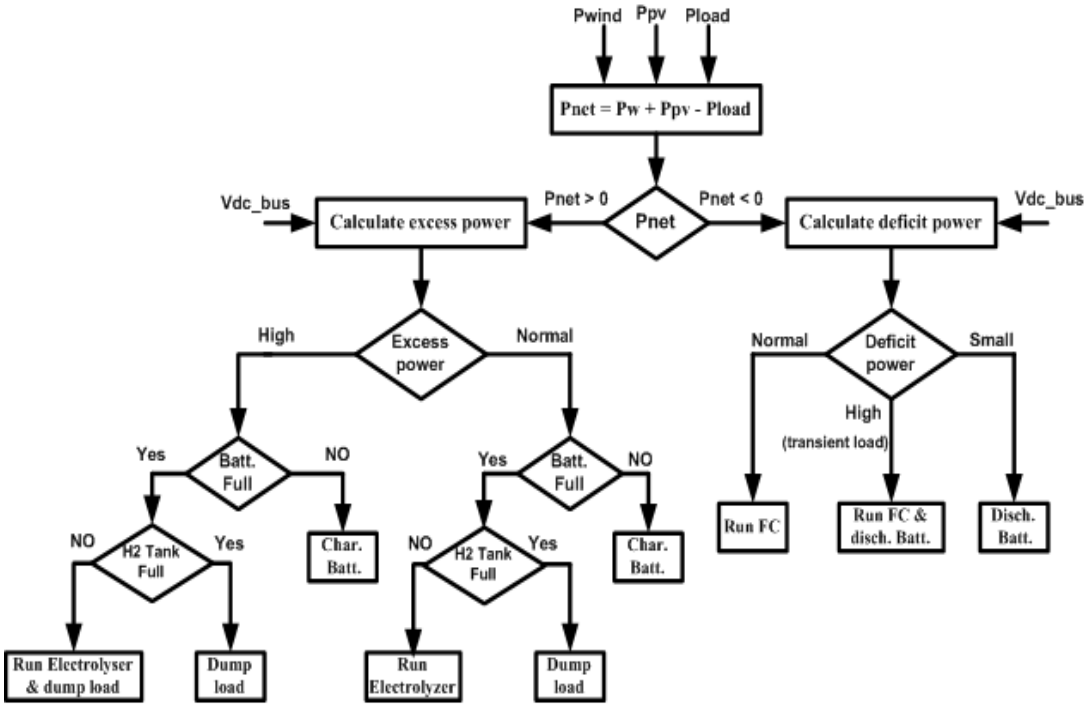

Figure 6.3. Power flows management

6.4 Fuzzy Logic Controller

6.4.1 Background information

The FL graphical user interface (GUI) toolbox implemented by MATLAB/Simulink has been used in this study. It is simple, effective and provides tools to create and edit fuzzy inference systems [79].

In can be defined as a logical system with an extension of multi-valued logic, also it is almost synonymous with the theory of fuzzy sets that relates to classes of objects with uncertain boundaries in which membership is a matter of degree [79].

The fuzzy inference is a method that interprets the values in the input vector and assigns values to the output vector. It includes five parts: fuzzification of the input variables, application of the fuzzy operator (AND or OR) in the antecedent, implication from the antecedent to the consequent, aggregation of the consequents across the rules, and defuzzification.

Step1: Fuzzification

The first step is to take the inputs and determine the degree to which they belong to each of the appropriate fuzzy sets via membership functions, this process is called *fuzzification*.

The membership function is a curve that defines how much points in the input space are mapped to a degree of membership which must vary between 0 and 1. The shape of each membership

function can be designed according to the target required that suits us from the point of view of simplicity, convenience, speed, and efficiency [79].

A classical set might be expressed as [79]:

$$C = \{x \mid x > 6\} \quad (6.2)$$

A fuzzy set is an extension of a classical set. If X is the universe of discourse and its elements are denoted by x, then a fuzzy set C in X is defined as a set of ordered pairs.

$$C = \{x, \mu C(x) \mid x \ X\} \quad (6.3)$$

$\mu_C(x)$ is called the membership function (or MF) of x in C. The membership function maps each element of X to a membership value between 0 and 1.

Several kinds of membership functions can be considered; the simplest is the triangular membership function, which is a collection of three points forming a triangle, and the trapezoidal membership function, which is just a truncated triangle curve. Some membership functions are built based on a simple Gaussian distribution curve or on a two-sided composite Gaussian distribution curve. The generalized bell membership function is specified by three parameters [79].

Step 3: Fuzzy operators

After the Fuzzy inference interprets the values in the input vector data, it assigns values to the output vector based on some set of rules. These if-then rule statements are used to formulate the conditional statements that comprise fuzzy logic which is in the form: 'if x is A then y is B', where A and B are linguistic values defined by fuzzy sets on the ranges X and Y, respectively. The if-part of the rule "x is A" is called the antecedent or premise, while the then-part of the rule "y is B" is called the consequent or conclusion.

If the antecedent of a given rule has more than one part, the fuzzy operator is applied to obtain one number that represents the result of the antecedent for that rule. This number is then applied to the output function. The input to the fuzzy operator consists of two or more membership values from fuzzified input variables [79].

Step3: Implication

The *implication* is applied after weighting the rules. Implication is implemented for each rule. The input for the implication process is a single number given by the antecedent, and the output is a fuzzy set [79]. The available options are minimum function which truncate the output fuzzy set and product function that scales the output fuzzy set which both used by the 'AND' method.

Step 4: Aggregation

The output fuzzy sets that represent the output of each rule are combined into a single output fuzzy set which is called *aggregation* which only occurs once for each output variable. As long as the aggregation method is commutative then the order in which the rules are executed is unimportant. Various methods are supported such as maximum (MAX), probabilistic OR and simply the sum (SUM) of each rule's output set.

The aggregate of a fuzzy set encompasses a range of output values, and so must be defuzzified in order to resolve a single output value from the set which is the final step.

Step 5: Defuzzification

Defuzzification is such inverse transformation which maps the output from the fuzzy domain back into the crisp domain. the most popular defuzzification method is the centroid calculation, which returns the center of area under the curve [79,81,82].

6.4.2 Fuzzy Logic Controller Design

The main task of the control strategy is to determine the references for the control systems of the subsystems of the hybrid generation system as shown in Figure 6.3. The FL strategy is built using a Mamdani inference with four input variables and two main outputs as shown in Figure 6.4.

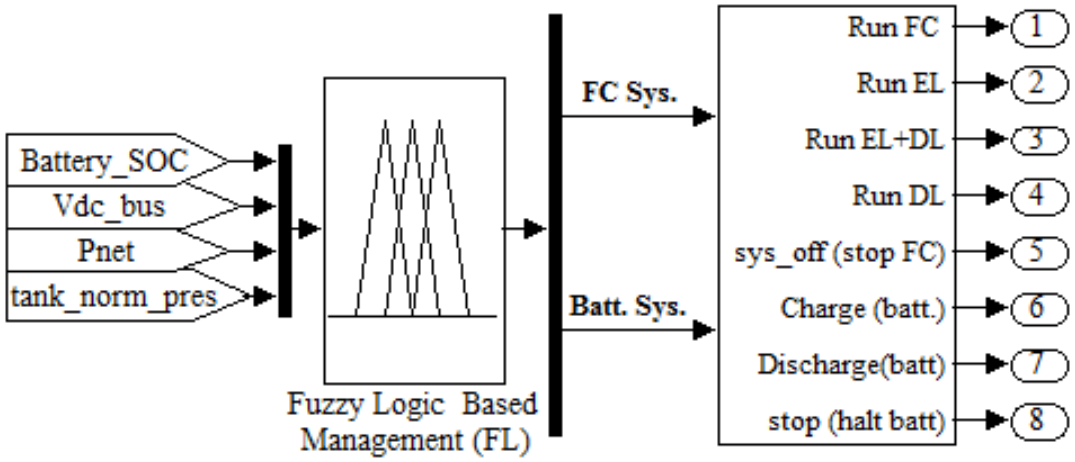

Figure 6.4. FL based management strategy

The input variables illustrated in Figure 6.4 are described below:

1. The net power (P_{net}) which is calculated using equation (6.1) is given in the range from -3kW to 3kW to determine the situation of the power flow in the system. The P_{net} range is defined based on the capacity of the system. The net power (P_{net}) is described through five linguistic terms based on triangular membership functions as shown in Figure 6.5:

- High-excess: The generated power is larger than the capacity of the system.
- Normal-excess: The generated power is within the range of the capacity of the system.
- Small lack: In this range, the system suffers from small energy lack.

- Normal lack: In this range the amount of energy lack is normal according to the control system.
- High lack: The system suffers from high energy lack.

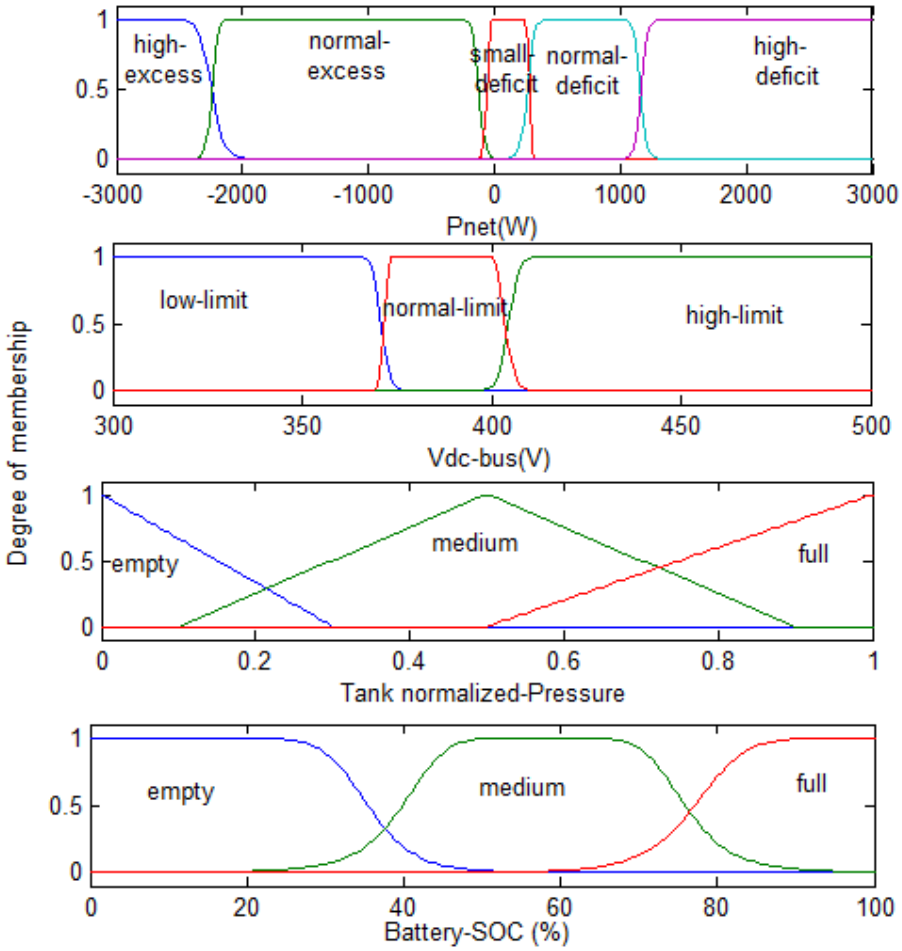

Figure 6.5. Fuzzy sets defining the four inputs

2. DC bus voltage: It is described through three linguistic terms based on triangular membership functions , which are:

- Low limit: In this range, the DC bus voltage decreases lower than the designed value.
- Normal limit: being in this range the DC bus voltage keeps within the controlled designed range.
- High limit: In some circumstances especially in a lower load demand with higher generated power, the DC bus voltage overcomes the designed range of the DC bus voltage.

3. Normalized Hydrogen tank pressure. It is described using three linguistic terms based on generalized bell membership functions: *Empty, Medium and Full.*
4. Battery state of charge (SOC). It is described using three linguistic terms based on triangular membership functions, namely: *Empty, Medium and Full*.

The output variables are described below and illustrated in Figure 6.6:

1. The battery power has three linguistic terms based on triangular membership functions:

- Charge mode: This means that DC/DC bidirectional converter should be controlled to charge the BSS.
- Discharge mode: This means that DC/DC bidirectional converter should be controlled to discharge the BSS.
- Stop (idle) mode: This means that BSS is neither in a charge nor in a discharge mode.

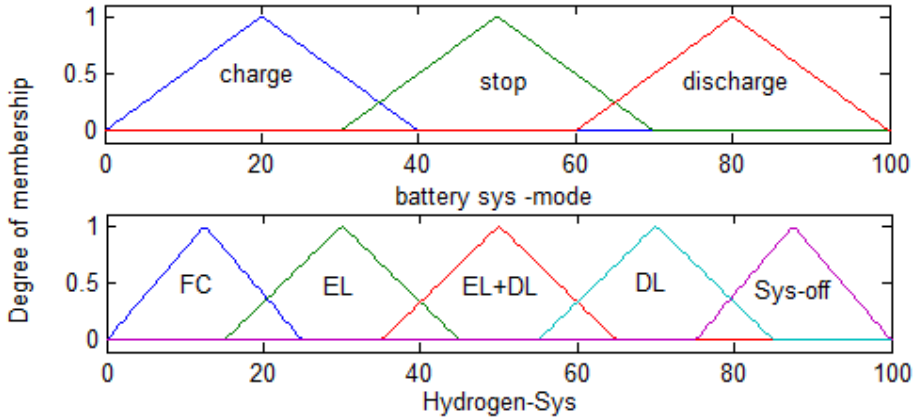

Figure 6.6: Fuzzy sets defining the two outputs

2. The FC/E-ESS operating mode has five linguistic terms based on triangular membership functions:

- Running fuel cell stack (FC): The FC power source must provide the system with energy, normally the amount of required energy is calculated and based on the capacity of the stack.
- Running electrolyser (EL): The electrolyser starts to convert the specified electrical energy from the control system.
- Running dump load (DL): part of excess energy is directed to dump load as specified by the control system.
- Running electrolyser and dump load (EL+DL).
- Turning off the FC system (Sys-Off): The hydrogen system is completely idled.

A connection between the cause and effect, or a condition and a consequence is made by reasoning which can be expressed by a logical inference as explained before or by the evaluation of inputs in order to draw a conclusion. This study follows rules of inference which have the form as shown in the example:

If Battery-SOC is at full mode and Vdc-bus is at high-limit and Pnet is at high-excess mode and the tank normalized-Pressure is at full mode then (battery-mode is stop)(Hydrogen-Sys is DL).

In this case 20 rules have been designed in order to fit with the power flow management of the hybrid system as shown in Figure 6.7.

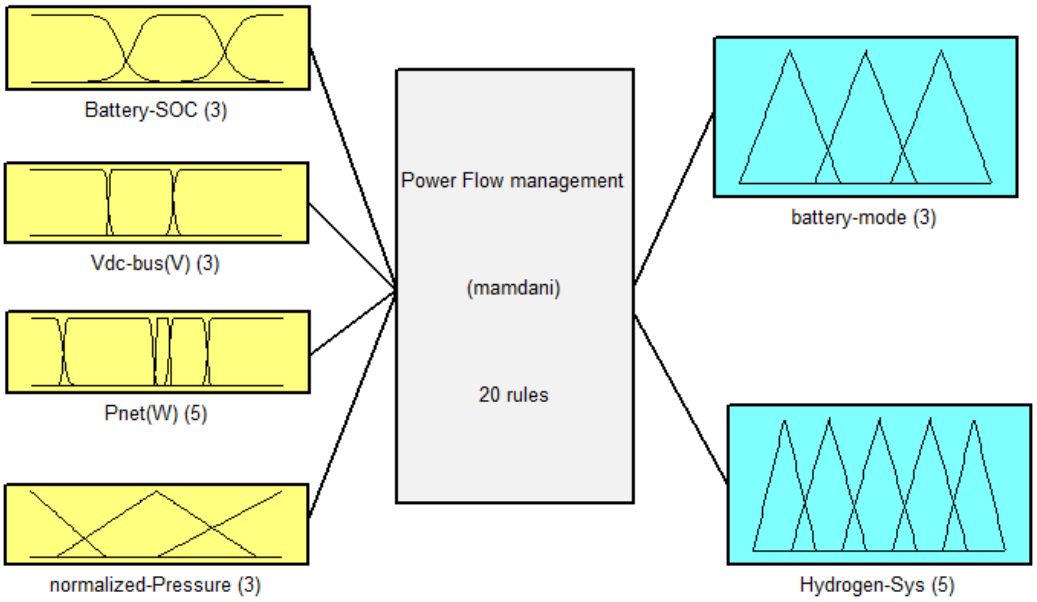

Figure 6.7. System power flow management: 4 inputs, 2 outputs and 20 rules

The output of the fuzzy inference are some surfaces as shown Figures 6.8a and 6.8b.

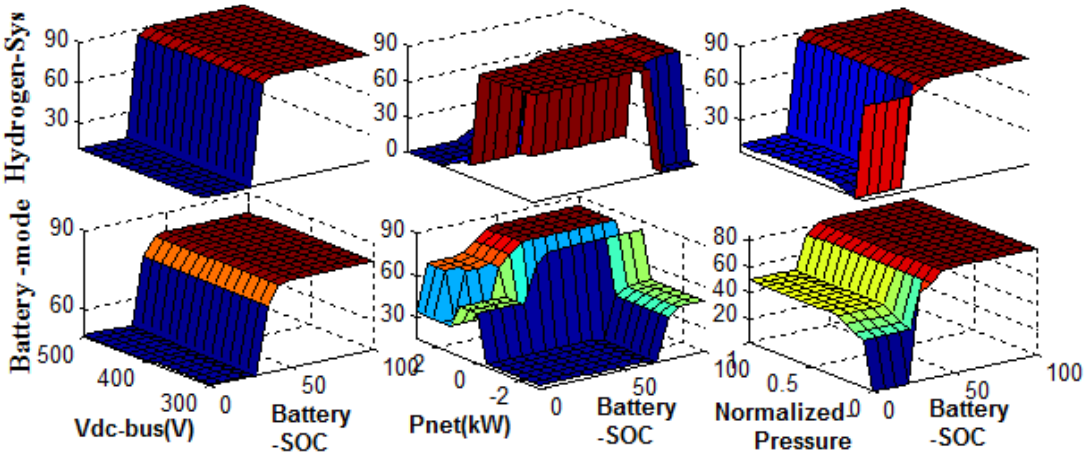

Figure 6.8a. FLC surface for BSS and hydrogen storage tank

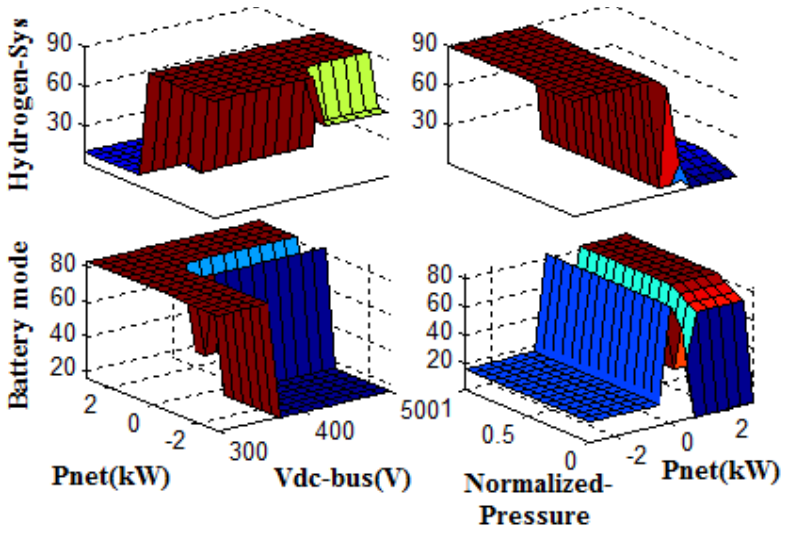

Figure 6.8b. Fuzzy logic controller surface for BSS and hydrogen storage system

6.5 Simulation Results

Two simulations have been accomplished to confirm the effectiveness of the FL based management using performance indexes as: the normalized frequency deviation, stability of the DC bus voltage and AC voltage total harmonic distortion of the output signal (THD). Definitions of those indexes are presented in the next section.

6.5.1 Time Domain Performance Indexes

Frequency Deviation

Frequency deviation is considered an important index. The normalized frequency deviation is calculated as shown in eq. (6.4).

$$\Delta f = (f - fr)/fr \qquad (6.4)$$

Where fr is the rated frequency (50 Hz) and f is the measured frequency (Hz). According to standard EN50160/2006 [83], under normal operating conditions, the mean value of the fundamental frequency of islanding system (standalone) measured over 10s must stay within range: 50Hz ± 2%. The frequency deviation index is adopted in this study as a stability index, which is allowing evaluation of a small frequency variation.

The Simulink model shown in Figure 6.9 illustrates the method of measuring Δf. Once the voltage signal is sensed, each voltage cycle is transferred to a pulse in the output of the flip flop. The two switches and clock are used to count up the time between the two successive pulses. The measured frequency (1/T) is compared and divided with the rated frequency (fr) to calculate the frequency deviation as illustrated in eq. (6.4).

Voltage Total Harmonic Distortion (THDv)

THD_V is an important index to evaluate the quality of output AC signal. It is calculated using the discrete THD_V block in Simulink depending on the eq. (6.5) [84].

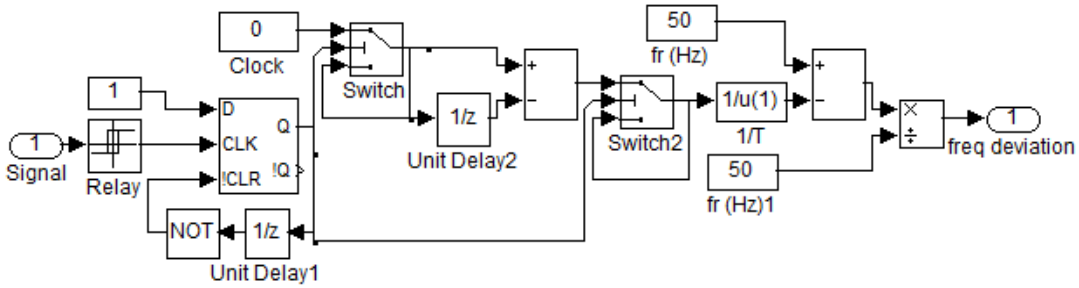

Figure 6.9. Simulink model for frequency deviation measurement

$$THD_v = \sqrt{\sum_2^{\infty} V_h^2}/V_1 \qquad (6.5)$$

Variation in DC Bus Voltage

Variation in DC bus voltage is taken as a system stability index. In general, the variation of voltage is caused from sudden changes in load and weather conditions. DC bus voltage is controlled to be within the range (380 - 420V) at the input of DC/AC inverter in order to secure $230V_{rms}$ at the connection point with AC load.

6.5.2 Performance of FL based management

Three cases are considered, dealing with different weather data and load demand day profiles. The ambient temperature is assumed to be constant (25°C) throughout the simulations. The solar radiation is expressed in per unit, the base value being $1kW/m^2$, the wind speed is expressed in actual values, the power flow and load demand is also expressed in per unit system at base value 1kW, and the DC bus voltage is normalized at 400V.

CASE 1: This case deals with an excess of generated power. The battery is assumed full charged at the beginning. Results of time domain simulation are shown in Figure 6.10 The simulation test can be divided into four intervals:

(0-20s): the average wind speed is about 8.5m/s and the average load is 0.45pu. The solar radiation is zero. WEG covers all the load demand and the net power is zero.

(20-60s): the average wind speed rises from 8.5 to 11m/s and load demand rises to 0.6pu. The solar radiation rises gradually to about 0.75pu. The excess power increases gradually to 2pu with the increase of the solar radiation and wind speed, as shown from the P_{net} diagram.

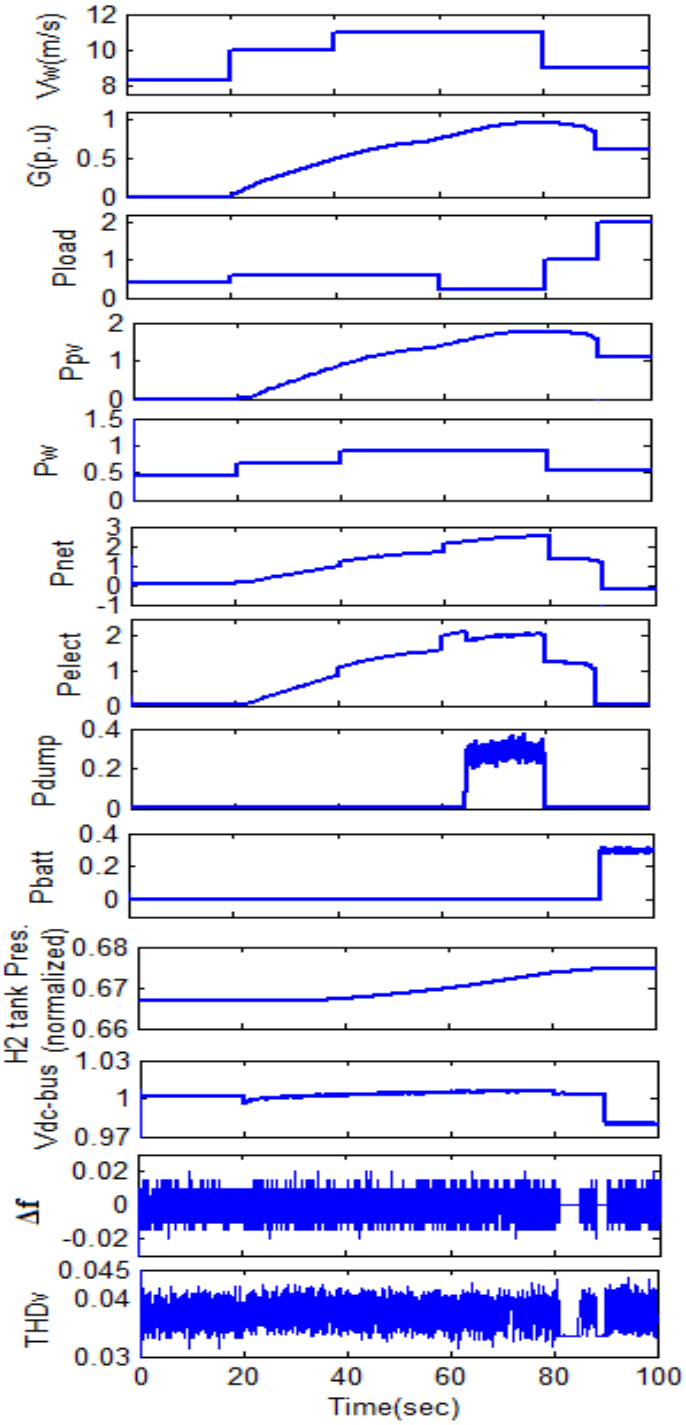

Figure 6.10. Case 1 - Time domain simulation

According to the developed power management strategy, the excess power is delivered to the electrolyser. Therefore, the storage tank normalized pressure increases as the hydrogen is pumped in.

(60-80s): The load demand decreases to 0.2pu, the solar radiation rises gradually to 0.95pu, while the wind speed is constant. The excess power in this interval is higher than the electrolyser rated

power. About 0.4pu is then delivered to the dump load, while about 2.2pu is delivered to the electrolyser. The storage tank normalized pressure increases as the Hydrogen is still pumped in.

(80-100s): The load demand abruptly rises from 0.2 to 1 to 2pu. The solar radiation and wind speed decreases to 0.6pu and 9m/s, respectively. Within this interval (at 90s) a small power lack occurs as the load rises to 2pu. The power lack is compensated by the batteries according to power management strategy.

The system is stable during all the considered intervals as it is possible to observe from the Δf diagram. In fact, the normalized frequency deviation is always less than 0.02; moreover, the DC bus voltage remains constant around 1pu. More precisely, after 90s, the DC bus voltage decreases to 0.98pu, which is still within the allowed range of variation.

CASE 2: Deals with an insufficient generated power. Results of the simulation test is shown in Figure 6.11. The simulation can be divided into five intervals:

(0-20s): The average wind speed and the load demand are 5m/s and 0.6pu, respectively. The solar radiation rises gradually from 0.2 to 0.3pu. As the power lack is small (< 0.2pu), it is compensated only by the batteries.

(20-40): The load demand increases to 1.6pu, while the wind speed and the solar radiation increase to 6.4m/s and 0.45pu, respectively. The lack of generated power increases. FC/E-ESS covers the difference while the power drawn from batteries is null. The H_2 storage tank pressure decreases as the H_2 is pumped out.

(40-60): The load demand rises to 2.8pu, while the wind speed decreases to 6m/s and the solar irradiation increases to 0.5pu. The FC/E-ESS and the batteries cover the power difference working together. The storage tank pressure decreases as the H_2 is still pumped out.

(60-80): The load demand suddenly decreases to 0.5pu, while the wind speed increases to 8m/s. the solar irradiation is constant. The excess power is transferred to the batteries.

(80-100s): The load demand and the wind speed increase to 1pu and 11.5m/s, respectively, while a sudden PVG shutdown occurs. In this interval two simultaneous changes are taken into account. The WEG supports all the load demand.

The system is stable during all the five intervals, as it is confirmed by the Δf index which is always less than 0.02. The DC bus voltage is sensitive to sudden changes in weather data and load, but it is still kept within the allowed range. Moreover, the AC voltage THD does not exceed 0.05.

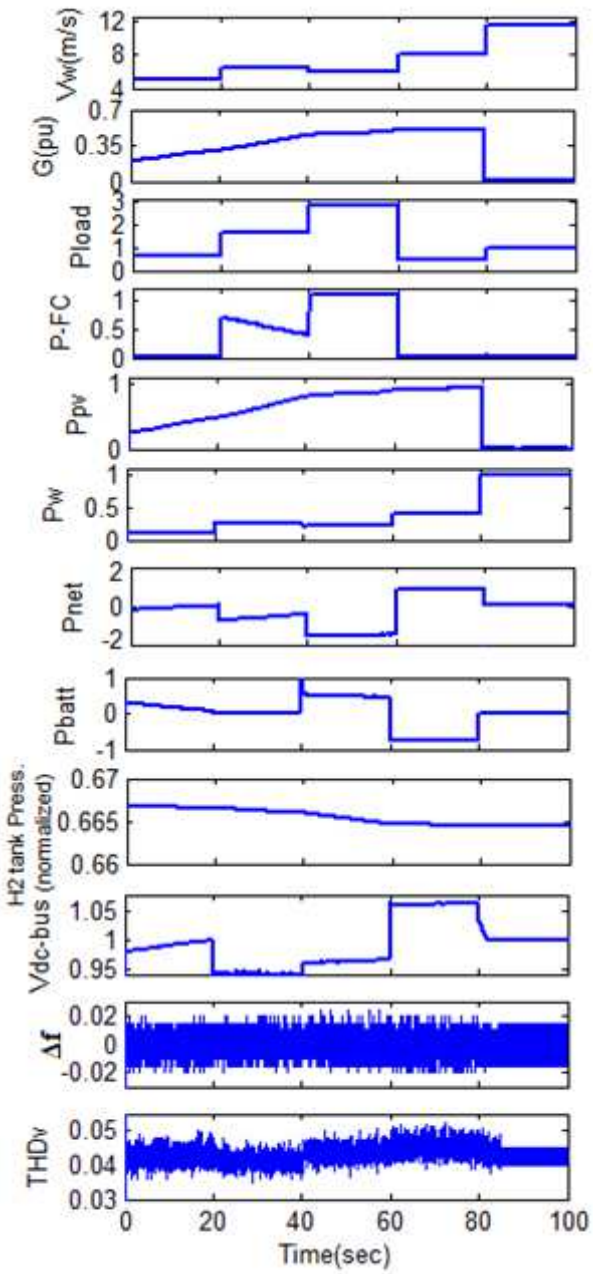

Figure 6.11. Case 2 - Time domain simulation

CASE 3: This case deals with zero power generation from WEG and PVG systems which means Pnet < 0 during all simulation test. Results of the time domain simulation is shown in Figure 6.12. The simulation test can be divided into three intervals:

(0-20s): The average load demand is about 0.2pu. As the power lack is small, it is compensated only by the batteries.

(20-80s): The load demand increases from 0.2pu to 1pu. According to power management strategy FC covers the lack of power during those periods, while the power drawn from batteries

is less than 0.1pu just to maintain the DC bus voltage in the designed range. The H_2 storage tank pressure decreases as the H_2 is pumped out.

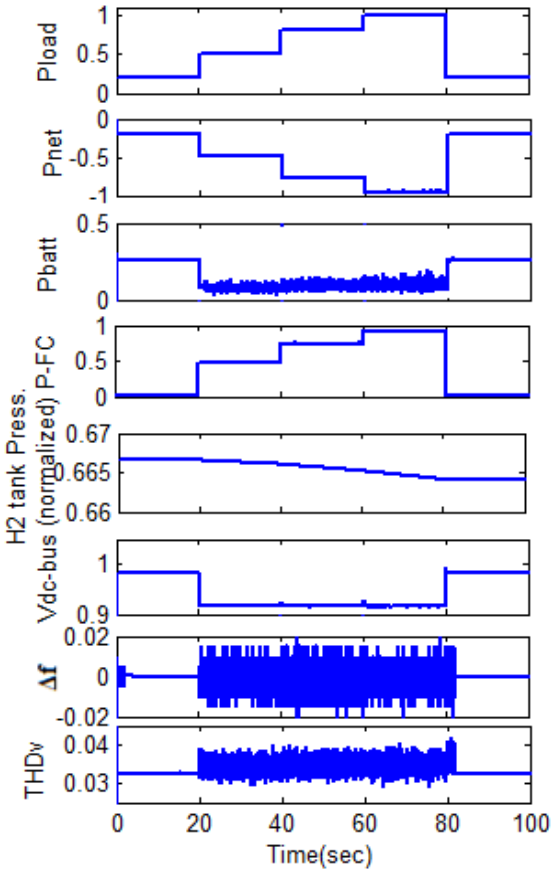

Figure 6.12. Case 3 - Time domain simulation

(80-100s): The load demand decreases again to 0.2pu. As the power lack is small, it is compensated only by the batteries. The storage tank pressure keeps constant as no H_2 is pumped out or pumped in.

The system is stable during all the intervals, as it is confirmed by the Δf index which is always less than 0.02. The DC bus voltage decreases suddenly as the FC stack covers the power lack, but it is still kept within the allowed range. Moreover, the AC voltage THD does not exceed 0.05, which is a standard requirement [85], all over the five intervals of the three cases.

6.5.3 Comparison between the FL based strategy and a conventional one based on a deterministic approach.

This simulation aims to compare the FL controller with a more conventional controller.
The performance of the developed FL based management strategy has been compared to that obtained by an optimally tuned conventional one. The last being implemented through deterministic management rules. Besides the performance indexes used in the FL based management in *section 6.5.2*, considered energy management performances indexes are:

- The amount of H_2 consumption by fuel cell,
- The amount of H_2 generated from Electrolyser and
- Final battery state of charge (SOC).

The designed dynamic model is not able to deal with long time simulation that is important to show up the energy performance. In order to overcome this problem 1728 seconds are used to simulate 24 hours of hourly average load demand for two residential users in Italy as well as real weather data measured in CNR-ITAE/Messina, Italy for a typical winter day: hourly average wind speed, hourly average solar radiation and hourly average ambient temperature.

The total hourly average residential load demand for one home in Italy in the cold season is shown in Figure 3.3 and weather data for a typical day in December are shown in Figures 3.4, 3.5 and 3.6.

Figure 6.13 shows the main benefits of the FL based management which are: a reduction of the fuel cell stack H_2 consumption, an higher amount of H_2 generated from Electrolyser, and an higher final battery SOC.

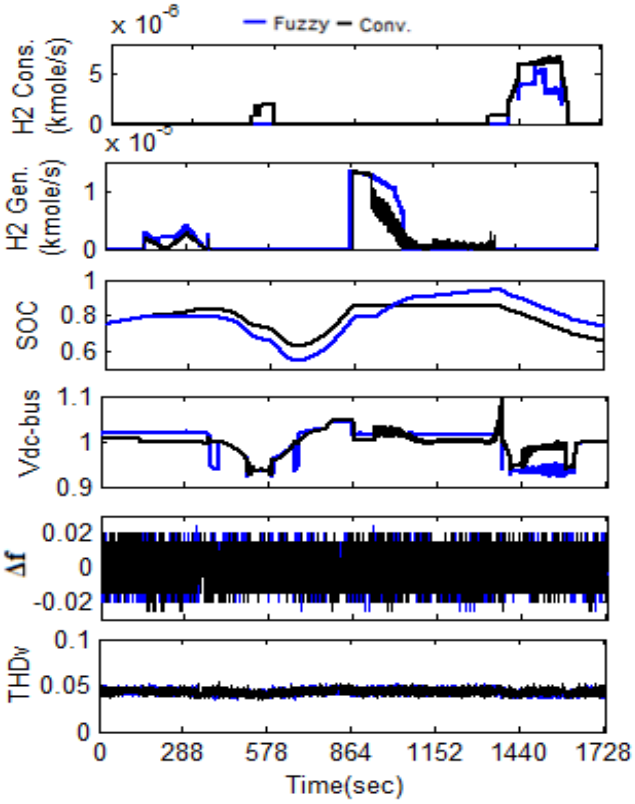

Figure 6.13. Simulation results of comparison study between FL based management and conventional controller

According to Figure 6.13 a great matching is obtained in THD, frequency deviation in both cases. The DC bus voltage in both cases is stable with dips and rises in some intervals but still within the accepted range.

It is worth to note that the conventional controller is optimally designed in order to perform a fair comparison with the FL controller. This is clear from the results obtained in the simulation test shown in Figure 6.13, which shows great matching in power performance indexes like stability of DC bus voltage, frequency deviation, and THD.

The comparison shows the superiority of FL controller to the conventional controller in terms of H_2 consumption and generation as well as the final SOC of battery.

6.6 Conclusion

- A FL approach has been proposed to the design of a power management strategy for a standalone hybrid system encompassing a WEG, a PVG, and a FC/E-ESS.

- The management approach based on fuzziness in values of excess/lack power, DC bus voltage, battery SOC, and H_2 storage tank capacity offers more realistic and practical decisions compared with conventional management based on deterministic logical rules.

- FL based management controller optimizes the energy generation and conversion in the single components (FC/E- ESS).

- Time domain stability analysis has been implemented to check the consistence of the developed strategy in different operating conditions. Simulation results confirm the effectiveness of the proposed power management strategy, providing the ground for the practical realization of a fuzzy logic based control system.

- The efficiency of the developed fuzzy logic controller is compared to that of a more conventional controller taking into account the fuel cell H_2 consumption, the amount of H_2 generated from the Electrolyser and the final battery SOC.

Part II

Sizing Step up Transformers for Grid Connected Wind Farms

Chapter 7

A Probabilistic Approach to Size Step-Up Transformers for Grid Connected Wind Farms

This chapter presents a general design methodology to optimally size step-up transformers for 4.5 MW grid connected wind farms with/without ESS on the basis of the statistical distribution of the wind energy in the selected site and the mathematical model of the plant.

The methodology is based on a probabilistic approach based on the evaluation of the so called LPPP (Loss of Produced Power Probability) index. The internal rate of return (IRR) and discount payback period (PBP) are utilized as economical indexes.

7.1 Introduction

On large wind farm plants directly connected to the medium voltage utility grid, a step-up transformer is required to boost the inverters output voltage from the low voltage range (380÷690) V to the medium voltage range (13.8÷46) kV as shown in Figure 7.1.

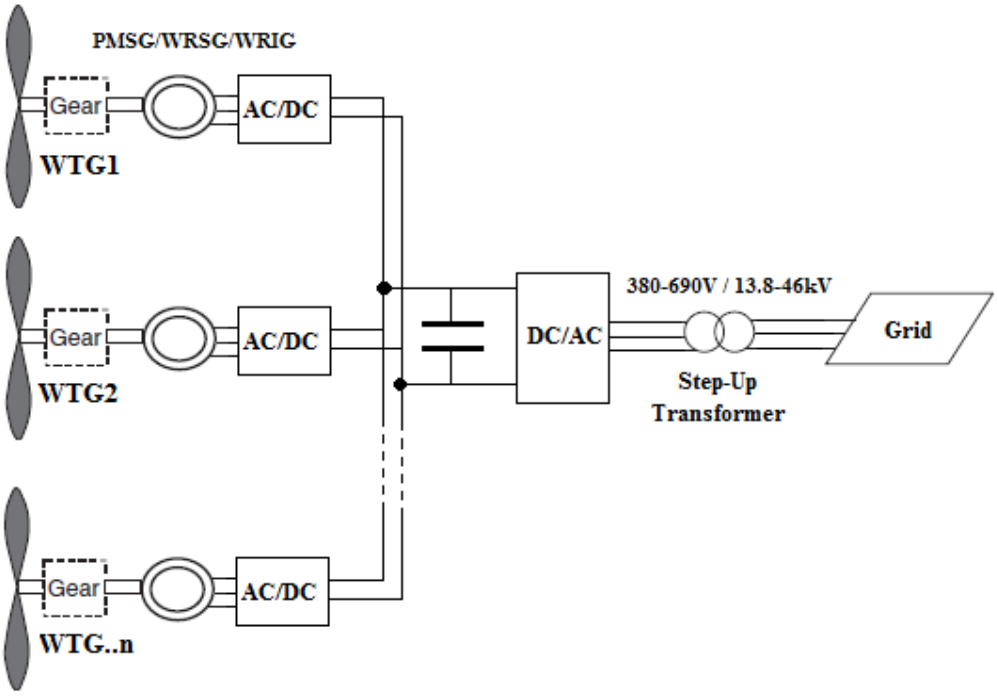

Figure 7.1. Schematic of the considered wind farm plant

The step-up transformer is a key element of a wind farm power system, as it processes the whole generated energy. Moreover, not only the efficiency and the cost are of primary concern, but also the influence of the transformer size either on the amount of energy delivered to the main utility, either on the stability of the network. In fact, while selecting a transformer rated power close to the wind farm peak power makes theoretically possible to fully transfer the captured wind energy to the utility network, such a design criterion will in practice lead to oversize the transformer, power converters and the power lines. Moreover, a too large transformer would operate for long times at a reduced efficiency, while generating a largely unpredictable power injection on the main grid. The last may lead to grid instabilities, causing frequent plant shutdowns, and requiring a remarkable reserve power to be provided by conventional generators. On the other hand, a too small step-up transformer would constitute a bottleneck, preventing an optimal exploitation of the solar energy.

To improve the reliability of wind farm plants resulted from the stochastic nature of the wind energy, some forms of energy storage system can be introduced. This may also enable highly remunerative new functions, such as peak shaving, load shifting, and utility grid power quality control. Several traditional energy storage technologies have been considered to accomplish this task. Among them: pumped hydroelectric storage, batteries and compressed air energy storage. Some advanced technologies have been also developed in the last years including: flywheels, superconducting magnets, fuel cells with electrolysers and redox flow cells.

Sizing of step-up transformer becomes more complex when considering plants with energy storage capabilities, as an optimal solution must be detected taking also into account the cost of the energy storage system, losses and their effects on the cost and efficiency of the whole system.

The aim of this work is to develop a general methodology to accomplish an optimal sizing of step-up transformers for grid connected wind farm plants, either directly delivering power to the utility network, either equipped with energy storage systems.

Common methods used to select the size of transformers equipping wind farm plants are based on deterministic approaches, fairly resulting in oversized designs. Therefore, a new probabilistic approach is carried out in this chapter based on an analysis of the LPPP (Loss of Produced Power Probability) index. Such an approach has been derived from the well-known LPSP (Lost of Power Supply Probability) technique used on PV plants operating in island mode [86, 87].

7.2 Schematic of the Proposed Wind Farm

Figure 7.1 shows a schematic of the wind farm considered in this study. This section illustrated the main components of the electrical system.

- Wind Turbine Generator (WTG)

The wind turbines can be classified into four types [88]:

Type A: Fixed speed with asynchronous squirrel cage induction generator (SCIG) and it is directly connected to grid via a transformer. It doesn't support any speed control.

Type B: Limited variable speed, it uses a wound rotor induction generator (WRIG) and it is directly connected to grid. A capacitor bank performs the reactive power compensation.

Type C: Variable speed with partial scale frequency converter. It corresponds to limited variable speed wind turbine with WRIG and known as the doubly fed induction generator (DFIG).

Type D: Variable speed with full-scale frequency converter corresponds to the full variable speed wind turbine, with the generator connected to the grid through a full-scale frequency converter. The frequency converter performs the reactive power compensation and a smooth grid connection. The generator can be excited electrically in wound rotor synchronous generator (WRSG) or WRIG) or by a permanent magnet in PM synchronous generators (PMSG) [89].

The WTG considered in this study belongs to the fourth generation Type D class.

- Power Electronics Converter

The introduction of any power electronic converter in a wind generation plant increases the costs, losses and harmonics, but has many significant advantages: Energy optimal operation, soft drive train, load control, gearless option, reduced noise, controllable active and reactive power, local reactive power source, improved network (voltage) stability, improved power quality [88,90].

In Figure 7.1, each wind turbine is connected to a three phase rectifier, while a common high power inverter is connected to the DC bus. The converters power losses can be computed according to efficiency diagrams as that of Figure 7.2 which shows the typical efficiency of a high power inverter.

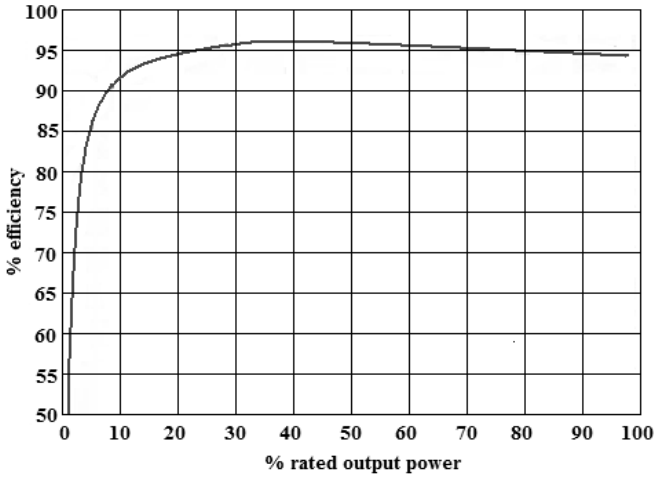

Figure 7.2. Typical inverter efficiency curve

- Step Up Transformer

Aero generators in a wind farm produce electrical energy at a low voltage (normally 690 V) which is transformed to a medium voltage (typical 20kV) by transformers which are usually of the dry type [91]. In this study the step up transformer is responsible for transforming the 575V low voltage to 25kV.

Two types of transformer losses are of major importance in determining the transformer efficiency: Core losses (no-load losses), which are the result of the cyclic magnetization/de-magnetization of the core during normal operations. They are constant and do not vary with load. The Coil losses (load losses) constitutes the second component of loss; it is a function of the resistance of the winding materials and varies with the load level and the temperature.

- Energy Storage System (ESS)

Vanadium Redox Batteries (VRB) have been selected among available energy storage systems to equip the considered wind farm plant. In a VRB-ESS the energy is transferred to the electrolyte, rather than being stored into the electrodes as in conventional batteries.

As a result, a VRB-ESS can be easily charged, discharged and recharged over 10,000 times (from 20% to 80% of the state of charge) with a high efficiency (65%÷ 75%), while ensuring a power availability greater than 98%.

Moreover, a VRB-ESS is easily scalable either in power, either in storage capability, respectively acting on the number of flow cells and the size of the electrolyte tanks. If compared with lead-acid batteries, VRB show some advantageous features, such as: compactness, shorter charge times, an increased discharge depth, longer lifetimes and lower maintenance costs. Moreover, VRB systems are suitable to perform either short time operations, such as compensation of load peaks and voltage drops, either medium or long time operations, as required by energy management strategies. More details about VRB-ESS are introduced in Chapter 2.

The ESS is normally connected with the system through bidirectional power electronic converter; this adds another costs and energy losses.

7.3 The Proposed Approach

Optimized designs can be theoretically carried out through probabilistic approaches, which make possible to determine the smallest (and thus the most economical) step up transformer able to deliver a given amount of energy to the utility grid on the basis of the size of wind farm and yearly wind speed of the selected geographical site.

In order to optimally determine the size of the step up transformer a probabilistic approach has been then developed to estimate the probability that the transformer is unable to deliver a part of the wind energy captured by wind turbines to the utility grid, due to power losses and/or transformer overloads.

The value assumed by the probabilistic LPPP index over a given observation time T, gives an estimation of the amount of energy converted by the wind farm but not delivered to the utility grid. It takes into account the energy lost due to the transformer efficiency, the energy lost due to the excess of produced power and converter losses. It may also take into account the presence of an ESS and limitations of the utility network in accepting the generated power due to grid stability reasons.

Once that the amount and the type of wind turbine is stated, the LPPP index can be computed as a function of the transformer rated power. In order to simplify the LPPP index analysis, it is assumed that the each rectifier rated power is equal to wind turbine rated power and the inverter rated power is equal to the transformer rated power.

The amount of energy produced from the proposed wind farm over each interval is computed through the annually average wind data measured in CNR/ITAE of Messina/Italy using the power curve of the wind turbines provided from the manufacturer. In this study, the wind farm consists of a set of 9 wind turbines each one rated at 500kW.

According to Figure 7.1, the wind turbines are connected to the step-up transformer through power electronic converters. The ESS is connected to DC bus through a bidirectional converter whose power losses can be computed according to its typical efficiency curve. Two configurations are investigated in this study:

7.3.1 Wind Farm Without ESS

The selection of step-up transformer for a wind farm plant without ESS is evaluated taking into account the following costs.

A. The initial cost of the step-up transformer and power electronic converters

The customer price of step up transformers can hardly be estimated. In fact, they often are custom built units with unlisted prices. Only considering commercial off the shelf transformers and neglecting taxes and marketing markups, the cost curve of Figure 7.3 can be considered, as function of the rated power.

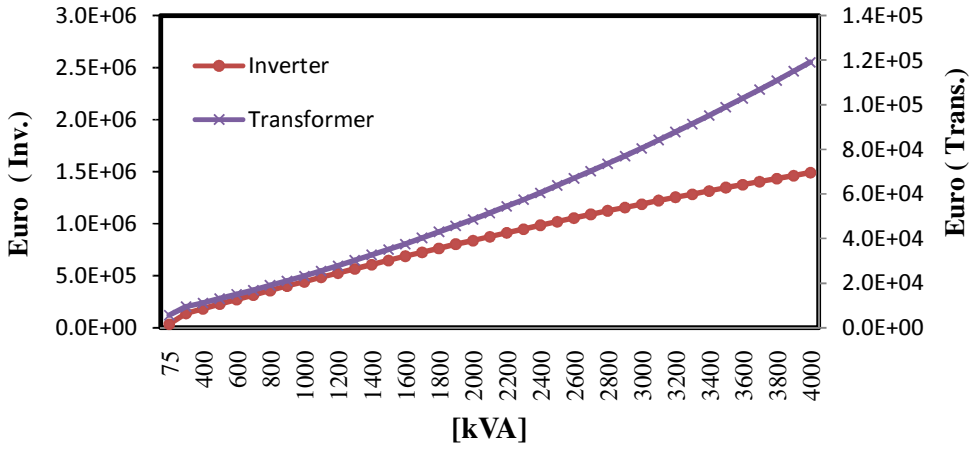

Figure 7.3 Step up transformer and inverter initial costs

Main contributions to the final cost are given from manufacturer selling price, shipping and installation costs. Moreover, as the size and the cost of the inverter serving the plant are also closely related to the transformer rated power, a specific cost function, shown in Figure 7.3 is assumed. The cost of the rectifiers attached to each wind turbine is obtained from Figure 7.3 assuming that it resembles the cost function of the inverter.

B. The cost of the energy wasted due to transformer overloads and efficiency

To accomplish the LPPP analysis over a given time window T, the last is divided into N intervals, each one Δt=T/N long. Typically, these intervals are taken to be of one hour duration. It is assumed that if the average input power during the k-th interval is greater than 110% of the transformer rated power, the excess power is lost as it cannot be processed. For each k-th time interval the transformer overload power losses is computed according to eq. (7.1)

$$P_{OL}(k) = [P_i(k) - 1.1P_n(k)\,] \qquad (7.1)$$

Where Pn is the transformer rated power and Pi(k) is the average input power during k-th interval.

The power wasted due to no load and copper losses during the k-th interval can be computed through eq. (7.2), assuming constant the amplitude of the inverter output voltage:

$$P_d(k) = P_v + (P_c/P_n^2) * P_i^2(k) \qquad (7.2)$$

Where P_v represents the no-load losses and Pc the rated copper losses.

Copper losses can be simply referred to an average operating temperature, or, more precisely, computed from an estimated operating temperature profile on the basis of the estimated ambient temperature and the load. Cooling power and stray power losses can be also considered for a better precision.

Considering a 4.5MW peak power wind farm plant, the transformers whose main data are summarized in Table 7.1 have been selected for comparison. To simplify the comparison only single units are considered, working at unity power factor. However, the proposed approach can be easily generalized to transformer banks working at an arbitrary power factor.

Table 7.1 : Step up Transformer Main Data

Rated power [kVA]	Pv[kW]	Pc[kW]
250	0.52	2.6
400	0.74	3.62
600	1.04	5.20
1000	1.3	8.97
1600	2	13.00
2000	2.4	16.08
2500	2.78	18.62
3750	3.8	25.46

C. The cost of energy wasted due to power electronic converters

The power electronic converters losses are obtained by summing the power losses of the rectifiers and inverters connected to each wind turbine:

$$P_{Conv-No\ ESS}(k) = \left[P_{rectifiers}(k) + P_{inverter}(k)\right] \quad (7.3)$$

According to the flowchart sketched in Figure 7.4, it is assumed that if Pi(k) is less than 1.1Pn, the LPP is computed as:

$$LPP(k) = [P_d(k) + P_{Conv-No\ ESS}(k)]\Delta t \quad (7.4)$$

While if it is greater than 1.1Pn, the energy delivered to grid is limited to 110% of the transformer rated power, in order to avoid heavy overload conditions. Therefore, the excess power is lost. To account for these losses, the LPP over the k-th interval is computed as:

$$LPP(k) = [P_{OL}(k) + P_d(k) + P_{Conv-No\ ESS}(k)]\Delta t \quad (7.5)$$

The value of the LPPP index is then determined as follows:

$$LPPP = \sum_{k=1}^{N} \mathrm{LPP(k)} / \sum_{k=1}^{N} \mathrm{P_i\,(k)} \quad (7.6)$$

The LPPP index is ideally zero when, at least theoretically, the wind energy converted over a day by the wind farm is fully delivered to the utility grid. The lost energy and the associated loss of profit can be evaluated as follows:

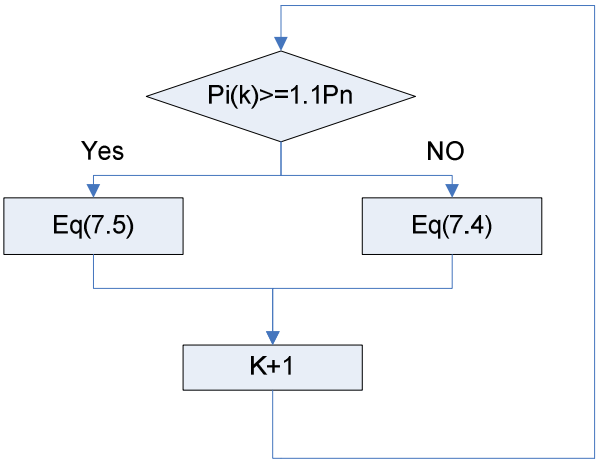

Figure 7.4. Flowchart of the LPP algorithm without ESS

$$E_W = \sum_{k=1}^{N} LPP(k) \quad (7.7)$$

$$C_{EW} = \sum_{k=1}^{N} C_e(k) LPP(k) \quad (7.8)$$

Where $C_e(k)$ is the energy selling price per kWh during the k-th interval. The selling price can be considered constant, or variable according to the rules of the modern energy market.
The energy effectively delivered to the network E_{grid} and the proceeds from the sale of this energy can be computed as:

$$E_{grid} = \sum_{k=1}^{N} [P_i(k)\Delta t - LPP(k)] \quad (7.9)$$

$$C_E = \sum_{k=1}^{N} C_e(k)[P_i(k)\Delta t - LPP(k)] \quad (7.10)$$

The load factor (LF) is a quality figure defined as the ratio between the energy yearly produced by the plant and what would be ideally produced by always operating the system at the rated power. It can be computed according to the following equation:

$$LF = E_{grid}/(P_n * 8760) \quad (7.11)$$

7.3.2 Wind Farm Plant With ESS

The cost of the energy storage system must be added to the other costs discussed in section 7.3.1. A cost curve for large VRB-ESS is shown in Figure 7.5 [92].

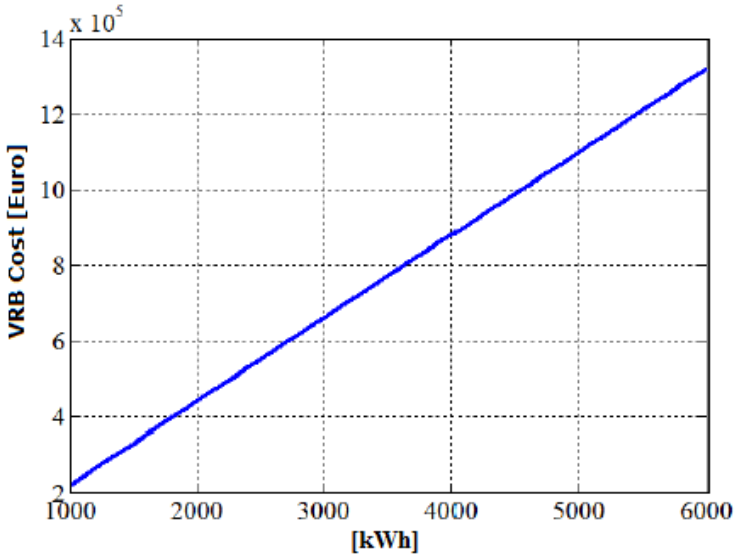

Figure 7.5. VRB Energy Storage System initial cost.

The power electronic converter losses shown in eq. (7.3) must be modified to include the losses of the ESS bidirectional converter ($P_{bi-conv.-ESS}$) as shown in eq. (7.12):

$$P_{Conv-ESS}(k) = \left[P_{rectifiers}(k) + P_{inverter}(k) + P_{bi-conv.-ESS}(k)\right] \qquad (7.12)$$

The LPP algorithm must be suitably modified as shown in Figure 7.6.

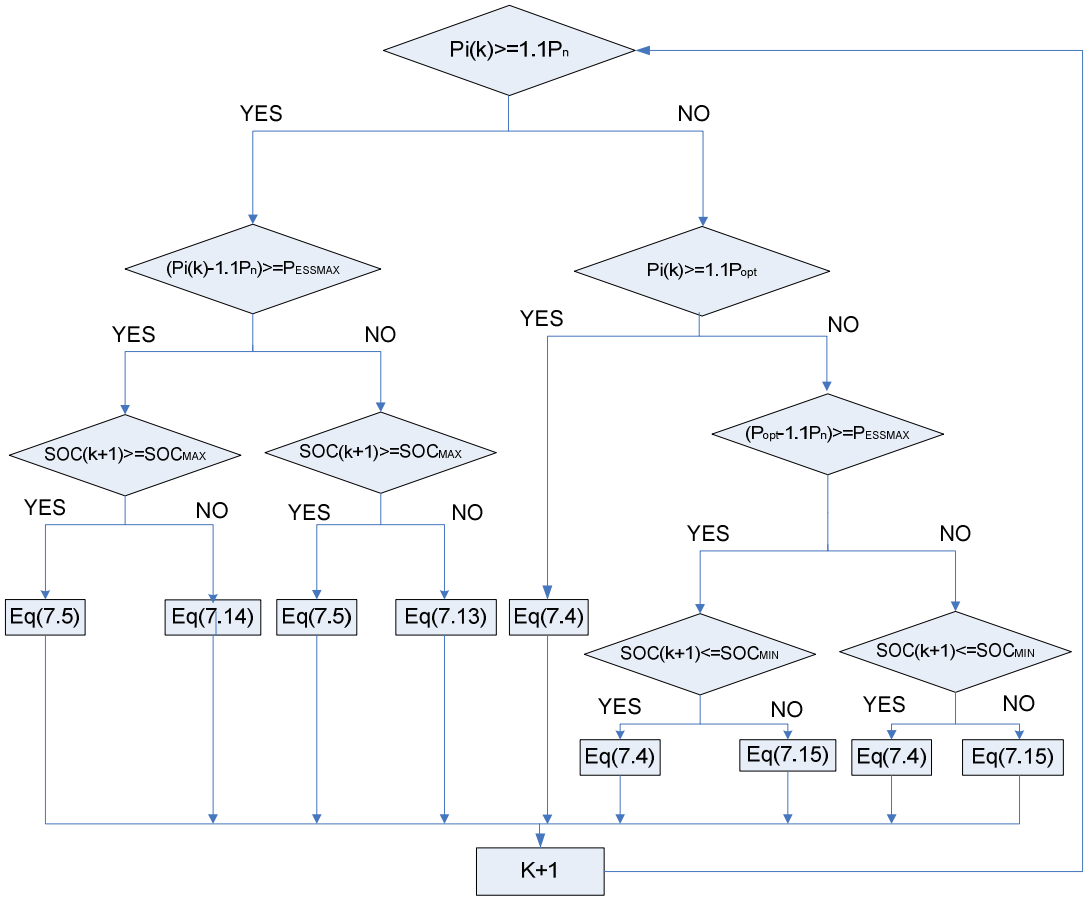

Figure 7.6. Flowcharts of the LPP algorithm calculation with BSS

In this case, if Pi(k) is larger than 1.1Pn and the state of charge (SOC) of the ESS is lower than 100%, the excess energy is not lost, as it can be stored into the ESS, taking into account the charge efficiency. The state of charge of the ESS is then suitably increased through a mathematical model of the specific ESS considered, and the LPP is computed as:

$$LPP(k) = \left[P_{OL}(k)(1-\eta_c) + P_a(k) + P_{Conv-ESS}(k)\right]\Delta t \qquad (7.13)$$

Where η_c is the ESS charge efficiency.

When the SOC reaches its maximum value, the ESS cannot be charged anymore and the LPP is then computed as in eq. (7.4):

However, if the excess power outreaches the ESS maximum power P_{ESSMAX} the surplus power is anyway lost. In this case the LPP is computed as:

$$LPP(k) = [P_{OL}(k) - P_{ESSMAX} + P_{ESSMAX}(1 - \eta_C) + P_d(k) + P_{Conv-ESS}(k)]\Delta t \quad (7.14)$$

If, in the last case, the SOC also reaches its maximum value, the LPP must be computed as in Eq. (7.4).

If $P_i(k)$ is lower than the transformer rated power, some energy can be drawn from the ESS to keep the transformer at the maximum efficiency working point at power P_{opt}. In this case, if the difference between the optimal power P_{opt} and $P_i(k)$ is greater than P_{ESSMAX} then the SOC of the ESS is decreased and the LPP is computed as shown in eq. (7.15):

$$LPP(k) = \left[\left(P_{opt} - P_i(k)\right)(1 - \eta_D) + P_d(k) + P_{Conv-ESS}(k)\right]\Delta t \qquad (7.15)$$

Where η_d is the ESS discharge efficiency and P_{opt} is maximum efficiency working point of the transformer.

Differently, if the SOC has reached its minimum level, then the LPP is computed using eq. (7.4).

If $P_{opt} - P_i(k)$ is lower than P_{ESSMAX} the LPP is calculated using eq. (7.15).

If $P_i(k)$ is greater than P_{opt} but lower than 1.1 Pn, all the power is delivered to the utility network and LPP is computed according to eq. (7.4). If $P_i(k)$ is lower than P_n and the SOC is close to the minimum allowable value, the LPP is computed according to eq. (7.4).

7.4 Sizing Step-Up Transformers Analysis

The proposed approach is exploited to size a step-up transformer for a 4.5MW grid connected wind farm. Technical and economical analysis is jointly used to accurately select the most feasible alternative.

The Technical Approach is based on a minimization of losses concept, i.e. low LPPP. This approach is illustrated in the previous sections through the flow chart depicted in Figures 7.4 and 7.6.

Although the data of any kind of transformer can be taken in to account, in order to simplify the application of the proposed approach only transformers whose rated power ranges from 1.2MVA to 4.5MVA, with steps of 0.1MVA, have been considered, all featuring Pc/Pv=5. Moreover, only single units are considered, working at unity power factor.

The low value of LPPP index and high amount of harvested yearly grid energy are good indication about the effectiveness of the transformer selection, but the last decision must be based on economical profitability indexes.

The Economical Analysis is significantly based on technical analysis and all costs are taken into account. The profitability of the selection is calculated using two important economic indexes:

- Discounted Payback Period (PBP):

It refers to the time required to recover the initial investment considering the time value of money, it may be defined also as a capital budgeting procedure used to determine the profitability of a project. It is calculated by dividing the investment costs over the annual cash inflow.

This method ignores any benefits that occur after the payback period and, therefore, does not measure profitability, for this reason other method of capital budgeting like internal rate of return is included in this study.

- The Internal Rate of Return (IRR) :

It is defined as annualized effective rate of return that makes the net present value of all cash flows from a particular investment is equal to zero.

$$\mathrm{IRR} = 1 + \frac{\mathrm{NPV}}{\mathrm{I}} \qquad (7.15)$$

Where NPV is the net present value. It is defined according to the following expression:

$$\mathrm{NPV} = \sum_{i=1}^{l} (\mathrm{CF_i})_{\mathrm{dis}} - \mathrm{I} \qquad (7.16)$$

Where $(CF_i)_{dis}$ is the discounted cash flow in the i^{th} year and I is the investment cost. The annual revenues are calculated on the basis of the value of green energy in the Italian electricity market. The economic parameters are shown in Table 7.2:

Table 7.2: Economic Parameter

Parameter	**Value (unit)**
Economic lifetime	20 years
Electricity price	0.30 €/kWh
Discount rate	5%
Depreciation	9%

7.4.1 Sizing Step-up transformers for Wind Farm plants without ESS

Simulation results:

Figure 7.7 shows the simulation results to find out the optimum size of the step up transformer of a 4.5MW grid connected wind farm plant without ESS.

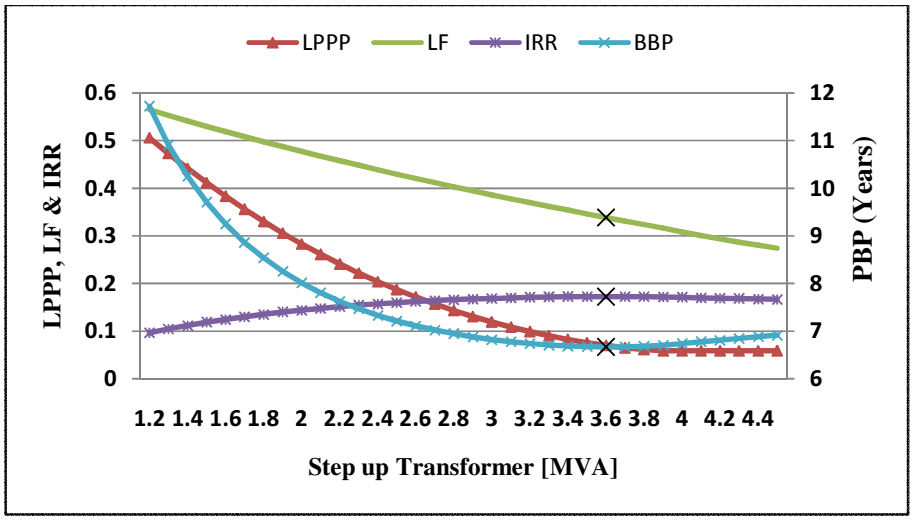

Figure 7.7. LPPP, LF, IRR and PBP with different capacities of step-up transformer

The optimum size of the step up transformer is 3.6 MVA and this is indicated in the figure by symbol (x). The optimum point presents the highest value of IRR and lowest value of PBP.

The LPPP decreases notably as the rating of the step-up transformer increases and this continues until reaching the optimum selection point indicated by symbol (x) in Figure 7.7, after this point, LPPP continues to slightly decrease, not affecting the economic indexes. This is considered an indication that LPPP is not the only dominant factor in the sizing methodology.

The load factor at the optimum selection point is about 33.8% which is not high enough. In this application the load factor is an indicator of how much the optimum selection of the transformer is compatible with the amount of energy transmitted to grid.

Sensitivity analysis:

The influence of the cost of energy and the site of wind farm on the feasible selection of step-up transformer for wind farm grid connected is investigated in this section.

- *Sensitivity analysis to selling price of green energy.*

Three different economical analyses with three different green energy selling prices have been performed to size the step up transformer of a 4.5MW grid connected wind farm plant without ESS. The green energy selling price rates are: 0.3, 0.35 and 0.4 €/kWh.

The cross symbol (x) in Figure 7.8 shows the optimum selection capacity of the step-up transformer which corresponds to the highest IRR and the lowest PBP in the three cases.

It is obvious from Figure 7.8 that values of economical indexes are significantly affected by the price of energy but the best profitability index always occurs at the same step-up transformer capacity which is 3.6MVA.

This is a good indication that the optimum selection of step-up transformer for wind farm grid connection doesn't depend on the price of energy.

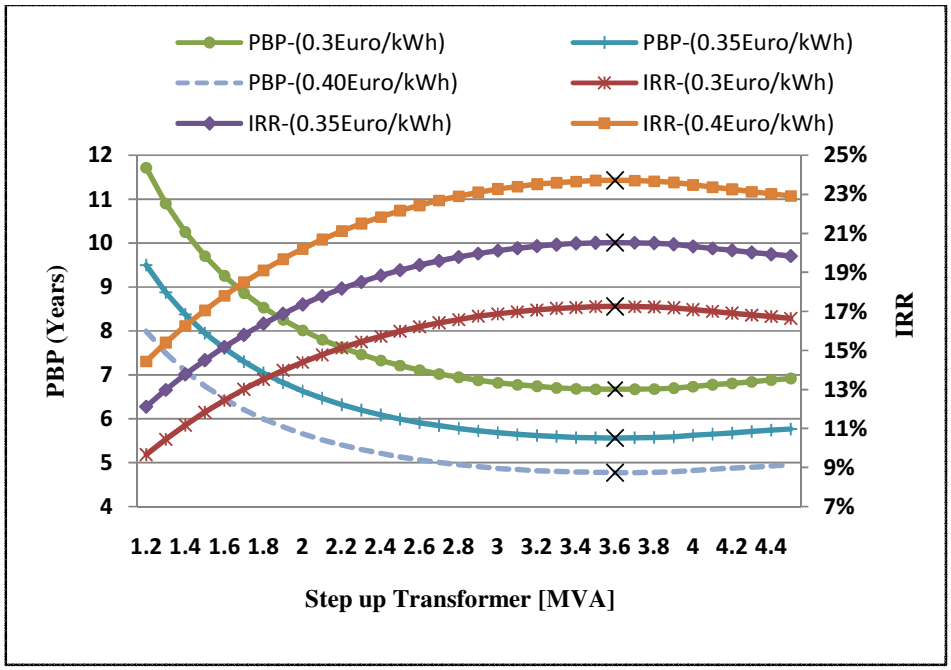

Figure 7.8. Sensitivity Analysis of Step-up transformer selection with energy cost

- *Sensitivity analysis to wind data variation*

For further analyses, the sensitivity of wind data variation (different sites) on the optimum size of the step up transformer of a 4.5MW grid connected wind farm plant without ESS is investigated. For this purpose, three sets of simulations have been run using three different wind data, economical analysis for each set has been performed to find the optimum size of the transformer.

To obtain three different wind data, the main data have been multiplied by a suitable factor: 0 variance factor, which means no variation to the original wind data. 1.30 and 0.7 variance factors which led to the wind data being multiplied by 1.30 and 0.70, respectively.

Figure 7.9 shows the influence of wind data variation on the selection of the step-up transformer. The symbols shows the optimum selection which corresponds to the highest IRR in each case.

As depicted from Figure 7.9 the wind data variation has significant effect on the optimum selection of the step-up transformer. The optimum step-up transformer size is 3.1MVA, 3.6 and 3.8 MVA in case of 0.7, 0 and 1.3 multiplication variance factors, respectively.

The economical indexes are extensively influenced by the variation in wind data as they directly affect the produced energy. The rising in wind speed improves IRR as shown in Figure 7.9.

The load factor is significantly affected by the wind data variation; this is clear from Figure 7.9 which shows that the load factor is positively related with wind speed. The LF at optimum points is 21.7%, 33.8% and 44.5% in case of 0.7, 0 and 1.3 multiplication variance factors, respectively.

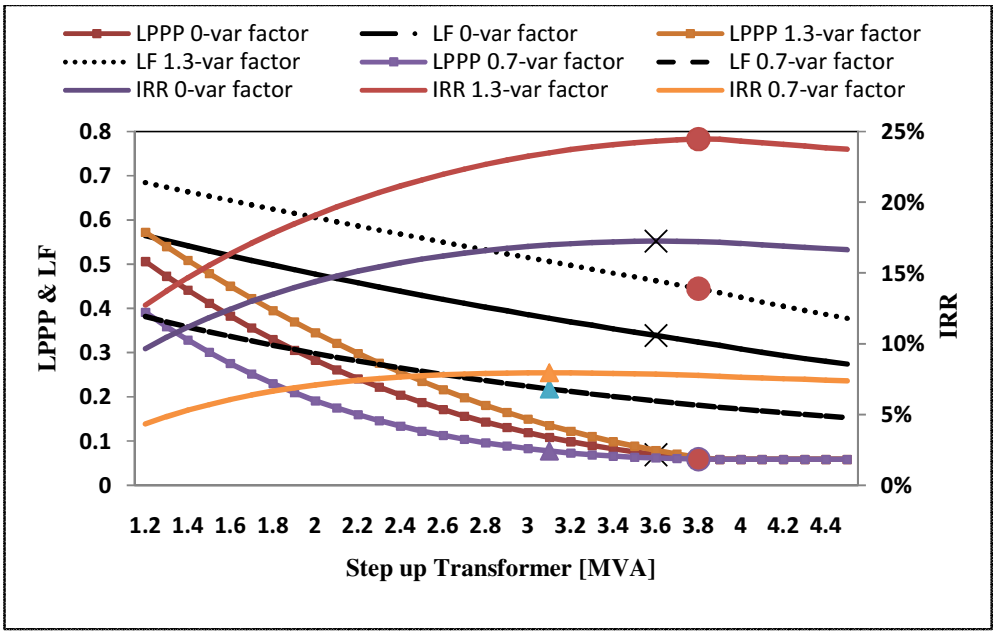

Figure 7.9. Sensitivity Analysis of Step-up transformer selection with wind speed variation

The LPPP is generally reduced with the reduction in wind speed, but the value of LPPP is not the only factor in sizing the step up transformer.

7.4.2 Sizing Step-up transformers for Wind Farm plant with ESS

In this section, the simulation results of sizing the step up transformer of 4.5MW grid connected wind farm with ESS. This analysis aims to find the effects of introducing an ESS on the optimum size of the step up transformer as well as on the load factor.

Simulation results:

Figure 7.10 shows the economical indexes (IRR and PBP) featured by different step-up transformers and VRB-ESS capacity combinations.

Transformer ranging from 1.2MVA to 4.5 MVA are considered for the same 4.5MW wind farm plant previously examined. Three different sizes of the VRB-ESS are considered, namely: 1500, 1000, 500kWh, moreover also the no ESS configuration is considered for comparison. The cross symbol (x) shows the optimum size of the step up transformer corresponding to the different capacities of ESS. It is shown that increasing ESS capacity reduces the corresponding optimum size of the step up transformer, for example the optimum size of step up transformer at 1500, 1000, 500kWh is 2.2, 2.5 and 3MVA, respectively. The capacity of the optimum step up transformer at zero ESS is 3.6 MVA.

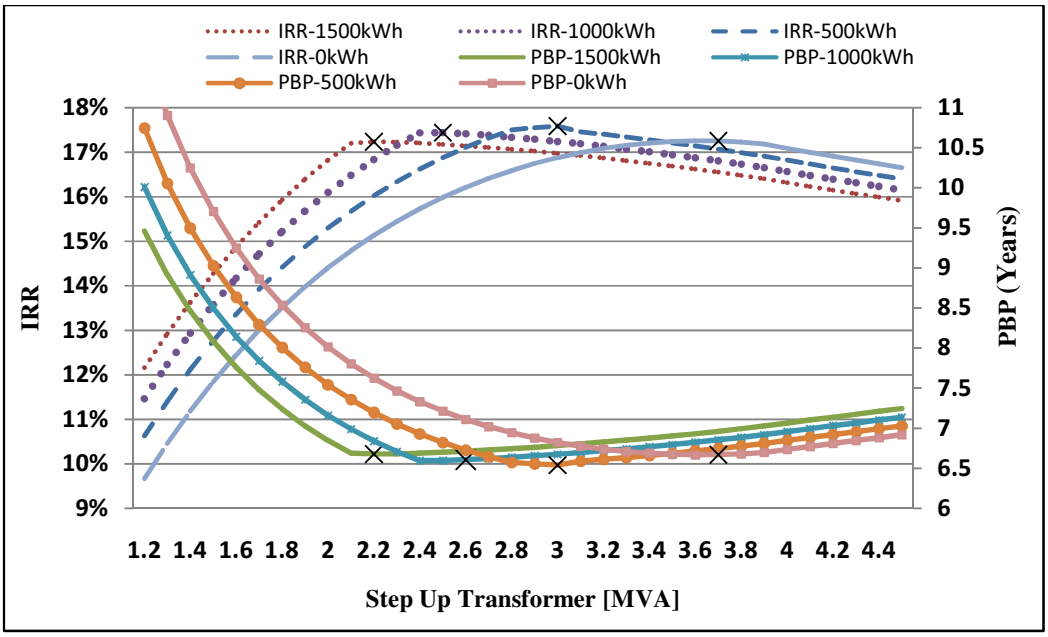

Figure 7.10. IRR and NPV versus step-up transformer ratings at different BES capacities

Figure 7.10 reveals that the optimum size of the step up transformer is 3MVA at 500kWh as IRR is the highest and PBP is the lowest among the different alternatives.

Figure 7.11 shows the LPPP and Load factor (LF) with corresponding step-up transformer at different ESS capacities, the markers on the figure shows the values of LPPP and LF at the corresponding optimum size of the step up transformer.

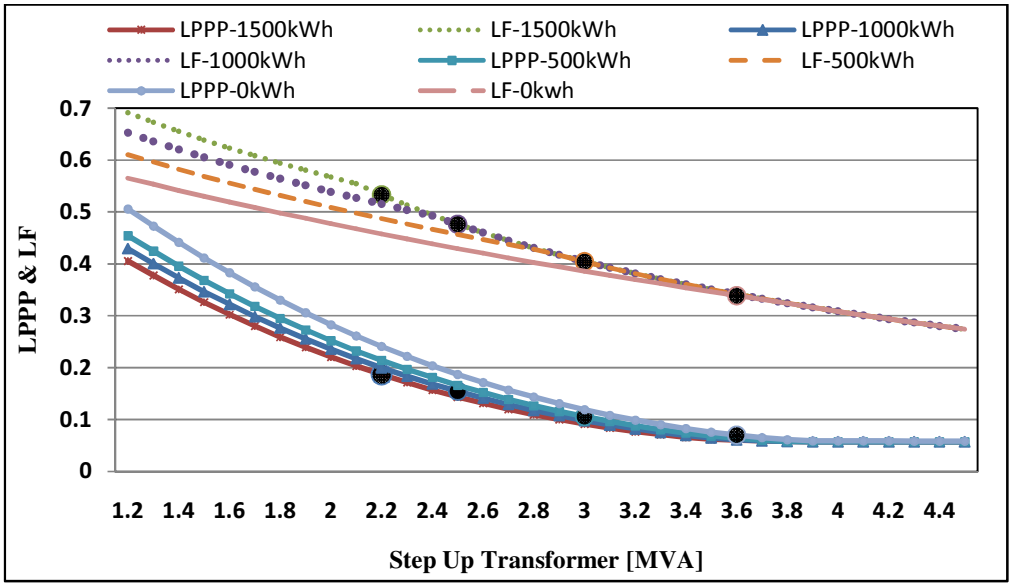

Figure 7.11. LPPP and load factor (LF) versus step-up transformer ratings at different BSS capacities

There is a strong relationship between the value of LPPP and the optimum size of transformer but

this is not the only factor that determines the optimal size between different alternatives as the economical indexes depend also on other factors such as the costs of the equipments.

The load factor (LF) is directly related to the installed capacity of ESS: this is clear in Figure 7.11 which illustrates that increasing the capacity of installed capacity of ESS improves the LF. The LF at the optimum selection of step up transformer is 40% which is accord with the standard load factor of wind power plants.

Sensitivity analysis:

The influence of the selling price of green energy and the wind farm site on the feasible selection of step-up transformer of a 4.5MW grid connected wind farm with 500kWh ESS is investigated in this section. A 500kWh ESS capacity is taken as a reference for this analysis as the optimum size of the transformer is verified at this capacity as already illustrated in the previous section.

- *Sensitivity analysis to selling price of green energy.*

Figure 7.12 describes the economical analysis for step-up transformer selection under three different selling cost rates of green energy: 0.3, 0.35 and 0.4 €/kWh using 500kWh as ESS.

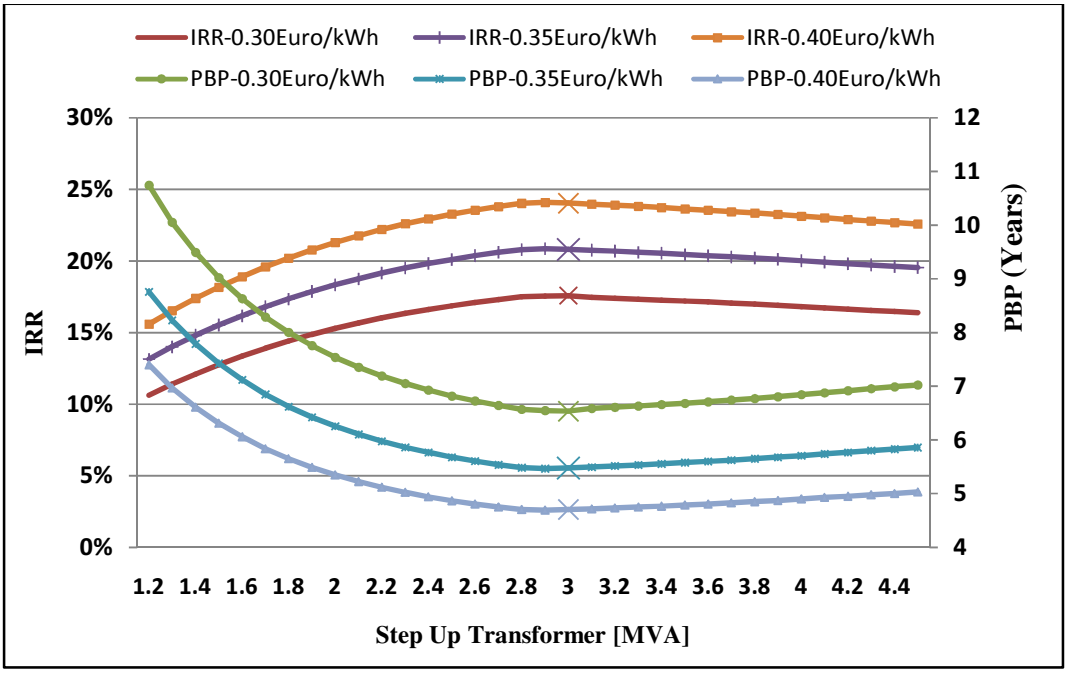

Figure 7.12. Sensitivity Analysis of Step-up transformer selection with different green energy prices

The cross symbol (x) shows the capacity of step-up transformer which corresponds to the best IRR and PBP in the three cases, the optimal selection in the three cases is 3MVA. This indicates that the optimum selection of the step up transformer of a grid connected wind farm with ESS is not sensible to the price of selling energy.

The variations of energy price affect the values of economic indexes but not the selection of the optimum step up transformer. These results agree with the results obtained in case of a grid connected wind farm plant without BSS.

- *Sensitivity analysis to wind data variation*

The same procedure is followed as in the case of a grid connected wind farm without ESS and the same three sets of wind data are also used in this analysis. A 500kWh ESS capacity is taken as a reference for this analysis.

Figure 7.13 shows the influence of wind data variation on the optimum selection of step-up transformer using a 500kWh BSS.

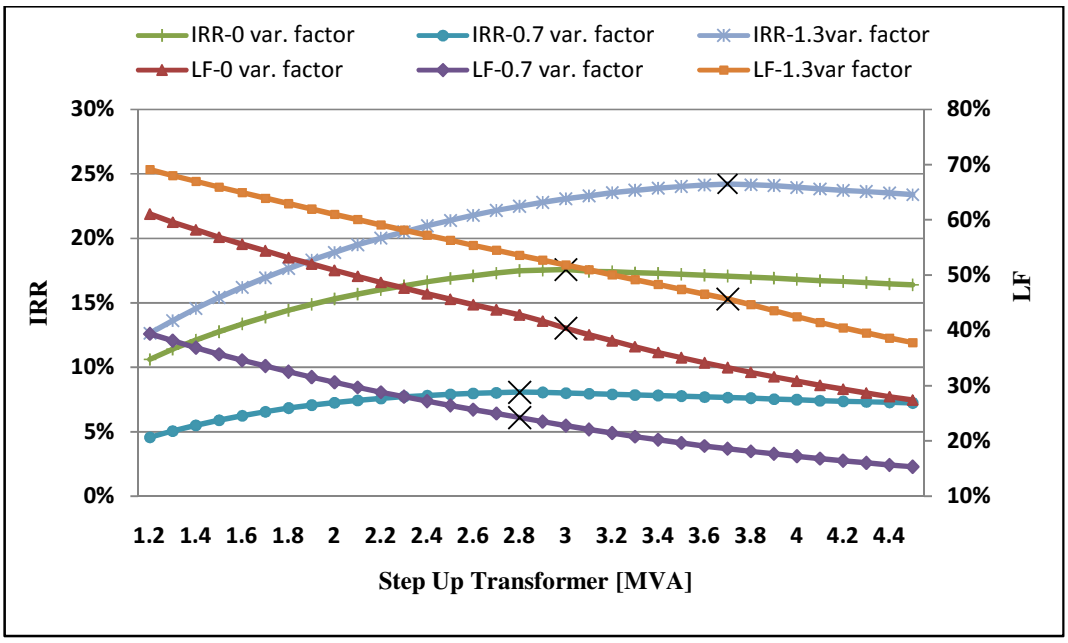

Figure 7.13. Sensitivity Analysis of Step-up transformer selection at different wind speed

The cross symbol (x) in the Figure 7.13 shows the feasible selection capacity of step-up transformer which corresponds to the best IRR in the three cases.

As depicted from Figure 7.13 the wind data variation has significant effect on the optimum selection of the step-up transformer. The optimum step-up transformer size is 2.8MVA, 3 and 3.7 MVA in case of 0.7, 0 and 1.3 multiplication variance factors, respectively.

The economical indexes are extensively influenced by the variation in wind data as it is directly affect the produced energy. The increase in wind speed improves the IRR.

The load factor is significantly affected by the wind data variation; this is clear from Figure 7.13 which shows that the load factor is positively related with wind speed.

7.5 Conclusion

- A general probabilistic methodology approach to accomplish an optimal selection of the rated power of step-up transformers in wind farm plants with or without energy storage systems has been presented.

- A correct selection of the size of the step-up transformer in a wind farm plant involves a deep analysis of the whole system, as several variables are related to the transformer rated power as: initial cost of the system, energy losses due to transformer efficiency, energy storage system efficiency and energy losses due to power electronic converters.

- The proposed approach is based on the evaluation of a probabilistic index LPPP to estimate the costs of energy losses related to the size of the transformer and the power and the storage capability of the ESS. Moreover, energy losses related to power electronic converters are also considered.

- Annual wind data measured at CNR/ITAE Messina/Italy are utilized in this study.

- When applying the presented methodology for sizing step-up transformer of a 4.5MW grid connected wind farm plant without ESS, it is found that the optimum size is 3.6MVA. In case of introducing ESS, it is found that the optimum size is 3MVA at 500kWh ESS.

- The introduction of ESS in wind farm plant has significant effect on the step-up transformer selection and improving the load factor (LF).

- The introduction of a 500 kWh ESS to the considered 4500 kW wind farm plant reduces the LPPP index but not significantly.

- The optimum selection of step up transformer is not sensible to price of produced energy but has a great sensitivity to wind data variation. However these parameters significantly affect the economic profitability values.

References

[1] International Energy Outlook 2010, Energy Information Administration (EIA), http://www.eia.gov/oiaf/ieo/electricity.html.

[2] World Crude Oil Prices, Energy Information Administration (EIA), http://www.eia.gov/dnav/pet/hist/LeafHandler.ashx?n=PET&s=WTOTWORLD&f=W

[3] Trends in photovoltaic applications: Survey report of selected IEA countries between 1992 and 2009, International Energy Agency Photovoltaic Power Systems Programme (IEA PVPS), August 2010.

[4] W. El-Khattam and M.M.A. Salama, "Distributed generation technologies, definitions and benefits ‘‘, Science direct, electric power systems research 71 (2004) 119–128.

[5] Global Power Source, Global Wind Energy Council, http://www.gwec.net/.

[6] El-Shater TF, Eskander M, El-Hagry M, "Hybrid PV/fuel cell system design and simulation", In: 36th intersociety energy conversion engineering conference, Savannah, Georgia, July 29–August 2, 2001.

[7] The Fuel Cell Today Industry Review 2011, Fuel Cell Today http://www. Fuelcelltoday .com/media /pdf/surveys/2011-Fuel-Cell-Patent-Review.pdf

[8] R. Messenger and J. Ventre, Photovoltaic Systems Engineering, CRC Press LLC, 2000.

[9] International Energy Agency (IEA): Trends in Photovoltaic Applications. Survey report of selected IEA countries between 1992 and 2003. Source: http://www.oja-services.nl/ieapvps/products/download/rep1_13.pdf.

[10] Texas State Energy Conservation Office, “Introduction to Photovoltaic Systems,” SECO Fact Sheet No. 11, p. 2, http://www.infinitepower.org/pdf/FactSheet-11.pdf. (Last visited August 1, 2011.)

[11] F. Iov, M. Ciobotaru, D. Sera, R. Teodorescu, F. Blaabjerg, Power Electronics and Control of Renewable Energy Systems, PEDS conference 2007 .

[12] Abou El-Maaty Metwally Metwally Aly Abd El-Aal, Modelling and Simulation of a Photovoltaic Fuel Cell Hybrid System, PhD Dissertation, Dissertation Day: April 15, 2005 Kassel, Germany, Faculty of Electrical Engineering University of Kassel.

[13] M.A.S. Masoum, H. Dehbonei and E.F. Fuchs, “Theoretical and experimental analyses of photovoltaic systems with voltage and current-based maximum power-point tracking,” IEEE Transactions on Energy Conversion, Vol. 17, No. 4, pp. 514 – 522, Dec. 2002.

[14] Hussein, K. H., Muta, I., Hoshino, T. and Osakada, M., “Maximum Photovoltaic Power Tracking: an Algorithm for Rapidly Changing Atmospheric Condition,” IEE Proc.-Gener. Transm. Distrib, Vol. 142, pp. 59_64 (1995).

[15] Chihchiang Hua, ‚Jongrong Lin, and Chihming Shen,“Implementation of a DSP Controlled Photovoltaic System with Peak Power Tracking”, IEEE transactions on industrial electronics, vol. 45, no. 1, February 1998 pp 99-107.

[16] American Wind Energy Association, The Most Frequently Asked Questions About Wind Energy (Washington, D.C., 1999), p. 1http://www.awea.org/pubs/factsheets/FAQ1999.PDF. (Last visited August 17, 2007.)

[17] Mukund R. Patel, Wind and solar power systems: design, analysis, and operation, CRC Mechanical Engineering Series, CRC Press, 2006, ISBN 9780849315701

[18] L. Barote, R. Weissbach, R.Teodorescu, "Stand-alone wind system with vanadium redox battery energy storage," in Proc. 2008 IEEE International Conference on Optimization of Electrical and Electronic Equipments, pp.407-412.

[19] Wenliang Wang, Baoming Ge, Daqiang Bi, and Dongsen Sun, 'Grid-Connected Wind Farm Power Control using VRB-based Energy Storage System', IEEE (2010) 978-1-PP. 4244-5287.

[20] S.R. Guda, "Modeling and power management of a hybrid wind-microturbine power generation system," MS thesis, Montana State University, 2005.

[21] Fuel cell handbook (sixth edition) EG&G Technical Services, Inc., Science Applications International Corporation, DOE, Office of Fossil Energy, National Energy Technology Lab, Nov. 2002.

[22] M. W. Ellis, M. R. Von Spakovsky, and D. J. Nelson, "Fuel cell systems: efficient, flexible energy conversion for the 21st century," Proceedings IEEE, Vol. 89, No. 12, Dec. 2001, pp. 1808-1818.

[23] E. Santi, D. Franzoni, A. Monti, et al, "A fuel cell based domestic uninterruptible power supply," in Proc. IEEE Applied Power Electronics Conference, 2002, pp.605-613.

[24] Felix A. Farret, M. Godoy Simoes, Integration of alternative sources of energy, Wiley-IEEE Press, January 2006, ISBN: 978-0-471-71232-9.

[25] Z. M. Salameh, M. A. Casacca, and W. A. Lynch, A mathematical model for lead–acid batteries, IEEE Transactions on Energy Conversion, Vol. 7, pp. 93–98, March 1992

[26] Paulo F. Ribeiro, Brian K. Johnson, Mariesa L. Crow, Aysen Arsoy, Yilu Liu, Energy Storage Systems for Advanced Power Applications. Proceedings Of The IEEE, Vol. 89, No. 12, December 2001.

[27] ITACA web site ,A guide to lead acid battery, http://itacanet.org/eng/elec/battery/battery. pdf. (last visited date 3/08/2011).

[28] Steeb, H., Brinner, A., Bubmann, H., Seeger, W., 1990. Operation experience of a 10 kW PV-electrolysis system in different power matching modes. In: Veziroglu, T.N., Takahashi, P.K. (Eds.), Hydrogen Energy Progress VIII, vol. 2. Pergamon Press, New York, pp. 691–700.

[29] Ulleberg O. Stand-alone power systems for the future: optimal design, operation and control of solar-hydrogen energy systems, PhD dissertation. Norwegian University of Science and Technology; 1998.

[30] Wendt H. and Plzak H. (1991) Hydrogen production by water electrolysis. Kerntechnik 56 (1), 22–28.

[31] T. Kato, M. Kubota, N. Kobayashi, and Y.Suzuoki: Effective Utilization of By- Product Oxygen of Electrolysis Hydrogen Production, Annual Meeting of the International Energy Workshop (IEW), Laxenburg, Austria, 2003.

[32] Griesshaber W. and Sick F. (1991) Simulation of Hydrogen-Oxygen–Systems with PV for the Self-Sufficient Solar House (in German). FhG–ISE, Freiburg im Breisgau, Germany.

[33] Taylor, J.B., Anderson, J.E.A., Kalyanam, K.M., Lyle, A.B., Philips, L.A., 1986. Technical and economic assessment of methods for the storage of large quantities of Hydrogen. Int. J. Hydrogen Energy 11 (1), 5–22.

[34] S.A. Sherif, F. Barbir, T.N. Veziroglu, Wind energy and the hydrogen economy—review of the technology, Solar Energy 78 (2005) 647–660

[35] Mitlitsky, F., 1996. Development of an advanced, lightweight, high pressure storage tank for on-board storage of compressed hydrogen. In: Proc. Fuel Cells for Transportation TOPTEC, Alexandria, VA, SAE, Warrendale, PA.

[36] Scientific-technical knowledge international view http://www.scienceandtrade.com/ en / vrb.html, (last visited date 5/08/2011).

[37] EPRI, 2002. Handbook for Energy Storage for Transmission or Distribution Applications. Report No. 1007189. Technical Update December 2002. Document can be found at: www.epri.com

[38] L. Barote, R. Weissbach, R.Teodorescu, "Stand-alone wind system with vanadium redox battery energy storage," in Proc. 2008 IEEE International Conference on Optimization of Electrical and Electronic Equipments, pp.407-412.

[39] Wenliang Wang, Baoming Ge, Daqiang Bi, and Dongsen Sun, 'Grid-Connected Wind Farm Power Control using VRB-based Energy Storage System', IEEE (2010) 978-1-PP. 4244-5287.

[40] Energy efficiency and renewable energy, Industrial distributed energy, http://www.eere.energy.gov/de/pdfs/distributed_generation_interfaces.pdf. (last visited in June 2010).

[41] Caisheng Wang, "Modelling and Control of Hybrid Wind/Photovoltaic/Fuel Cell Distributed Generation Systems", PhD Dissertation, Montana State University, July 2006.

[42] M. Ibrahim: Decentralized Hybrid Renewable Energy Systems Control Optimization and Battery Ageing Estimation Based on Fuzzy Logic, Ph.D. dissertation, Kassel University, Germany, 2002.

[43] W. Kleinkauf and J. Sachau: Components for modular Expandable and Adaptable PV systems, 12th EPVSEC, Amsterdam, the Netherlands, 1994, pp. 1711-1713.

[44] R. H. Lasseter, "MicroGrids," Proceedings, 2002 IEEE PES Winter Meeting, Vol. 1, pp. 305-308, 2002.

[45] IEEE Std 1547, IEEE Standard for Interconnecting Distributed Resources with Electric Power Systems, 2003.

[46] H. Ribberink and I. knight, 2007. European and Canadian non HVAC electric and DHW load profiles for use in simulating the performance for residential cogeneration systems. Annex42 of international energy Agency, May2007.

[47] Tozzi Nord wind turbine company,2009 http://www.tozzinord.com/admin/ PagPar.php?op=fg&id_pag_par= 188&fld=file. (Jan. 2010)

[48] Alwitra company, Brochure SOLYNDRA Solarhttp: www.alwitra. de / index.php? id =produkte&L = 1.(Jan. 2010).

[49] Tommaso Scimone, Energy Storage in Electric Power Generation Plants from Renewable Sources, PhD dissertation, University of Catania/Italy , 2010.

[50] Ballard Power Systems Inc, NexaTM Power Module User's Manual, Document Number: MAN5100078, Release Date: June 16, 2003.

[51] T. Schucan, Case studies of integrated hydrogen energy systems, International Energy Agency Hydrogen Implementing Agreement, Final Report, Paul Scherrer Institute, Switzerland, 2000.

[52] Loferski J. J. An introduction to the physics of solar cells. In Solar Cells—Outlook for Improved Efficiency, National Academy of Sciences–Space Science Board, Washington, DC, pp. 47–53,1972.

[53] H. S. Rauschenbach. Solar cell array design handbook. Van Nostrand Reinhold, 1980.

[54] T.U. Townsend, A Method for Estimating the Long-Term Performance of Direct-Coupled Photovoltaic Systems, MS thesis, University Of Wisconsin – Madison, 1989.

[55] Ross, R.G. and Smockler, M.I. 'Flat-Plate Solar Array Project Final Report, Volume VI: Engineering – Sciences and Reliability, Jet Propulsion Laboratory, Publication 86–31, 1986.

[56] Mukund R. Patel, Wind and solar power systems: design, analysis, and operation, CRC Mechanical Engineering Series, CRC Press, 2006, ISBN 9780849315701.

[57] Nord wind turbine company, 2009 http://www.tozzinord.com/admin /PagPar.php?op=fg&id_pag_ par= 188&fld= file. (Jan. 2010)

[58] P.C. Krause, O.Wasynczuk, S.D. Sudhoff, Analysis of Electric Machinery and drive systems, 2nd ed., IEEE Press, 2002.

[59] MATLAB SimPowerSystems for Use with Simulink User's Guide, Version7.8.0.http:// www.mathworks.com/access/helpdesk/help/toolbox/physmod/powersys/ref/permanentmagnets ynchronousmachine.html.

[60] MATLAB SimPowerSystems for Use with Simulink User's Guide, Version 7.8.0. http://www.mathworks.com/ help/ toolbox /physmod /powersys/ref/ fuelcellstack.html.

[61] Khan MJ, Iqbal MT. Dynamic modelling and simulation of a small wind-fuel cell hybrid energy system. Renewable Energy 2005;46(3):421–39.

[62] Ø. Ulleberg, "Modelling of advanced alkaline electrolysers: a system simulation approach," International Journal of Hydrogen Energy, Vol. 28, pp. 21-33, 2003.

[63] Caisheng Wang, "Modelling And Control Of Hybrid Wind/Photovoltaic/Fuel Cell Distributed Generation Systems", PhD Dissertation, Montana State University, June 2006.

[64] Gorgun H. Dynamic modelling of a proton exchange membrane (PEM) electrolyzer. International Journal of Hydrogen Energy 2006;31(1):29–38.

[65] Çengel Y. A. and Boles M.A. (1989). Thermodynamics – An Engineering Approach. McGraw-Hill, Inc., London.

[66] Hunter R, Infield D, Kessler S, de Bonte J, Toftevaag T, Sherwin B. Designing a system. In: Hunter R, Eliot G, editors. Wind-diesel systems: a guide to the technology and its implementations. Cambridge, UK: Cambridge University Press; 1994.chapter 4.

[67] R. Sebastia , J. Quesada, Distributed control system for frequency control in a isolated wind system, Renewable Energy 31 (2006) 285–305.

[68] MATLAB SimPowerSystems for Use with Simulink User's Guide, Version 7.8.0. http ://www.mathworks.com/access/helpdesk/help/toolbox/physmod/powersys/ref/battery.html

[69] Tremblay, O.; Dessaint, L.-A.; Dekkiche, A.-I., A Generic Battery Model for the Dynamic Simulation of Hybrid Electric Vehicles,Vehicle Power and Propulsion Conference, 2007. VPPC 2007. IEEE 9-12 Sept. 2007, pp. 284-28.

[70] B. Nelson, M. H. Nehrir, and C. Wang, "Unit sizing and cost analysis of stand-alone hybrid wind/PV/fuel cell power generation systems," Renewable Energy, vol. 31, pp. 1641-1656, 2006.

[71] Testa, S. De Caro, R. La Torre, T. Scimone ,"Optimal size selection of Step-Up Transformers in PV Plants" International Conference on Electrical Machines (ICEM 2010), 6-8 September, Rome, Italy.

[72] Das, D, Esmaili, R, Xu, L, Nichols, D. An Optimal Design of a Grid Connected Hybrid Wind / Photovoltaic / Fuel Cell System for Distributed Energy Production. The 31st Annual Conference of the IEEE Industrial Electronics Society, IECON, 2005, pp. 2499-2504.

[73] Dan Burger, Eric Dougan , Joe Oberle, Sean Periyathamby, DC/DC Converter. Senior Project Final Report. Design Team 7 :, .www.ecgf.uakron.edu/~elec/ SDmaterial/ spr2003final /DT7final.pdf.

[74] H. J. Cha and P. N. Enjeti, "A three-phase AC/AC high-frequency link matrix converter for VSCF applications," Proceedings, IEEE 34th Annual Power Electronics Specialist Conference 2003 (PESC '03), Vol. 4, No. 15-19, pp. 1971 – 1976, June 2003.

[75] R. Lasseter, A. Abbas, C. Marnay, J. Stevens, J. Dagle, R. Guttromson, A. Sakis Meliopoulos, R. Yinger, and J. Eto, "Integration of distributed energy resources: The CERTS microgrid concept," California Energy Commission, P500-03-089F, Oct. 2003.

[76] Gabler, H. and E. Wiemken. "Modelling of Stand-Alone PV-Hybrid Systems and Comparison of System Concepts". Proceedings of 2nd World Conference on Photovoltaic Solar Energy Conversion, Vienna, Austria, 6-10 July, 1998.

[77] Ross, Michael M.D. Comparison of AC, DC, and AC/DC Bus Configurations for PV Hybrid Systems. Report submitted to CETC-Varennes in fulfilment of Contract #3-1542SR. Varennes, Québec, Canada: Natural Resources Canada, 2004.

[78] L.A. Zadeh, "Fuzzy Sets," Inform. Contr., vol. 8, pp. 338-353, 1965.

[79] Fuzzy Logic Toolbox™ 2, User's Guide, http://www.mathworks.com/help/toolbox/fuzzy/fp61.html , (Last visited: 17/08/2011)

[80] Hunter R, Infield D, Kessler S, de Bonte J, Toftevaag T, Sherwin B, et Wind-diesel systems: a guide to the technology and its implementations. Cambridge, UK: Cambridge University Press; 1994. Chapter 4.

[81] Ian S. Shaw and Marcelo G Simoes, M.G. (1999) Controle e Modelagem Fuzzy ("in Portuguese"), Edgard Bluchert Company; ISBN: 8521202482.

[82] Ian S. Shaw (1998), Fuzzy Control of Industrial Systems : Theory and Applications, Kluwer Academic Publishers; ISBN: 0792382498.

[83] EN 50160/1999, Voltage characteristics of electricity supplied by public distribution systems.

[84] G.W. Mack, S. Santoso, Understanding power system harmonics, Power Engineering Review, IEEE, Volume: 21, Issue: 11, Nov. 2001, pp. 8 – 11.

[85] IEEE Standards 519-1992, "Recommended Practices and Requirements for Harmonic Control in Electric Power Systems", 1992.

[86] Testa A., De Caro S., Scimone T. "Analysis of a VRB energy storage system for a tidal turbine generator" Power Electronics and Applications, 2009. EPE '09. 13th European Conference on 8-10 Sept. 2009 Page(s):1 – 10.

[87] D.B. Nelson, M.H. Nehrir, and C. Wang, "Unit Sizing of Stand-Alone Hybrid Wind/PV/Fuel Cell Power Generation Systems", IEEE Power Engineering Society General Meeting, 2005, Vol. 3, page. 2115-2122.

[88] Hansen A.D (2004). Generators and power electronics for wind turbines. Chapter 4 in ''Wind Power in power systems', John Wily&Son,Ltd,75P.

[89] E. Muljadi, N. Samaan, V. Gevorgian, Jun Li, Member, S. Pasupulati, 'Short Circuit Current Contribution for Different Wind Turbine Generator', IEEE Power and Energy Society General Meeting, NREL/CP-550-47193, March 2010.

[90] Sørensen, P., Bak-Jensen, B., Kristian, J., Hansen, A. D., Janosi, L., Bech, J. (2000)'Power Plant Characteristics of Wind Farms', in Wind Power for the 21st Century; Proceedings of the International Conference Kassel, Germany.

[91] ABB group , Automation and power technologies, Transforming wind power www.abb.com.

[92] A. Testa, S. De Caro, R. La Torre and T. Scimone, 'Optimal size selection of Step-Up Transformers in PV Plants', XIX International Conference on Electrical Machines - ICEM 2010, Rome.